A Role For Microtubule Dynamics For The Induction Of Chromosomal Instability And Cell Migration And Invasion In Human Cancer Cells

Dissertation

for the award of the degree

"Doctor rerum naturalium"

of the Georg-August-Universität Göttingen

within the doctoral program "Molecular Biology of Cells"

of the Georg-August University School of Science (GAUSS)

submitted by

Katharina Berger

from Brandenburg an der Havel, Germany

Göttingen, September 2016

Thesis Committee

Prof. Dr. Holger Bastians
Institute for Molecular Oncology
Section of Cellular Oncology
University Medical Center Göttingen

Prof. Dr. Michael Thumm
Department of Cellular Biochemistry
University Medical Center Göttingen

Prof. Dr. Dieter Kube
Department of Haematology and Oncology
University Medical Center Göttingen

Members of the Examination Board

Referee: Prof. Dr. Holger Bastians
Institute for Molecular Oncology
Section of Cellular Oncology
University Medical Center Göttingen

2nd Referee: Prof. Dr. Dieter Kube
Department of Haematology and Oncology
University Medical Center Göttingen

Further members of the Examination Board

Prof. Dr. Michael Thumm
Department of Cellular Biochemistry
University Medical Center Göttingen

Prof. Dr. Matthias Dobbelstein
Institute for Molecular Oncology
University Medical Center Göttingen

Prof. Dr. Heidi Hahn
Department of Human Genetics
Section of Developmental Genetics
University Medical Center Göttingen

Prof. Dr. Peter Burfeind
Department of Human Genetics
University Medical Center Göttingen

Date of oral examination

18th of November 2016

Affidavit

Hereby I declare that my doctoral thesis entitled "A Role For Microtubule Dynamics For The Induction Of Chromosomal Instability And Cell Migration And Invasion In Human Cancer Cells" has been written independently with no other sources and aids than quoted.

Göttingen, September 2016 _____

Katharina Berger

Table Of Contents

List Of Figures

List Of Tables

Abstract

Aneuploidy and increased cell migration and invasion are hallmarks of aggressive human cancers. Aneuploidy derives from an increased rate of perpetual chromosome missegregation during mitosis, referred to as chromosomal instability (CIN). CIN contributes to the development of genetic heterogeneity and is thought to support rapid adaptation of cancer cells. Significantly, late tumor stages, which exhibit metastasis, are not only characterized by increased cancer cell migration and invasion, but also by high levels of CIN, both of which correlate with poor patient prognosis. Therefore, I aimed to investigate a potential link between CIN and increased cell migration and invasion in aggressive human cancer cells.

In this study, I found that CIN *per se* is not sufficient to trigger increased cancer cell migration and invasion. However, a hyperactive TRIO-Rac1-Arp2/3 pathway acts as a shared trigger for both, the development of CIN and cancer cell migration and invasion. Hyperactivation of TRIO, Rac1 and the Arp2/3 complex depends on increased microtubule plus-end assembly rates and on the localization of the Rac1-GEF TRIO to microtubule plus-ends *via* the microtubule end-binding protein EB1. In mitosis, microtubule dependent hyperactivation of the pathway causes spindle positioning defects leading to erroneous microtubule-kinetochore attachments and the generation of lagging chromosomes, which constitute a common cause for chromosome missegregation and CIN. Inhibition of TRIO, Rac1 or the Arp2/3 complex suppressed these phenotypes and prevented the development of aneuploidy in chromosomally instable colon cancer cells. In interphase, the hyperactivity of TRIO, Rac1 and the Arp2/3 complex resulted in highly enhanced cancer cell migration and invasion. Analogous to the situation in mitosis, restoration of proper microtubule dynamics in interphase suppressed the migratory and invasive phenotype in invasive colorectal cancer and melanoma cells. Thus, these results demonstrate a mechanistic link between the regulation of the actin and the microtubule cytoskeleton important for the development of CIN as well as for triggering cancer cell migration and invasion.

As one important trigger that can cause increase of microtubule plus-end assembly rates in both, mitosis and in interphase I identified a concomitant loss of the transcription factors p53 and p73. In fact, my studies suggest that p53 and p73 cooperate in maintaining chromosomal stability and suppressing cancer cell migration and invasion.

1 Introduction

1.1 The Eukaryotic Cell Cycle

The cell cycle enables the generation of two daughter cells that are accurate copies of the parental cell. This process is divided into two main phases: mitosis and interphase. Mitosis again is subdivided into a successive series of phases: prophase, prometaphase, metaphase, anaphase and telophase, whereas interphase is subdivided into G_1-, S- and G_2-phase (Fig. 1.1). Each phase of the cell cycle is characterized by the time-dependent activation and inactivation of enzymatic cascades, that are regulated through various protein complexes (Nigg 2001).

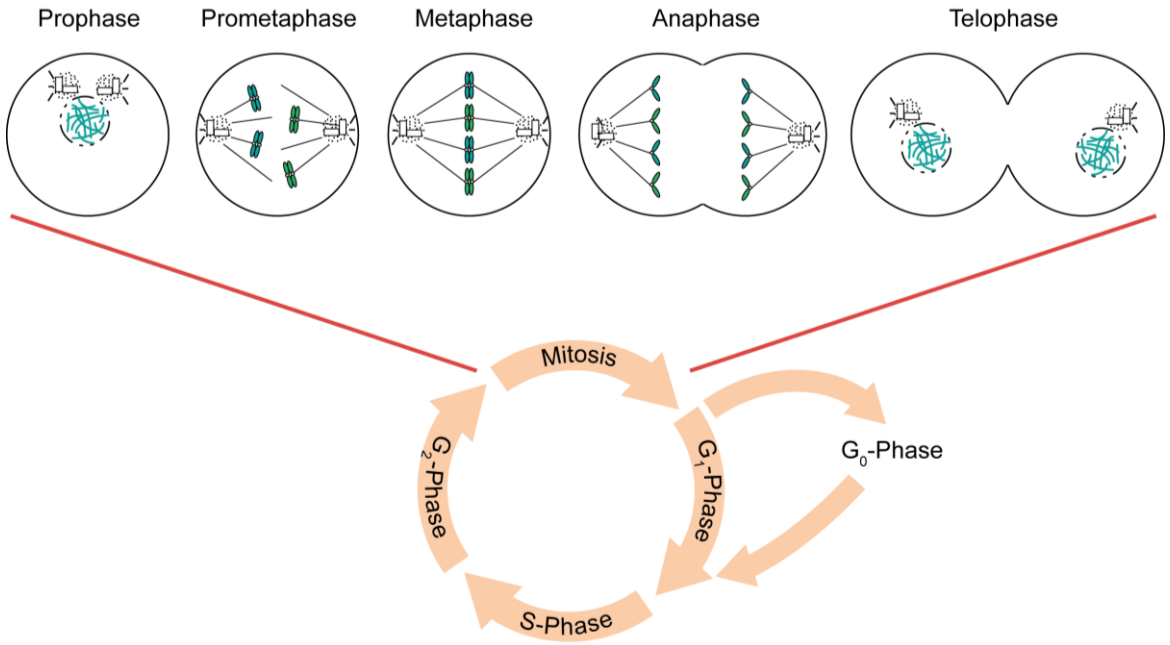

Figure 1.1: The eukaryotic cell cycle. The eukaryotic cell cycle is divided into interphase with its sub-phases G_1-, S- and G_2-phase and mitosis with its sub-phases prophase, prometaphase, metaphase, anaphase and telophase. During prophase, the centrosomes separate and the chromosomes starts to condense. The nuclear envelope breaks down in prometaphase and the mitotic spindle assembles. When all chromosomes are attached to spindle microtubules emanating from the opposing spindle poles and fully aligned on the cell equator, the cell is said to be in metaphase. During anaphase the chromosomes are separated and pulled towards the opposing spindle poles. A new nuclear envelope is build in telophase and the chromosomes decondense.

During G_1-phase (gap-phase 1), the cell grows in size and many genes required for cell division are switched off. In case of poor nutrient supply or during differentiation, the cell is able to exit the cell cycle to enter the resting phase G_0. But upon proliferative environmental stimuli, the cell overcomes the restriction point, whereupon genes required for the transition

into S-phase (DNA synthesis phase) are transactivated. The transition from G_1- to S-phase needs to be tightly regulated, since the misregulation promotes oncogenesis (Bertoli *et al.* 2013). During S-phase, the centrosomes, which are the main microtubule organizing centers in mammals, are duplicated and the DNA is replicated. As a result, two sister chromatids exist, which are linked by the cohesin protein complex (Losada *et al.* 1998; Sumara *et al.* 2000). This complex is important for a symmetrical segregation of the sister chromatids during mitosis (Michaelis *et al.* 1997). The G_2-phase is characterized by the accumulation and activation of enzymes, which trigger mitotic entry when reaching a critical threshold.
During the following mitosis, the replicated DNA is segregated equally onto two daughter cells. Chromosome condensation, movement of centrosomes towards the opposing spindle poles (Nigg 2001) and the formation of the mitotic spindle (Nigg & Stearns 2011) starts in prophase. During prometaphase, the nuclear envelope breaks down and the mitotic spindle is further established. Moreover, the kinetochores assemble at the centromeric region of the sister chromatids, thereby generating binding sites for the microtubules (Cheeseman & Desai 2008). First, the chromosomes become randomly attached by microtubules emanating from the spindle poles in a process termed "search and capture" (Kirschner & Mitchison 1986). Then they are aligned at the metaphase plate in an accurate manner. Once all chromosomes are properly attached to spindle microtubules and fully aligned, the cell is said to be in metaphase. During anaphase A, cohesin protein complexes, which link the sister chromatids, are cleaved by the enzyme separase (Nakajima *et al.* 2007), the sister chromatids are separated and move towards the spindle poles due to microtubule shortening, while in anaphase B the two spindle poles themselves move apart (Rieder & Salmon 1994). In telophase, the chromatids reach the spindle poles thereby forming the new daughter nuclei. The separation of the daughter cells is completed by cytokinesis.

1.2 Cell Cycle Regulation And Checkpoints

The cell cycle needs to be highly regulated to avoid the formation of abnormal daughter cells. The timely ordered progression of cells through the cell cycle is mediated by the oscillating activation and inactivation of cyclin-dependent kinases (CDKs) (Arellano & Moreno 1997). The catalytic activity of CDKs requires the binding of regulatory subunits known as cyclins (Malumbres & Barbacid 2005). The cell cycle dependent synthesis and degradation of cyclins regulate CDK activity in a timely manner (Malumbres & Barbacid 2009). However, binding of cyclins to CDKs is not sufficient to fully activate the complex. CDK activity is also regulated by activating and inhibitory phosphorylations and dephosphorylations (Coleman & Dunphy 1994; Lolli & Johnson 2005). The kinases Wee1 and Myt1 inhibit CDK-cyclin complexes by phosphorylation, whereas the phosphatase Cdc25 removes these inhibitory

phosphorylation (Malumbres & Barbacid 2005). Furthermore, an activating phosphorylation through the CDK activating kinase (CAK) is required (Lolli & Johnson 2005). Specific CDK-cyclin complexes control cell cycle progression: D-type cyclins bind to CDK4 and CDK6 during G_1-phase, E-type cyclins preferentially bind to CDK2 at the G_1-S-transition, CDK2-cyclin A is active during S-phase and CDK1-cyclin A and CDK1-cyclin B at the transition to mitosis as well as during mitosis (Malumbres & Barbacid 2009) (Fig. 1.2).

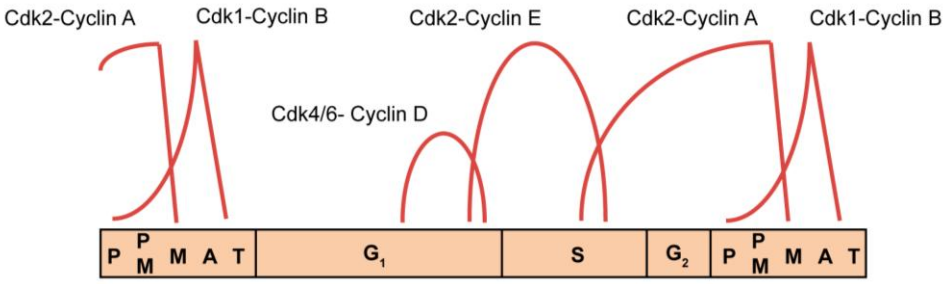

Figure 1.2: Regulation of the cell cycle by CDK-cyclin complexes. In early mitosis, Cdk1 and Cdk2 bound to cyclins A and B are highly active. The G_1-S-transition is mediated by Cdk4/6-Cyclin D and Cdk2-Cyclin E activity, which also lead to the synthesis of proteins needed for DNA replication in S-phase. Cdk2-Cyclin A is active during S-phase until early mitosis. P: prophase, PM: prometaphase, M: metaphase, A: anaphase, T: telophase. Modified from Pollard & Earnshaw 2007.

Signaling pathways control the progression of the cell during the cell cycle and regulate the transition between the different phases by modulating CDK activity. For instance, the DNA-damage checkpoint is activated upon diverse alterations in the DNA caused by environmental or endogenous stress (Bartek *et al.* 2004). Central checkpoint proteins are ATM (ataxia telangiectasia mutated) and ATR (ATM-Rad3-related) and their effectors Chk1 (Liu *et al.* 2000), Chk2, BRCA1 (Cortez 1999) and p53 (Banin *et al.* 1998; Matsuoka *et al.* 1998). DNA double strand breaks during G_1-phase activate ATM and Chk2, which leads to the stabilization of the transcription factor p53 (Banin *et al.* 1998). This in turn results in the induction of the cyclin-dependent kinase inhibitor p21, which binds to CDK-cyclin complexes, thereby blocking cell cycle progression into S-phase (Harper *et al.* 1993; Harper *et al.* 1995). During G_2-phase, the activation of Chk1 by ATR leads to a phoshorylation and thereby inhibition of Cdc25. As a consequence, Cdc25 is not able to activate CDK1-cyclin B, thus preventing mitotic entry in the presence of damaged DNA (Sanchez 1997).

During mitosis, the spindle assembly checkpoint (SAC) ensures genomic stability by delaying chromosome segregation until all kinetochores are properly attached to spindle microtubules. During prometaphase, the mitotic checkpoint complex (MCC), consisting of the proteins BubR1, Bub3, Cdc20 and Mad2, assembles at unattached kinetochores (Lara-Gonzalez *et al.* 2012). Due to this complex formation, Cdc20 is not able to activate the E3 ubiquitin ligase

anaphase-promoting complex/cyclosome (APC/C) (Musacchio & Salmon 2007). When all chromosomes are bi-oriented and aligned at the metaphase plate, the SAC is satisfied and the generation of the MCC declines. Cdc20 is released from the complex and can activate APC/C, which leads to the ubiquitylation of cyclin B and securin and their subsequent proteasomal degradation. Proteolysis of securin results in the release of the protease separase. In turn, separase cleaves the cohesin complexes that are responsible for sister chromatid cohesion, thereby enabling chromosome segregation. On the other hand APC/C-mediated proteasomal degradation of cyclin B inactivates the cyclin-dependent kinase 1 (CDK1), thereby promoting mitotic exit (Peters 2006).

1.3 The p53 Tumor Suppressor Family

The *TP53* gene encoding for p53 is among the most frequently altered tumor suppressor genes in human cancers. About 50% of human cancers harbor mutations in this gene, leading to an overproduction of mutant protein in high concentrations. p53 is a sequence specific transcription factor, which is involved in regulating the expression of genes controlling cell cycle arrest and apoptosis. p53 is activated upon genotoxic damage or metabolic stress and plays a central role in G_1 and DNA damage checkpoints. Upon DNA damage p53 induces DNA repair proteins with subsequent cell cycle arrest until the damaged DNA is repaired. In case of irreparable DNA damage, p53 is also able to induce programmed cell death, thus preventing the proliferation of cells with highly damaged DNA (Amundson *et al.* 1998).

The p53 family members p73 and p63 were found to have a high structural and functional similarity to p53 (Yang *et al.* 1998; Kaghad *et al.* 1997). They share the hallmark features of p53´s structure: an amino-terminal transactivation domain, a highly conserved DNA-binding domain and a carboxy-terminal oligomerization domain (Levrero *et al.* 2000). Therefore, they might be able to fulfill redundant functions of p53. Indeed, it was shown, that TA isoforms of p73 and p63 can bind to p53-responsive promotor elements of well-known p53 target genes like *CDKN1A*, *BAX* or *MDM2* (Yang & McKeon 2000). In addition, so-called ΔN isoforms, which are truncated at their N-terminus, have been shown to act antagonistically to p53 as well as to TAp73 and TAp63 (Yang *et al.* 1998; Grob *et al.* 2001). These ΔN isoforms are still capable of DNA-binding and thus might compete with p53, TAp73 and TAp63 for DNA-binding sites. Because of the conserved oligomerization domain, ΔN proteins are also able to bind to p53, TAp73 and TAp63 leading to sequestration of the proteins and formation of inactive hetero-oligomers (Yang & McKeon 2000; Grob *et al.* 2001). Furthermore, *ΔNp73* is highly overexpressed in various tumors (Concin *et al.* 2004) including ovarian and skin cancer. The overexpression is associated with poor patient prognosis and decreased survival

(Concin *et al.* 2005). *ΔNp73* expression can also be found in metastases of skin cancer patients (Tuve *et al.* 2004). Here, ΔNp73 induces epithelial-mesenchymal-transition (EMT), with loss of E-cadherin and induction of N-cadherin (Engelmann *et al.* 2014).

A frequent lesion in colorectal cancer is a mutation in *TP53* (Muller & Vousden 2013), which causes loss of lost wild-type function. Mutant p53 protein exerts a dominant-negative regulation towards the remaining wild-type p53 (Petitjean *et al.* 2006). Mutations can be found throughout the *TP53* gene but they cluster within the DNA-binding domain. Several hot spot mutations were identified, including occurrence at R175, G245, R248 and R273. These mutations affect folding of the protein and also alter the DNA-binding ability of p53. Mutant p53 still exerts DNA-binding activity, nevertheless, the binding to p53 responsive elements is impaired (Muller & Vousden 2013; Thukral *et al.* 1995). However, mutant p53 can also bind to unique DNA-elements, which indicates a gain of function and gives mutant p53 the function of an oncogenic transcription factor (Kim & Deppert 2004; Muller & Vousden 2013). Transcriptional functions of mutant p53 are also achieved *via* a direct interaction with other transcription factors to prevent or even enhance their function. An inhibitory interaction can be found between mutant p53 and p73 as well as p63. Thereby, mutant p53 binds to and inhibits the TA isoforms of p73 and p63 (Gaiddon *et al.* 2001).

1.4 p21 As Mediator Of p53 Tumor Suppressor Activity

p21 is a member of the Cip and Kip family of CDK inhibitors, which includes p21, p27 and p57. The gene encoding for p21 (*CDKN1A*) is activated upon DNA-damage by p53 and p21 protein mediates a cell cycle arrest (Deng *et al.* 1995) by inhibiting CDK2, CDK4 and CDK6 (Harper *et al.* 1995). CDK2 activity is required for phosphorylation of the Rb (retinoblastoma) protein. Upon phosphorylation, Rb is released from a complex consisting of Rb and the transcription factor E2F. This complex disruption leads to E2F-dependent gene expression, which is needed to overcome the restriction point. p21 is frequently deregulated in cancers and is able to promote proliferation and oncogenesis (Rufini *et al.* 2011). This deregulated expression is often associated with a loss of function of transcriptional regulators such as p53 (Abbas & Dutta 2009). Reduced *CDKN1A* expression is detected in colorectal, cervical, head and neck as well as small-cell lung cancers (Ogino *et al.* 2010). Ahead from p21´s role in the DNA damage checkpoint, p21 deficiency was shown to induce mitotic defects (Kreis *et al.*, 2014). These defects include prolonged metaphase and anaphase as well as erroneous chromosome segregation and cytokinesis, which promote genomic instability. However, the underlying mechanisms are unclear.

1.5 The Cellular Cytoskeleton

1.5.1 The Microtubule Cytoskeleton

The microtubule cytoskeleton is important for a large number of cellular functions. During mitosis the most prominent function is the assembly of the mitotic spindle and the precise chromosome segregation (Wittmann *et al.* 2001), whereas during interphase microtubules participate in organelle positioning, intracellular transport as well as maintaining cell shape and facilitating cellular motility (Goode *et al.* 2000). Microtubules are assembled of α- and β-tubulin heterodimers, which form a protofilament. 13 protofilaments form the hollow tube of microtubules. Microtubules exhibit a certain polarity with α-tubulin exposed at the minus-end and β-tubulin exposed at the plus-end. Assembly and disassembly of tubulin heterodimers occurs solely at their ends. Each end switches between growth and shrinkage, whereby dissociation of tubulin mainly occurs at the minus-end and association at the plus-end. Thereby, microtubules grow and shrink at a steady state, a process termed ´treadmilling´ (Margolis & Wilson 1998*;* Grego *et al.* 2001).

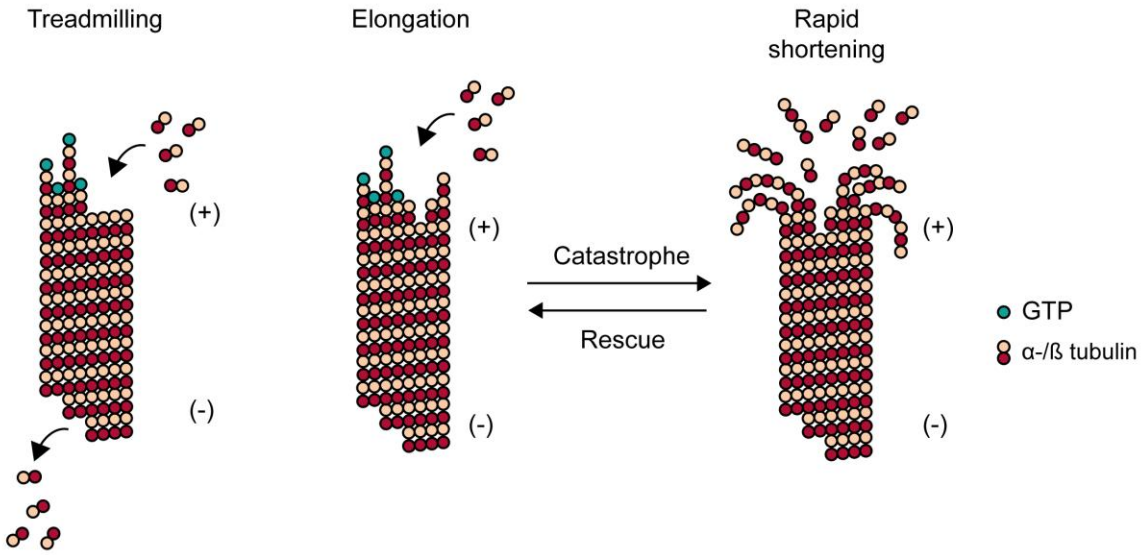

Figure 1.3: Dynamic instability of microtubules. Microtubules are assembled by α-/β- tubulin heterodimers that are incorporated at the microtubule plus-end. The assembly at the plus-end and disassembly of heterodimers at the minus-end, without changes in length is termed treadmilling. However, microtubules are characterized by dynamic instability. They undergo transition to rapid shortening, which is termed catastrophe. This process can be terminated by a rescue event whereupon the microtubule grows again. Modified from Pollard & Earnshaw 2007.

Microtubule growth is regulated by the incorporation of the tubulin heterodimer into the microtubule end and the hydrolysis of β-tubulin bound GTP. GTP hydrolysis occurs with a delay, resulting in a so-called GTP-cap at the microtubule tip. The GTP-cap stabilizes the microtubule and loss of the cap leads to a catastrophe event with microtubule

depolymerization and shrinkage. The switch between growth and shrinkage is known as catastrophe, while the switch from shrinkage to growth is termed ´rescue´. Microtubule disassembly can be rescued by the presence of GTP-islands on the surface of the microtubule lattice, which mimic the GTP-cap (Desai & Mitchison 1997; Akhmanova & Steinmetz 2015) (Fig. 1.3).

The dynamicity of microtubules is regulated by microtubule associated proteins (MAPs) and their sub-class of microtubule plus-end tracking proteins (+TIPs) (Schuyler & Pellman 2001). Microtubule polymerases, such as ch-TOG (colonic and hepatic tumour-overexpressed gene), bind to microtubule plus-ends and promote the incorporation of tubulin heterodimers into the growing plus-end (Gard & Kirschner 1987; Brouhard *et al.* 2008). Microtubule depolymerases, such as MCAK (mitotic centromere-associated kinesin), regulate microtubule disassembly by removing heterodimers from the microtubule minus-ends (Hunter *et al.* 2003; Burns *et al.* 2014). Indirectly, also the end-binding proteins (EBs) of +TIPs can regulate microtubule polymerization rates. Hundreds of EB proteins like EB1 can bind to a growing microtubule tip (Vaughan 2005), thereby serving as a binding platform for other proteins like CLIP-170 (cytoplasmic linker protein) (Lansbergen *et al.* 2004), CLASP1 and CLASP2 (cytoplasmic linker protein associated proteins 1/2) (Mimori-Kiyosue *et al.* 2005) and $p150^{Glued}$ (Ligon *et al.* 2003; Watson & Stephens 2006). These proteins appear to promote rescue events or suppress catastrophe events (Akhmanova & Steinmetz 2015).

1.5.2 The Actin Cytoskeleton

Actin plays an important role in several cellular processes like cell motility, establishment and maintenance of cell shape, cytokinesis and muscle contraction. Actin filaments are assembled of actin polymers and a variety of actin-binding proteins (ABPs), which include filament crosslinkers, motor proteins as well as nucleation and elongation factors (Lee & Dominguez 2010; Mullins & Hansen 2013).

In the cell, actin is present in a monomeric, globular (G-actin) or polymeric, filamentous (F-actin) form. G-actin is able to bind ATP, which is hydrolyzed to ADP, when actin is incorporated into a growing filament. F-actin forms a double-stranded helix and exhibits a certain polarity with a barbed (+) end and a pointed (-) end. Spontaneous addition of ATP-bound G-actin at the barbed (+) end leads to growing of the actin filament, whereas depolymerization of F-actin occurs at the pointed (-) end by dissociation of ADP-bound G-actin (Lee & Dominguez 2010) (Fig. 1.4). This so-called actin filament treadmilling is regulated by ABPs. Among them, ADF/cofilin and profilin accelerate the dissociation of G-actin from the pointed end and the incorporation to the barbed end, respectively. ADF/cofilin and profilin are ABPs that bind to G-actin, thereby controlling the pool of

unpolymerized actin in the cell (Lee & Dominguez 2010). During actin polymerization, an actin/profilin complex is guided to the barbed end of a filament and incorporated into the filament by the filament elongation factor Eva/VASP (Lee & Dominguez 2010).

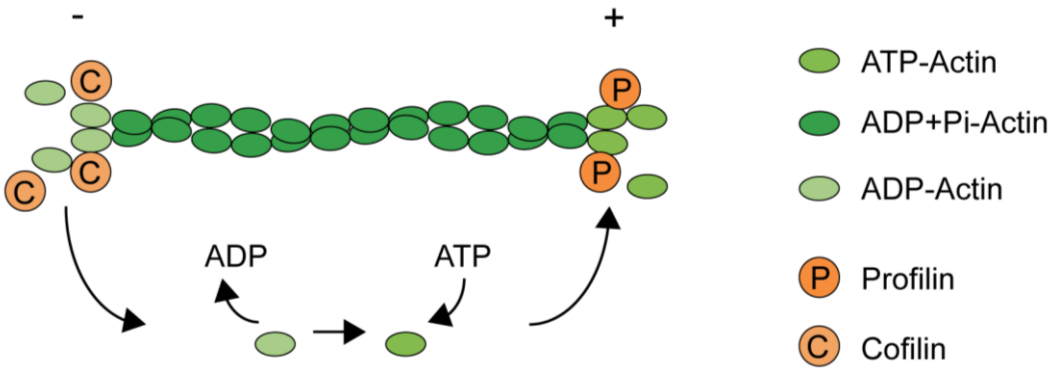

Figure 1.4: Actin filament nucleation. Actin filaments form a double-helix and exhibit a barbed (+) and a pointed (-) end. Association of ATP-bound actin monomers mainly occurs at the barbed end, whereas the pointed end is mainly characterized by dissociation of ADP-bound actin monomers. Actin binding proteins (ABPs) regulate actin treadmilling. Profilin promotes incorporation of actin monomers at the barbed end, whereas cofilin promotes actin disassembly from the pointed end. Modified from Lee & Dominguez 2010

Actin filaments can exhibit different types of organization: branched and crosslinked networks, parallel bundles and anti-parallel contractile structures (Blanchoin *et al.* 2014). The Arp2/3 complex (actin related protein 2/3) is responsible for branching of a pre-existing actin filament. This complex is activated by the Nucleation Promoting Factors (NPF) WASP (Wiskott-Aldrich syndrome protein) or WAVE (WASP-family verprolin-homologous protein), which interact with Arp2/3 and actin monomers to create a nucleation core at the side of a mother filament (Lee & Dominguez 2010; Achard *et al.* 2010). The presence of capping protein (CP) limits the growth of the filament by binding to the barbed end (Akin & Mullins 2008). Surprisingly, this CP-mediated termination of filament elongation promotes actin network assembly and cell motility (Achard *et al.* 2010). Whereas the Arp2/3 complex is involved in the initiation of actin assembly as well as in the organization of the actin network, there are also proteins, which solely connect actin filaments without modulating their assembly, e.g. the long crosslinkers alpha-actinin and filamin, and the short crosslinkers fimbrin and fascin. Depending on the crosslinking proteins, actin is packed into tight parallel or antiparallel bundles or a filament network is built. Branched and crosslinked filaments make up the lamellipodium, whereas aligned bundles are the basis for filopodia and stress fiber formation (Blanchoin *et al.* 2014). Alterations in the actin cytoskeleton are associated with cancer metastasis and invasion, since the invasion process is characterized by the formation of lamellipodia, filopodia and invadopodia (Yamaguchi & Condeelis 2007).

During mitosis, the actin cytoskeleton is subjected to dynamic rearrangements. Actin filaments localize to the cortical plasma membrane, to retraction fibers and also to the contractile ring during late stages of mitosis and cytokinesis (Mitsushima *et al.* 2010). The cortical actin influences spindle positioning, thereby defining the cell´s division axis (Théry *et al.* 2005; Toyoshima & Nishida 2007). Furthermore, an amorphous cluster known as ´actin cloud´ was recently described to be present during mitosis (Mitsushima *et al.* 2010), which interacts with astral microtubules, influencing mitotic spindle alignment (Fink *et al.* 2011). The actin cloud forms at the cell cortex early during mitosis, persists until late anaphase and was shown to be dependent on the activity of the Arp2/3 complex (Mitsushima *et al.* 2010).

1.6 Mitotic Spindle Assembly

The dynamic properties of microtubules along with many proteins that modulate microtubule organization and stability are required to set up a bipolar spindle during mitosis to separate the sister chromatids (Gadde & Heald 2004). Three sub-populations of microtubules exist within a mitotic spindle: kinetochore microtubules connect the chromosomes to spindle poles, interpolar microtubules form an overlapping, antiparallel network and astral microtubules interact with the cell cortex (Wittmann *et al.* 2001; Gadde & Heald 2004). The first step towards a bipolar spindle is the separation of the centrosomes, which is mediated by motor proteins (Wittmann *et al.* 2001). Motor proteins can be classified into plus-end directed motors, known as kinesins, and minus-end directed motors, known as dyneins. Among them, the kinesin Eg5 plays an important role during centrosome separation (Whitehead & Rattner 1998; Tanenbaum *et al.* 2008). Due to the antiparallel sliding activity of Eg5, the centrosomes are pushed to opposing sides (Tanenbaum & Medema 2010). A second important player is the minus-end directed motor dynein (Tanenbaum & Medema 2010). Dynein localizes to astral microtubules or to the cell cortex (Kardon & Vale 2009). The cortical dynein is able to pull on astral microtubules, thereby positioning the mitotic spindle (Grill *et al.* 2003). The main function of the mitotic spindle is the alignment and the segregation of the chromosomes. For this, microtubules are attached to kinetochores, which involves several kinetochore and microtubule associated proteins. Chromosome alignment and segregation requires the function of different kinesins, including chromokinesins.

Precise spindle positioning is an important process, since it provides the axis of the following cell division. Usually, the axis of cell division is oriented along the planar axis, thereby ensuring the attachment of the newly formed daughter cells to the substratum (Toyoshima & Nishida 2007). The polarization depends on external factors such as the extracellular matrix or neighboring cells (Fink *et al.* 2011). Astral microtubules interact with cortical proteins *via* +TIPs, including EB1, APC (adenomatous poliposis coli) and dynein (Schuyler & Pellman

2001). The dynein-dynactin complex binds to NuMA (Nuclear mitotic apparatus protein), that is linked to the cell cortex *via* LGN (GPSM2, G-protein-signaling modulator 2). The minus-end directed motor activity of dynein-dynactin then provides a pulling force on astral microtubules (Bergstralh & St Johnston 2014).

Furthermore, the actin cytoskeleton is necessary during spindle positioning, since the disruption of actin was shown to induce spindle misorientation (Toyoshima & Nishida 2007). The actin cytoskeleton provides information about the cell´s shape and adhesion. The distribution of adhesions in interphase cells was described to determine the mitotic spindle orientation (Théry *et al.* 2005). Thereby, the actin cytoskeleton is associated with membrane ruffles in interphase, which contain microtubule stabilizing proteins such as APC (Etienne-Manneville & Hall 2003) and motor proteins such as dynein (Busson *et al.* 1998). These proteins remain located in this area during cell division and promote the localization of the spindle poles (Dujardin *et al.* 2003). Additionally, forces generated by retraction fibers lead to Arp2/3-based subcortical actin structures in mitotic cells, which exert pulling forces on the mitotic spindle (Fink *et al.* 2011). These actin structures are possibly coupled to microtubules, thereby influencing spindle positioning, but its function is largely unknown.

1.7 Chromosomal Instability And Aneuploidy

Accurate progression of mitosis is pivotal to ensure a correct euploid karyotype. However, many human diseases including cancer and neurodegenerative diseases are characterized by aneuploidy. A common cause for aneuploidy in human cancer cells is chromosomal instability (CIN) (Lengauer *et al.* 1997). One can distinguish between structural chromosomal instability (S-CIN) that describes the susceptibility to structural rearrangements including translocations, deletions, inversions and duplications of chromosomal parts (Ricke *et al.* 2008; Thompson *et al.* 2010) and whole chromosomal instability (W-CIN), which is defined as the perpetual gain or loss of whole chromosomes during mitosis. In a typical aneuploid cancer cell, one chromosome in every one to five cell divisions becomes missegregated (Lengauer *et al.* 1997; Thompson & Compton 2008). It is thought that these low missegregation rates allow the acquirement of new cancer phenotypes and the adaptation to the environment (Thompson *et al.* 2010). In contrast, high rates of chromosome missegregation induced by a highly deregulated mitosis are lethal (Kops *et al.* 2004). Furthermore, CIN and aneuploidy is of disadvantage for tumor growth, probably caused by metabolic changes and proteotoxic stress (Torres *et al.* 2007; Sheltzer & Amon 2011; Ertych *et al.* 2014).

The molecular mechanisms causing CIN in human cancer cells are not well understood, but could involve abnormalities during interphase as well as various alterations in mitotic progression (Orr & Compton 2013).

A controversially discussed mechanism is an impaired spindle assembly checkpoint (SAC). The SAC senses improper kinetochore-microtubule attachments and maintains genomic stability by delaying the metaphase-to-anaphase-transition until all chromosomes are amphitelically attached (Fig. 1.5). A defective SAC leads to a premature anaphase onset in the presence of faulty kinetochore-microtubule attachments, resulting in chromosome missegregation. However, in human cancer cells exhibiting CIN, a weakened SAC due to mutations in SAC related genes is rarely found (Tighe *et al.* 2001; Barber *et al.* 2008) and the complete loss of SAC function was even shown to be lethal (Kops *et al.* 2004).

Chromosome missegregation can also result from the presence of supernumerary centrosomes, which occur from an aberrant cytokinesis or from defects in centrosome biogenesis or centrosome amplification during interphase. In principal, cells containing more than two centrosomes can build up a multi-polar spindle resulting in massive chromosome missegregation. However, this was shown to be unviable for progenies arising from multi-polar cell divisions (Ganem *et al.* 2009). Instead, supernumerary centrosomes often cluster to form a pseudo bi-polar spindle (Brinkley 2001). But still, the transient occurrence of a multi-polar spindle promotes transient spindle geometry defects, erroneous kinetochore-microtubule attachments and lagging chromosomes (Ganem *et al.* 2009), leading to chromosome missegregation.

Lagging chromosomes are widely recognized as a cause for chromosomal instability and arise from merotelic kinetochore attachments (Fig. 1.5a). In this case, one kinetochore is concomitantly attached to spindle microtubules emanating from the two opposing spindle poles (Cimini *et al.* 2001; Cimini *et al.* 2002; Thompson & Compton 2008). Normally, sister chromatids are attached to opposing poles of the spindle, known as amphitelic attachments. During chromosome alignment, one kinetochore becomes attached first and orients towards the spindle pole (Rieder & Salmon 1998). This monotelically attached chromosome moves poleward until microtubules bind to the unattached kinetochore, resulting in an amphitelic attachment and chromosome bi-orientation (Rieder & Salmon 1998; Cimini *et al.* 2002). But errors in kinetochore attachment can occur, including syntelic attachments, where both sister chromatids are attached to spindle microtubules emanating from the same spindle pole. In addition, merotelic attachments are often detectable in cancer cells (Fig. 1.5a). Merotelic attachments support chromosome alignment and the establishment of the metaphase plate, but these errors are not detected by the SAC and lead to a chromosome remaining near the spindle equator (Cimini *et al.* 2001) (Fig. 1.5b). During the following cytokinesis, the lagging chromosome is distributed onto one of the daughter cells by chance.

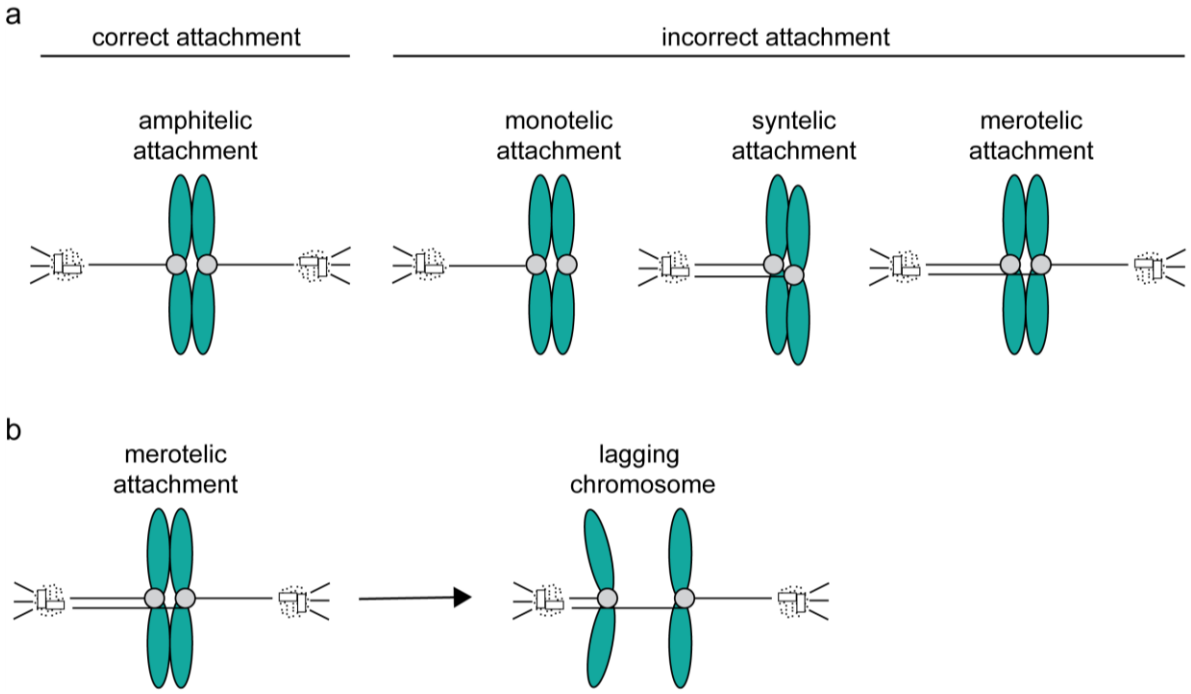

Figure 1.5: Classification of kinetochore-microtubule attachments. (a) Amphitelic attachments describe the state in which both sister kinetochores are attached to spindle microtubules emanating from the opposing spindle poles. In case of monotelic attachments, only one kinetochore is attached to microtubules emanating from one spindle pole, while syntelic attachments refer to the attachment of both sister kinetochores to spindle microtubules emanating from the same spindle pole. Lagging chromosomes arise from merotelic attachments, which describes the attachment of sister kinetochores to spindle microtubules emanating from the opposing spindle poles, whereby one kinetochore is also attached to microtubules from both spindle poles. **(b)** Merotelic attachments lead to the generation of lagging chromosomes during anaphase. The chromatid is randomly segregated onto the daughter cells.

During progression through mitosis, erroneous attachments can be corrected. Monotelic attachments will be sensed by the SAC (Rieder *et al.* 1995), whereas syntelic attachments generate low tension between sister kinetochores (Pinsky & Biggins 2005; Nezi & Musacchio 2009). Like syntelic attachments, merotelic attachments can be resolved by an error correction machinery involving the Aurora B kinase (Cimini *et al.* 2003; Knowlton *et al.* 2006; Holland *et al.* 2009). Aurora B is localized to the inner centromere and phosphorylates outer kinetochore components like Ndc80 (Cheeseman *et al.* 2006; DeLuca *et al.* 2006), Dam1 (Cheeseman *et al.* 2002), Ska1 (Chan *et al.* 2012; Schmidt *et al.* 2012) and MCAK (Gorbsky 2004), thereby destabilizing kinetochore-microtubule attachments. However, increased rates of the generation of erroneous microtubule-kinetochore attachments might overload the error correction machinery leading to the persistence of lagging chromosomes.

Increased microtubule plus-end assembly rates constitute a novel route to chromosomal instability, recently described by our lab (Ertych *et al.* 2014). MIN/MSI and CIN cell lines were analyzed regarding their microtubule plus-end assembly rates during mitosis. These analyses revealed elevated rates in all analyzed CIN cell lines. It is assumed, that increased

microtubule plus-end assembly rates lead to transient spindle geometry defects, which result in hyper-stable kinetochore-microtubule attachments, the occurrence of lagging chromosomes and CIN. In turn, restoration of proper microtubule assembly rates by genetic means or chemicals suppresses the CIN phenotype. *Vice versa*, an increase of microtubule plus-end assembly rates by genetic means also induced CIN and aneuploidy (Ertych *et al.* 2014).

Furthermore also abnormalities in interphase might contribute to whole CIN. In fact, replication stress during S-phase was shown to affect chromosome segregation but this observation is still debated (Bakhoum *et al.* 2014).

1.8 The Ras Homologous (Rho) Family Of Small GTPases

Small GTPases of the Rho family are intracellular signaling molecules, best known for their role in regulating the actin cytoskeleton, in vesicle trafficking, cell cycle regulation and transcriptional reprogramming (Cain & Ridley 2009).

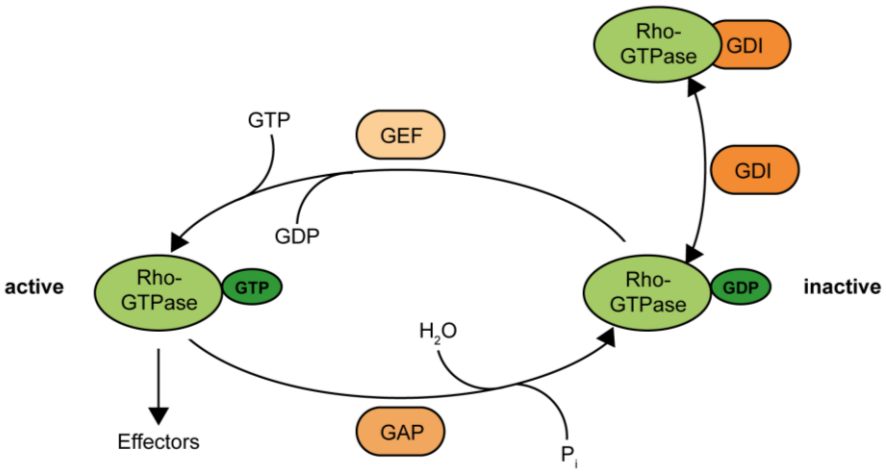

Fig. 1.6: Regulation of small GTPases of the Rho family. Inactive Rho-GTPases are activated by the exchange of GDP for GTP mediated by GEFs. GAPs inactivate Rho-GTPases by catalyzing the hydrolysis of GTP to GDP. GDIs bind inactive Rho-GTPases in the cytosol and prevent the nucleotide exchange. Modified from Lawson & Burridge 2014

Rho GTPases exist in either an inactive GDP-bound form or in an active GTP-bound form (Fife *et al.* 2014). Three different classes of regulatory molecules modulate the activity of the Rho-family small GTPases: guanine nucleotide exchange factors (GEFs), GTPase-activating Proteins (GAPs) and guanine nucleotide dissociation inhibitors (GDIs) (Lawson & Burridge 2014). While GEFs catalyze the exchange of bound GDP for GTP, GAPs stimulate the intrinsic GTPase activity, turning the Rho-family proteins into an inactive state. GDIs maintain

a cytosolic pool of inactive Rho-family small GTPases. If required, they can be transported to cell membranes, where the nucleotide exchange takes place (Leung *et al.* 1995; Zheng 2001; Rossman *et al.* 2005; Bos *et al.* 2007) (Fig. 1.6).

Among Rho GTPases, the best-studied members are RhoA, Rac1 and Cdc42 and their role during cell motility (Burridge & Wennerberg 2004). For a long time, RhoA was thought to be inhibitory for cell migration, since it promotes stress fiber formation and strong adherence mediated by focal adhesions (Lawson & Burridge 2014). But RhoA was also found to be active at the leading edge of migrating cells, where it is responsible for membrane ruffling and the formation of lamellipodia (O'Connor *et al.* 2000; Machacek *et al.* 2009; El-sibai *et al.* 2009). The switch between stress fiber formation and lamellipodia formation is not well understood but might be mediated by two different GEFs, whereby one potentially activates Rho at the leading edge and the other one at the rear of the cell (Sadok & Marshall 2014). The two homologs RhoA and RhoC were described to have different roles in cell migration since they act through different targets (Vega *et al.* 2011). While RhoC inhibits the development of lamellipodia through the formin FMNL3, RhoA promotes tail retraction *via* its effectors mDia (mammalian homolog of *Drosophila* diaphanous) and ROCK (Rho-associated kinase) (Narumiya *et al.* 2009; Vega *et al.* 2011). Both are well described regarding their roles in stress fiber formation. The activation of mDia and ROCK constitutes the trigger for the assembly of actomyosin filaments (Hall 2012). Here, ROCK phosphorylates and inactivates the myosin phosphatase and activates myosin light chain, resulting in an enhancement of actomyosin contractility (Kimura *et al.* 1996). Subsequently, contraction leads to bundling of actin filaments and clustering of integrins into focal adhesions (Narumiya *et al.* 2009). Actin polymerization itself is then stimulated by mDia.

During cell motility, RhoA acts in concert with Rac1 and Cdc42 (El-sibai *et al.* 2009; O'Connor *et al.* 2012). In contrast to RhoA, Rac1 and Cdc42 promote Arp2/3-based actin polymerization and branching in the lamellipodium by activating the WAVE or WASP protein complexes (Bid *et al.* 2013; Blanchoin *et al.* 2014). Effectors of Rac1 and Cdc42 are, among others, p21-activated kinase (PAK), WAVE/WASP, IQGAP1 (IQ motif containing GTPase activating protein 1) and IQGAP2 (IQ motif containing GTPase activating protein 2) (Kuroda *et al.* 1999). Rac1 activates the p21-activated kinases PAK1, PAK2 and PAK3, which themselves activate the actin-binding LIM kinases LIMK1 and LIMK2. These in turn phosphorylate the actin binding protein cofilin, thereby inactivating its activity of converting F-actin into G-actin and allowing actin growth (Ridley 2006; Bid *et al.* 2013). Rac1 and Cdc42 were also described to recruit mDia to RhoA, thus facilitating its activity during lamellae formation (Kurokawa & Matsuda 2005).

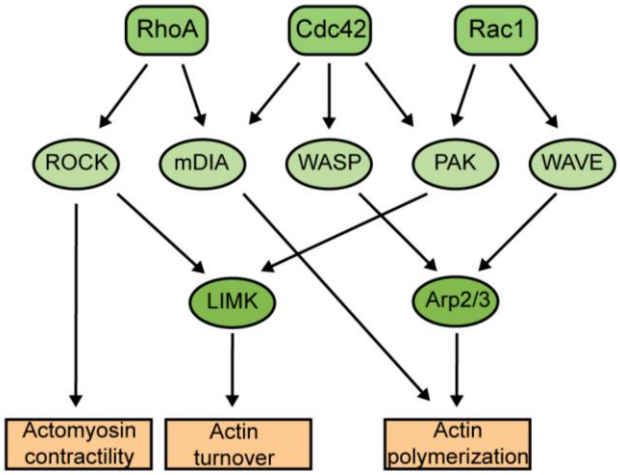

Abb 1.7: Rho-family of small GTPases regulating actin remodeling. RhoA promotes actomyosin contractility *via* ROCK. ROCK itself phosphorylates LIMK, thereby leading to inhibition of cofilin. RhoA also affects mDIA, which in turn promotes actin polymerization. Rac1 antagonizes RhoA´s function. It activates PAK and WAVE. WAVE-dependent activation of Arp2/3 leads to actin polymerization, whereas PAK-mediated activation of LIMK results in actin turnover. Cdc42 activates Arp2/3 *via* WASP resulting in actin polymerization. Adapted from Sadok & Marshall 2014.

Altered expression or dysregulated activity of the Rho-family of small GTPases is frequently associated with tumorigenesis and the development of different cancer types including colorectal cancer (Mack *et al.* 2011). While no mutations for Rho GTPases have been described so far, the Rac1-specific GEF TIAM 1 (T-lymphoma invasion and metastasis-inducing protein-1) and the RhoA-specific GEF RGNEF (p190RhoGEF) were shown to be up-regulated in colorectal cancer (Leve & Morgado-Díaz 2012). *TIAM 1* was identified as an invasion and metastasis gene and shown to be required for the initiation of colon cancer growth (Cook *et al.* 2013). In addition to invasion and metastasis, a mitotic role was also suggested for TIAM 1, since it was found to localize to mitotic centrosomes antagonizing the function of Eg5 in centrosome separation during prophase (Whalley *et al.* 2015). In axons, TIAM 1 was shown to localize to microtubules *via* MAP1B (Montenegro-Venegas *et al.* 2010). TRIO constitutes another Rac1-GEF with possible functions in mitosis. TRIO was identified as a microtubule plus-end binding protein in neurons (Van Haren *et al.* 2014). In these cells, binding is achieved *via* EB1/Nav1 complexes and requires dynamic microtubules. High expression of *TRIO* is found in different tumor types, including breast and lung cancer and glioblastoma and is associated with poor patient prognosis (Schmidt & Debant 2014).

A variety of tumor cells exhibit a deregulated expression or activity of Rho GTPases (Boettner & Van Aelst 2002). Especially Rac1 hyperactivation is associated with aggressive tumor growth (Bid *et al.* 2013). Aggressive tumor growth is accompanied by a high migration and invasion potential. These processes require the formation of certain cell surface extensions like lamellipodia or invadopodia, which emerge from Rac1-mediated

reorganization of the actin cytoskeleton (Parri & Chiarugi 2010). Therefore, Rac1 or other members of the Rac1 pathway would represent interesting therapeutic targets for anti-cancer therapy (Bid *et al.* 2013).

1.9 Cellular Migration

The activation of invasion and metastasis represents a hallmark of cancer (Hanahan & Weinberg 2011). Upon a migration promoting stimulus the cell starts to polarize and forms protrusions into the direction of migration. Thereby, the formation of protrusions is mainly driven by actin polymerization, whereas the establishment and maintenance of cell polarity is mediated by different factors like Rho-family GTPases, phosphoinositide 3-kinases (PI3Ks), vesicular transport and also microtubules (Ridley *et al.* 2003). Cell migration and invasion can be exemplified by a five step model (Lauffenburger & Horwitz 1996; Friedl & Wolf 2003): 1. Pseudopod protrusion at the leading edge, 2. Formation of a focal contact, 3. Focalized proteolysis, 4. Actomyosin contraction, 5. Detachment of the trailing edge (Fig. 1.8).
Cells can respond to very small differences of chemoattractant concentrations occurring between their front and rear. The signaling molecules PtdInst(3,4,5)P_3 (PIP_3) and PtdInst(3,4)P_2 (PIP_2) rapidly polarize along this gradient, whereby PIP_3 is located at the front and PIP_2 at the rear and the sites of the cell. This leads to the accumulation and activation of PI3Ks and PTEN (Phosphatase and Tensin). PTEN is responsible for the cleavage of the 3´ phosphate from PIP_3 to generate PIP_2. Thereby PTEN antagonizes the function of PI3K (Yamada & Araki 2001). PI3K accumulates at the leading edge of a cell, whereas PTEN localization is confined to the cell´s rear and sides. PIP_3 and PIP_2 have downstream effects on Rac1 and Cdc42 (Yamada & Araki 2001). Several Rac1-GEFs are activated by PI3K products. Active Rac1 can then regulate itself *via* different positive feedback loops. On the one hand, active Rac1 is able to recruit and activate PI3Ks at the plasma membrane. On the other hand, microtubule polymerization activates Rac1 whereupon Rac1 stabilizes microtubules (Waterman-Storer *et al.* 1999). Both, Cdc42 and Rac1 stimulate actin polymerization by activating the Arp2/3 complex *via* the WASP or WAVE complex, leading to the nucleation of a highly branched actin network (Rohatgi *et al.* 1999; Lawson & Burridge 2014), thereby inducing pseudopod extension (Nobes & Hall 1995). The growing actin filaments bind to a complex consisting of α-actinin, vinculin and paxillin within the cell membrane (Calderwood *et al.* 2000). Continuous actin assembly pushes the cell membrane outwards. The growing cell protrusion touches the ECM and transmembrane receptors of the integrin family initiate binding to it. Actin filaments are coupled to integrins, which are accumulated and clustered at these sides and form a focal contact. These contacts are highly dynamic and can therefore stably adhere to or slowly glide along the substratum.

Upon binding of integrins, surface proteases like MMP1 (matrix metalloproteinase 1) are recruited, which degrade ECM components like collagen, fibronectin and laminins (Ohuchi *et al.* 1997). During invasion, ECM degradation is an important process since it provides space for cell expansion and movement

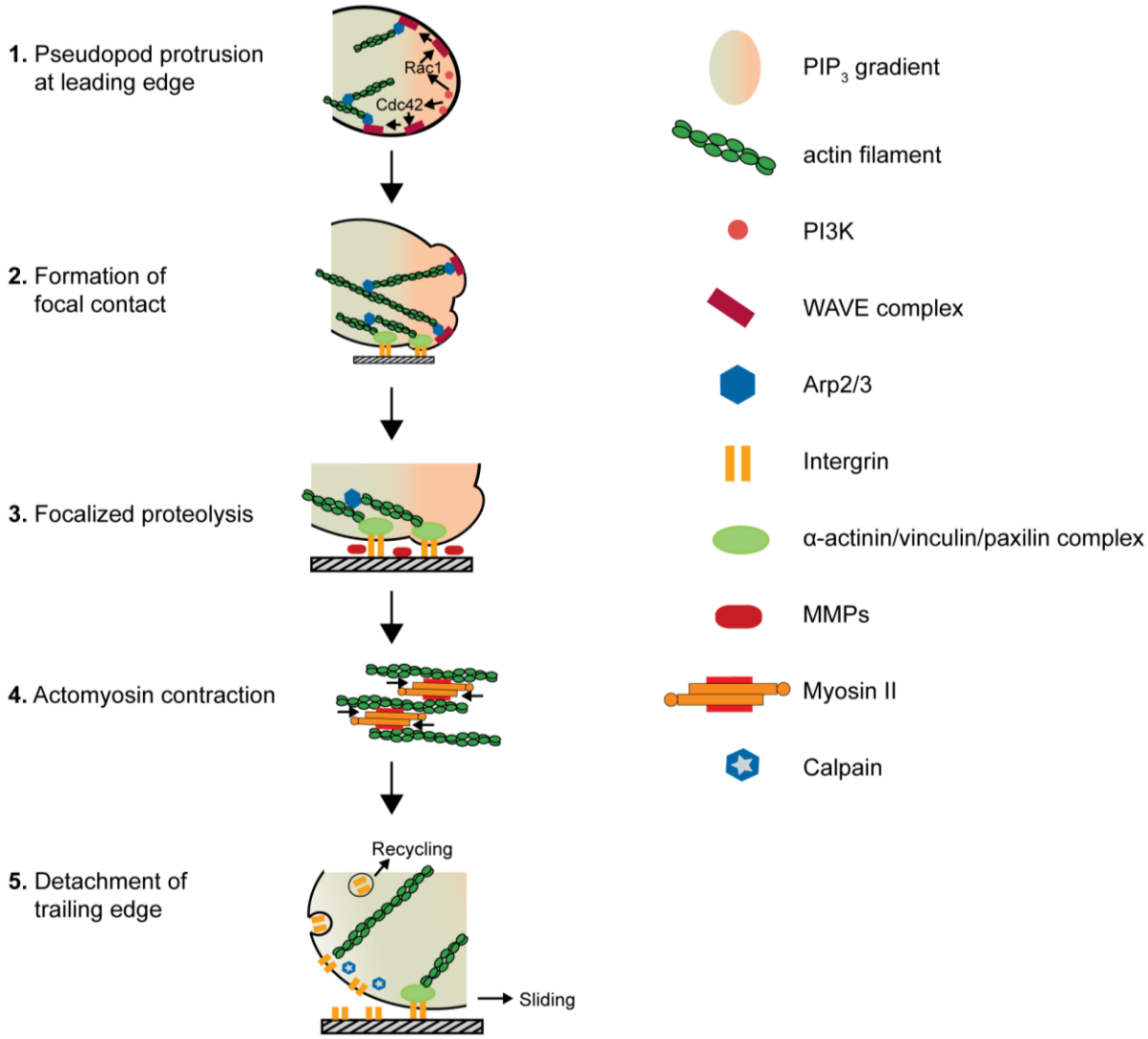

Figure 1.8: Model of cell migration. Migration can be divided into five steps: At first, the leading edge protrudes due to Arp2/3 mediated actin assembly. Second, a focal contact is formed *via* clustered integrins, whereupon surface proteases cleave ECM components during focalized proteolysis. The fourth step involves cell contraction by actomyosin, followed by the detachment of the trailing edge, which is mainly driven by focal contact disassembly. Modified from Friedl & Wolf 2013

After the initial phase of adhesion, Rac1 activity in the lamellipodium diminishes whereas RhoA activity in the rear increases. RhoA promotes the formation of stress fibers and mediates the maturation of focal adhesions by activating myosin *via* Rho kinase (ROCK) (O'Connor & Chen 2013; Lawson & Burridge 2014). ROCK inactivates the myosin phosphatase by phosphorylating its myosin-binding subunit. Contraction of actin-bound

myosin II, leads to bundling of actin fibers (O'Connor & Chen 2013). Actin fibers are crosslinked by α-actinin, thereby forming highly regulated actomyosin. Contraction of the actomyosin leads to shortening of the cell resulting in an inward tension towards the focal contacts (Chew *et al.* 2002). Cell-substrate-linkages are then resolved preferentially at the rear of the cell. Here, the cytoplasmic protease calpain cleaves focal contact components (Potter *et al.* 1997). In contrast, the leading edge stays attached and further elongates (Friedl & Wolf 2003). After disassembly of the focal contact, the cell glides forward and detached integrins become recycled at the leading edge (Bretscher 1996).

1.10 Microtubules In Cell Migration

Microtubules are well described for their role in mitotic spindle assembly, but they are not only important during cell division, but also required to establish cell polarity during cell motility (Bershadsky *et al.* 1991). Already in 1970, the inhibitory effect of spindle poisons onto fibroblasts and their locomotory behavior was reported (Vasiliev *et al.* 1970). However not only a full depolymerization of microtubules but also abolished microtubule dynamics was detected to alter cell motility (Liao *et al.* 1995). Nowadays, it is well established, that microtubule dynamics polarize a motile cell in an asymmetric fashion. The main characteristic of the polarized microtubule cytoskeleton is its alignment with the cell migration axis (Etienne-Manneville 2013). Microtubules predominantly grow towards the leading edge and only few of them reach the cell´s rear (Etienne-Manneville 2013). Furthermore, polarization is achieved by microtubule stabilization in the leading edge and microtubule destabilization at the trailing edge (Kaverina & Straube 2011). At the front of a cell, microtubules are captured and stabilized at cortical sides by several +TIPs including CLASP1 and CLASP2 (Mimori-Kiyosue *et al.* 2005), CLIP-170 (Fukata *et al.* 2002) and EB3 (Straube & Merdes 2007). Furthermore, leading edge microtubules are also target of Rho-GTPase regulation (Wittmann *et al.* 2003). On the one hand microtubules activate Rac1, thereby promoting lamellipodia formation, through delivering GEFs such as TIAM 1, TIAM 2 or TRIO (Waterman-Storer *et al.* 1999; Blangy *et al.* 2000; Rooney *et al.* 2010). But in a positive feedback loop, this enhanced activity of Rac1 further selectively promotes persistent growth of leading edge microtubules (Wittmann *et al.* 2003). Thereby, activation of Rac1 results in PAK1-mediated phosphorylation of the microtubule destabilizing protein Stathmin/Op18 (Daub *et al.* 2001). Due to this inactivation, catastrophe events are diminished and microtubule growth is promoted (Larsson *et al.* 1997).

At the rear of a cell, catastrophes are observed especially at focal adhesion sides (Bershadsky *et al.* 1996; Salaycik *et al.* 2005; Efimov *et al.* 2008). In fibroblasts, dynamic microtubules target mature focal adhesions. Due to their dynamic instability, microtubules

can repeatedly contact a focal adhesion, resulting in its disassembly (Kaverina *et al.* 1998; Krylyshkina *et al.* 2003). Furthermore, depolymerizing microtubules at the trailing edge result in the activation of RhoA *via* its GEF GEF-H1 (Ren *et al.* 1999; Waterman-Storer *et al.* 1999), leading to the formation of stress fibers and increased contractility (Bershadsky *et al.* 1996). Thus, microtubules transduce signals to the cell migration machinery depending on their dynamic behavior (Kaverina & Straube 2011): GEFs binding to microtubules can either be sequestered and inactivated by growing microtubules or released and activated by catastrophe events (Nalbant *et al.* 2010; Chang *et al.* 2007).

Hence, changes in microtubule dynamics implies alterations of cell migration (Kaverina & Straube 2011). Microtubule associated proteins (MAPs) regulate the dynamic behavior of microtubules. EB1 and APC stabilize microtubules at the leading edge in a RhoA-mDia-mediated fashion (Wen *et al.* 2004). EB1 and EB3 were described to suppress catastrophes but they promote persistent microtubule growth (Komarova *et al.* 2009). EB1 was also shown to increase membrane protrusion and cell migration in melanoma cells (Schober *et al.* 2009). In these cells, depletion of EB1 resulted in a loss of polarized cell morphology. Furthermore, APC accumulates at leading edge microtubules, promotes their growth and diminishes shrinkage, thus exerting a stabilizing function (Kita *et al.* 2006). Interestingly, microtubules in the leading edge are often post-translationally modified by acetylations or detyrosination (Gundersen & Bulinski 1988), resulting in increased stability (Tran *et al.* 2007) and a potentially increased recruitment of MAPs (Etienne-Manneville 2013).

Additionally, microtubules serve as tracks for directed membrane and organelle transport, thereby providing building material for protrusion formation (Nabi 1999) as well as molecular motors for focal adhesion turnover (Krylyshkina *et al.* 2002), which is mediated by integrin recycling (Pellinen & Ivaska 2006). Furthermore, endosomes carry membrane-associated molecules such as Rac1 and Cdc42, that are delivered to the plasma membrane (Palamidessi *et al.* 2008; Osmani *et al.* 2010). The traffic is facilitated by the existence of long microtubule tracks between the cell center and the periphery (Komarova *et al.* 2009).

In cancer, the microtubule-dependent control of cell migration is often impaired (Kaverina & Straube 2011).

1.11 Cell Invasion

The motility of a cell is often studied in 2D, where a cell migrates on a substratum towards a chemoattractant forming filopodia and lamellipodia. In contrast, invasion is the process of moving into or within a 3D matrix (Fife *et al.* 2014), which can arise from an aberrant regulation of cell migration (Sahai 2005; Yamaguchi *et al.* 2005). The invasion process occurs during cell morphogenesis, wound healing and in malignant cells allowing the

metastatic growth into distant organs (Friedl & Wolf 2003). Therefore, tumor cells need to detach from the primary tumor, invade the surrounding tissue, intravasate the blood or lymphatic vessels, extravasate into distant organs and grow to form secondary tumors (Hofmann *et al.* 2000). For these processes, specialized structures like invadopodia and podosomes and the proteolysis of the extracellular matrix (ECM) are required (Friedl & Wolf 2003). Podosomes are sides of contact to the substratum similar to focal adhesions, but they differ in some criteria. In contrast to focal adhesions, podosomes contain actin organizing structures like the Arp2/3 complex, N-WASP and fimbrin, which is an actin bundling protein (Buccione *et al.* 2004). Furthermore, they are more dynamic and form from pre-existing podosomes and therefore do not require ongoing protein synthesis (Buccione *et al.* 2004). Podosomes continuously probe the substratum and invadopodia are formed by their extension (Buccione *et al.* 2004). Invadopodia are membrane protrusions with ECM degradation activity (Buccione *et al.* 2004) and their formation is dependent on Arp2/3 activity. The knock down of Arp2/3 was shown suppress the development of these membrane protrusions (Yamaguchi *et al.* 2005). In malignant cells, an excessive cell protrusive activity was found, which is mainly driven by aberrant signaling regarding the activation of actin rearrangements (Wang *et al.* 2004). This signature of invasion involved deregulated genes in mammary tumors further includes *LIMK1* (LIM-kinase 1), *CFL1* (cofilin) and *ACTN3* (actinin) (Wang *et al.* 2004).

The degradation and remodeling of the ECM requires matrix-metalloproteinases (MMPs) (Coussens & Werb 1996; Chambers & Matrisian 1997). Several MMPs interact with surface receptors like integrins or are located to the ECM (Kessenbrock *et al.* 2010). The up-regulation of MMPs is often found in human cancers including breast cancer and melanoma (Rudolph-Owen *et al.* 1998; Hofmann *et al.* 2000). Interestingly, in breast cancer, the activation of MMPs was implicated in tumor progression and promotion of EMT (Radisky & Radisky 2010). The direct activation of the EMT program is mediated by MMP-3 stimulated expression of a constitutively active Rac1 splice variant (Rac1b), which increases reactive oxygen species in the cell, resulting in expression of SNAIL and induction of EMT (Radisky *et al.* 2005). Furthermore, MMP-3 is able to cleave E-cadherin, resulting in a bioactive E-cadherin fragment, which is capable of stimulating cancer cell motility (Lochter *et al.* 1997; Noë *et al.* 2001).

1.12 Epithelial-Mesenchymal-Transition (EMT)

Cancer cells invade into tissues by moving as single epithelial or amoeboid cells or as clusters. Thereby, the process of invasion accompanies morphological and phenotypical changes (Van Zijl *et al.* 2011).

The epithelial-mesenchymal-transition (EMT) is a conserved mechanism occurring during embryogenesis, chronic inflammation and fibrosis, but it is also a common process during cancer progression and the development of metastasis (Van Zijl *et al.* 2011). A hallmark of EMT is the loss of epithelial characteristics. Instead, the cell gains mesenchymal features (Spaderna *et al.* 2006). As a result, cells destabilize cell-cell-contacts due to the downregulation of *CDH1*, encoding for epithelial E-cadherin (Thiery & Sleeman 2006). E-cadherin exhibits an extracellular domain, which enables binding to E-cadherins of a neighboring cell. Downregulation of *CDH1* is mediated by the transcriptional repressors Snail/SNAI1, Slug/SNAI2, SIP1/ZEB2 or Twist. The disassembly of adherence junctions leads to the translocation of membrane bound β-catenin into the nucleus. There, it affects the transcription of genes like c-myc or cyclin D (Van Zijl *et al.* 2011). Subsequently, mesenchymal markers are upregulated. Among them, N-cadherin is responsible for the formation of Rho-induced stress fibers and activation of Rac1 and Cdc42, leading to the development of filopodia and lamellipodia. Cells, that have undergone EMT, are also able to regain epithelial properties. The mesenchymal-epithelial-transition (MET) leads to epithelial reorganization resulting in the ability for colonization at secondary sites, which is an important process during metastasis (Van Zijl *et al.* 2011). Thus, EMT can contribute or even be a prerequisite for cancer cell migration and invasion.

Scope Of The Study

Chromosomal instability is a hallmark of most solid tumors (Orr & Compton 2013) and has been associated with tumorigenesis and the development of therapy resistance (Bakhoum & Compton 2012). CIN enables the development of genetic heterogeneity and thus the emergence of novel phenotypes in cancer cells. Among them, cell migration and invasion are major characteristics that are acquired during the development of aggressive metastatic human tumors (Hanahan & Weinberg 2000). Both, CIN and cancer cell invasion are associated with tumor stage and poor patient prognosis. Although both phenotypes often appear concomitantly in late tumor stages, little is known about a possible shared link between CIN and cancer cell migration and invasion. Thus, the aim of this study was to investigate a potential shared mechanistic link between the development of CIN and a highly migratory and invasive phenotype.

2 Material and Methods

2.1 Material

The used working materials including cell culture dishes, pipette tips, disposable syringes and reaction tubes were purchased from Sarstedt (Nümbrecht, Germany), Greiner BioOne (Frickenhausen, Germany), Eppendorf (Hamburg, Germany) and Ibidi (Martinsried, Germany).

2.1.1 Equipment

Table 2.1 lists the equipment, which was used for the implementation of this study.

Table 2.1: Equipment

Equipment	Model	Company
CO_2 Incubator	HERAcell 240 CO_2 Incubator	Thermo Fisher Scientific, Karlsruhe, Germany
Cooling Centrifuge	Multifuge X3R	Thermo Fisher Scientific, Karlsruhe, Germany
Electroporation Device	GenePulser Xcell©	BioRad Laboratories, München, Germany
Electrophoresis Power Supply	Power Supply EV231	Peqlab, Erlangen, Germany
Flow Cytometer	BD FACSCanto© II	Becton Dickinson, San Jose, CA, USA
Gel Documentation	Gel iX Imager	Intas, Göttingen, Germany
Heating Block	Thermomixer Comfort R	Eppendorf, Hamburg, Germany
	TDB-120 Dry Block Thermostat	Biosan, Riga, Latvia
Horizontal Gel Electrophoresis System	Sub-Cell GT cell	BioRad Laboratories, München, Germany
Laboratory Scale	Sartorius Research R200D	Sartorius, Göttingen, Germany
Magnetic Mixer	IKAMAG© RCT	IKA Labortechnik, Stauffen, Germany
Medical X-Ray Film	Fuji Super RX	Christiansen und Linhardt, Planegg, Germany

Equipment	Model	Company
Microscope	Delta Vision Elite©	Applied Precision, Chalfont St. Giles, UK
	Leica DMI6000B	Leica, Wetzlar, Germany
	Zeiss Axio Imager Z1	Zeiss, Göttingen, Germany
Microscope Camera	sCMOS camera	GE Healthcare, Chalfront St. Giles, UK
	Leica DFC369 FX	Leica, Wetzlar, Germany
	Hamamatsu 1394 ORCA-II ER	Hamamatsu Photonics, Hamamatsu, Japan
Microscope Camera Adaptor	A3474-07	Hamamatsu Photonics, Hamamatsu, Japan
Multilabel Reader	Victor© X3	PerkinElmer, Rodgau, Germany
Nitrocellulose Membrane	Protran BA 83	GE Healthcare, Chalfront St. Giles, Great Britain
Pipettes	Pipetman©	Gilson International, LimburgOffheim, Germany
Pipettor	Pipetboy acu	Integra Biosciences, Fernwald, Germany
PVDF Membrane	ImmobilionR-P	Merck Millipore, Darmstadt, Germany
Semidry Western Blotting Device	Perfect Blue©	Peqlab, Erlangen, Germany
Sterile Workbench	HERAsafeM	Thermo Fisher Scientific, Karlsruhe, Germany
Spectrophotometer	NanoDrop 2000	Thermo Fisher Scientific, Karlsruhe, Germany
Tabletop Centrifuge	Biofuge pico	Thermo Fisher Scientific, Karlsruhe, Germany
Tabletop Centrifuge, cooling	Biofuge fresco	Thermo Fisher Scientific, Karlsruhe, Germany
Vertical Electrophoresis System		Own Manufacturing
Vortex Mixer	VORTEX-GENIE© 2	Scientific Industries inc., Bohemia, NY, USA
X-Ray film processor	Optimax	Protec, Oberstenfeld, Germany

2.1.2 Software

The following table lists the software, which was used for data analyses.

Table 2.2: Software

Software	Company
Hokawo Launcher	Hamamatsu Photonics, Hamamatsu, Japan
ImageJ	NIH Image, Bethesda, MD, USA
Leica Application Suite	Leica, Wetzlar, Germany
Soft Worx© 5.0	Applied Precision Inc., Issaquah, WA, USA

2.1.3 Chemicals

All used chemicals were purchased from Carl Roth (Karlsruhe, Germany), Sigma-Aldrich (Taufkirchen, Germany), VWR International (West Chester, PA, USA), BD Biosciences (Heidelberg, Germany), Fermentas (St. Leon-Roth, Germany), Promega (Madison, WI, USA), Merck Millipore (Darmstadt, Germany), Roche Diagnostics (Mannheim, Germany), Thermo Fisher Scientific (Waltham, MA, USA), Th. Geyer (Renningen, Germany), Enzo Life Sciences (New York, NY, USA) AppliChem (Darmstadt, Germany), Amersham Biosciences (Buckinghamshire, Great Britain).

Table 2.3 lists chemicals and inhibitors used in this study and their respective working concentration.

Table 2.3: Chemicals

Chemical	Used concentration	Effect	Company
Adriamycin	600 nM	Intercalates into DNA and stabilizes topoisomerase II	Th. Geyer, Höxter, Germany
CK666	20 µM	Inhibition of actin assembly by the Arp2/3 complex	Merck Millipore, Darmstadt, Germany
Dimethylenastron	2 µM	Inhibition of EG5-kinesin	Calbiochem, La Jolla, CA, USA
Doxycycline	200 ng/ml	Induction of gene expression	Sigma-Aldrich Taufkirchen, Germany
ITX3	15 µM	Inhibition of GEF-activity of TRIO	Merck Millipore, Darmstadt, Germany

Chemical	Used concentration	Effect	Company
Nocodazol	2-300 nM	Depolymerization of microtubules	Sigma-Aldrich Taufkirchen, Germany
NSC23766	40 µM	Inhibition of Rac1	Santa Cruz, Dallas, TX, USA
Ponasterone A	5 µmol/l	Induction of gene expression	Sigma-Aldrich Taufkirchen, Germany
Puromycin	1 µg/ml	Inhibition of translation	Sigma-Aldrich Taufkirchen, Germany
Taxol	0.2-150 nM	Stabilization of microtubules	Sigma-Aldrich Taufkirchen, Germany
TGF-β (human, recombinant)	10 ng/ml	Stimulation of TGF-β signaling	PeproTech, Hamburg, Germany
Thymidine	2 mM	Inhibition of nucleotide synthesis	Sigma-Aldrich Taufkirchen, Germany

2.1.4 Antibodies

Primary Antibodies

Primary antibodies, including their host species, antibody type and the used dilutions are listed in Table 2.4.

Table 2.4: Primary Antibodies

Antigen	Host Species	Antibody Type	Used Dilution	Company
α-Tubulin (B-5-1-2)	mouse	monoclonal	IF 1:700	Santa Cruz, Dallas, TX, USA
β-Actin (A5441)	mouse	monoclonal	WB 1:5000	Sigma-Aldrich, Taufkirchen, Germany
ch-TOG (H-4)	mouse	monoclonal	WB 1:750	Santa Cruz, Dallas, TX, USA
EB1 (clone 5)	mouse	monoclonal	WB 1:500	BD Biosciences, Heidelberg, Germany
E-Cadherin (clone 36)	Mouse	Monoclonal	WB 1:1000	BD Biosciences, Heidelberg, Germany
ɣ-Tubulin (T3559)	rabbit	polyclonal	IF 1:700	Sigma-Aldrich, Taufkirchen, Germany
ɣ-Tubulin (T6557)	mouse	monoclonal	WB 1:2000	Sigma-Aldrich, Taufkirchen, Germany
Human Nuclear ANA-Centromere (CREST)	human	polyclonal	IF 1:700	Europa Bioproducts, Wicken, Ely, UK

Antigen	Host Species	Antibody Type	Used Dilution	Company
MCAK	sheep	polyclonal	WB 1:250	Kindly provided by Prof. Linda Wordemann (Seattle, WA, USA)
Mep21	mouse	polyclonal	IHC 1:500	Kindly provided by Prof. Jörg Wilting (Göttingen, Germany)
p21 (Ab-1)	mouse	monoclonal	WB 1:1000	Oncogene, Cambridge, MA, USA
p53 (Ab-6)	mouse	monoclonal	WB 1:800	Oncogene, Cambridge, MA, USA
p73 (EP436y)	rabbit	monoclonal	WB 1:1000	GeneTex, Irvine, CA, USA
Rac1 (Arc03)	mouse	monoclonal	WB 1:500	Cytoskeleton Inc., Denver, CO, USA
TRIO (D-20)	goat	Polyclonal	WB 1:300	Santa Cruz, Dallas, TX, USA

Secondary Antibodies

Table 2.5 lists the used secondary antibodies including the host species, antibody type, the conjugated molecule and the used concentration.

Table 2.5: Secondary Antibodies

Antigen	Species	Antibody Type	Conjugate	Used Dilution	Company
Anti-Human	goat	polyclonal	Alexa-Fluor594	IF 1:1000	Invitrogen, Carlsbad, CA, USA
Anti-Mouse	goat	polyclonal	Alexa-Fluor488	IF 1:1000	Invitrogen, Carlsbad, CA, USA
Anti-Rabbit	goat	polyclonal	Alexa-Fluor594	IF 1:1000	Invitrogen, Carlsbad, CA, USA
Anti-Goat	mouse	polyclonal	Horseradish Peroxidase (HRP)	WB 1:10000	Dianova, Hamburg, Germany
Anti-Mouse	goat	polyclonal	Horseradish Peroxidase (HRP)	WB 1:10000	Dianova, Hamburg, Germany
Anti-Rabbit	goat	polyclonal	Horseradish Peroxidase (HRP)	WB 1:10000	Dianova, Hamburg, Germany
Anti-Sheep	goat	polyclonal	Horseradish Peroxidase (HRP)	WB 1:10000	Dianova, Hamburg, Germany

2.1.5 Chromosome Enumeration Probes

The used chromosome enumeration probes including the chromosome region of their hybridisation are listed in Table 2.6.

Table 2.6: Chromosome Enumeration Probes

Chromosome	Chromosome Region	Company
6	6p11.1-q11.1	Cytocell aquarius, Cambridge, UK
7	7p11.1-q11.1	Cytocell aquarius, Cambridge, UK
15	15p11.1-q11.1	Cytocell aquarius, Cambridge, UK
18	18p11.1-q11.1	Cytocell aquarius, Cambridge, UK

2.1.6 Oligonucleotides

The oligonucleotids used in this study were synthesized by Sigma-Aldrich (Taufkirchen, Germany) and stored at -20°C.

qRT-PCR Primer

The qRT-PCR primer used for this study and their respective sequence are listed in Table 2.7.

Table 2.7: qRT-PCR Primer

Gene	Primer		Reference
36B4	forward	5´-GATTGGCTACCCAACTGTTG-3´	Kindly provided by Matthias Dobbelstein (Göttingen, Germany)
	reverse	5´-CAGGGGCAGCAGCCACAAA-3´	
CDKN1A	forward	5´-TAGGCGGTTGAATGAGAGG-3	Kindly provided by Matthias Dobbelstein (Göttingen, Germany)
	reverse	5´-AAGTGGGGAGGAGGAAGTAG-3	

siRNA

Table 2.8 lists the used siRNAs, their sequence and the corresponding reference.

Table 2.8: siRNAs

Target Gene	Sequence	Reference
CDKN1A	5´-AAUCCCAGCUACUUGGAAGGC-3´	Zhang *et al.* 2005
CKAP5	5´-GAGCCCAGAGTGGTCCAAA-3´	De Luca *et al.* 2008
EB1	5´-AUUCCAAGCUAAGCUAGAA-3´	Watson & Stephens 2006
LUCIFERASE	5´-CUUACGCUGAGUACUUCGAUU-3´	Elbashir *et al.* 2001
RB	5´-AAGUUUCAUCUGUGGAUGGAG-3´	Guo *et al.* 2011
TP53	5´-GUAAUCUACUGGGACGGAA-3´	Ertych *et al.* 2014
	5´-GACUCCAGUGGUAAUCUAC-3´	Brummelkamp *et al.* 2002
TP73	5´-CAGGUGACCGACGUCGUGAAA-3´	Qiagen, Hilden, Germany
	5´-CUCGGGAGGGACUUCAACGAA-3´	
	5´-CCCGGGAUGCUCAACAACCAU-3´	
	5´-CCCGCUCUUGAAGAAACUCUA-3´	
TRIO	5´-GAUAAGAGGUACAGAGAUU-3´	Cannet *et al.* 2014
	5´-GGAAGUCGCUCCUUGACAA-3´	

2.1.7 Plasmids

The used plasmids including their purpose and reference are listed in Table 2.9.

Table 2.9: Plasmids

Vector	Purpose	Reference
pcDNA3.1	CMV-promotor driven expression vector for human cells	Invitrogen, Carlsbad, CA, USA
pcDNA3.1-∆*Np73*	CMV-promotor driven expression of ∆*Np73* in human cells	Kindly provided by Prof. Matthias Dobbelstein (Göttingen, Germany)

Vector	Purpose	Reference
pcDNA3.1-*E1A*	CMV-promotor driven expression of *E1A* in human cells	Kindly provided by Prof. Matthias Dobbelstein (Göttingen, Germany)
pBabe-puro-HPV16-*E7*	CMV-promotor driven expression of *E7* in human cells	Kindly provided by Prof. Matthias Dobbelstein (Göttingen, Germany)
pcDNA3.1-*MCAK*	CMV-promotor driven expression of *MCAK* in human cells	Kindly provided by Prof. Linda Wordeman (Seattle, WA, USA)
pcDNA3.1-*CDKN1A*	CMV-promotor driven expression of *TP21* in human cells	Kindly provided by Prof. Matthias Dobbelstein (Göttingen, Germany)
pEGFP-C1	CMV-promotor driven expression vector for human cells	Clontech, Saint-Germain-en-Laye, France
pEGFP-*CKAP5*	CMV-promotor driven expression of GFP-tagged *CKAP5* in human cells	Kindly provided by Prof. Linda Wordeman (Seattle, WA, USA)
pEGFP-*EB3*	CMV-promotor driven expression of GFP-tagged *EB3* in human cells	Kindly provided by Prof. Linda Wordeman (Seattle, WA, USA)
pEGFP-*HMMR*	CMV-promotor driven expression of GFP-tagged *HMMR* in human cells	Kindly provided by Prof. Tony Reiman (Westmount, Canada)
pEGFP-mCherry-*EB3*	CMV-promotor driven expression of mCherry-tagged *EB3* in human cells	Kindly provided by Prof. Linda Wordeman (Seattle, WA, USA)
pEGFP-*Rac1* Q61L	CMV-promotor driven expression of GFP-tagged constitutively active Rac1 in human cells	Kindly provided by Prof. Robert Grosse (Marburg, Germany)
pEGFP-*Rac1* T17N	CMV-promotor driven expression of GFP-tagged dominant negative Rac1 in human cells	Kindly provided by Prof. Robert Grosse (Marburg, Germany)
pInducer	Doxycycline inducible expression vector for human cells	Kindly provided by Prof. Thorsten Stiewe (Marburg, Germany)
pInducer20-*TAp73α*	Doxycycline inducible expression of *TAp73α* in human cells	Kindly provided by Prof. Thorsten Stiewe (Marburg, Germany)
pLOK.1-sh-*TP73*	Expression of a *TP73* shRNA in human cells	Kindly provided by Prof. Matthias Dobbelstein (Göttingen, Germany)

Vector	Purpose	Reference
pRcCMV-p53-R175H-72R	CMV-promotor driven expression of p53 R175H in human cells	Kindly provided by Prof. Matthias Dobbelstein (Göttingen, Germany)

2.1.8 Human Cell Lines

Table 2.10 provides the used human cell lines, their origin and references.

Table 2.10: Human Cell Lines

Cell Line	Origin	Reference
HCT116	colon carcinoma	Brattain *et al.* 1981
SW48	colon carcinoma	Leibovitz *et al.* 1976
SW620	colon carcinoma	Leibovitz *et al.* 1976
SW480	colon carcinoma	Leibovitz *et al.* 1976
SW837	rectum carcinoma	Leibovitz *et al.* 1976
CaCo2	colon carcinoma	Heinen *et al.* 1995
HT29	colon carcinoma	Adachi *et al.* 1987
LS411N	colon carcinoma	Suardet *et al.* 1992
LS513	colon carcinoma	Suardet *et al.* 1992
Colo201	colon carcinoma	Semple *et al.* 1978
LoVo	colon carcinoma	Drewinko *et al.* 1976
HCT116-*TP53*$^{-/-}$	colon carcinoma	Langermann 1998
HCT116-*TP73* shRNA	colon carcinoma	kindly provided by Dr. Daniela Kramer (Göttingen, Germany)
RKO	colon carcinoma	Brattain *et al.* 1984
RKO *CDKN1A* inducible	colon carcinoma	Schmidt *et al.* 2000
SK-Mel-19	melanoma	Carey *et al.* 1976
SK-Mel-28	melanoma	Carey *et al.* 1976

Cell Line	Origin	Reference
SK-Mel-103	melanoma	Gruis *et al.* 1995
SK-Mel-147	melanoma	Gruis *et al.* 1995

Generated Human Cell Lines

The following table lists the cell lines that were generated during this study.

Table 2.11: Generated Human Cell Lines

Cell line	Parental cell line	Plasmid	Selection Marker
HCT116-*TP53*$^{-/-}$- ctr	HCT116 *TP53*$^{-/-}$	pRetroSuper-scrambled	Puromycin
HCT116-*TP53*$^{-/-}$-*TP73* shRNA	HCT116 *TP53*$^{-/-}$	pLKO.1-sh-*TP73*	Puromycin
HCT116- ctr	HCT116	pInducer20	Puromycin
HCT116- *TAp73α*	HCT116	pInducer20-*TAp73*α	Puromycin
HCT116-*TP53*$^{-/-}$ - ctr	HCT116 *TP53*$^{-/-}$	pInducer20	Puromycin
HCT116-TP53$^{-/-}$ - *TAp73α*	HCT116 *TP53*$^{-/-}$	pInducer20-*TAp73*α	Puromycin
HCT116-*TP53*$^{-/-}$-*TP73* shRNA- ctr	HCT116 *TP53*$^{-/-}$	pInducer20	Puromycin
HCT116-*TP53*$^{-/-}$-*TP73* shRNA-*TAp73α*	HCT116 *TP53*$^{-/-}$	pInducer20-*TAp73*α	Puromycin
HCT116-p53-R175H-ctr	HCT116 p53 R175H	pRetroSuper-scrambled	Puromycin
HCT116-p53-R175H-*TP73* shRNA	HCT116 p53 R175H	pRcCMV-p53-R175H-72R	Puromycin

Cultivation of Human Cells

Human cells were cultivated at 37°C and 5% CO_2. Cells were cultured in RPMI medium (Sigma-Aldrich, Taufkirchen, Germany) supplemented with 10% FCS (GE Healthcare, Chalfont St. Giles, Great Britain), 100 µg/ml streptomycin and 100 U/ml penicillin (Sigma-Aldrich, Taufkirchen, Germany). Cells were passaged three times a week. For this, cells were washed once with PBS and detached by using trypsin (Sigma-Aldrich, Taufkirchen, Germany). A defined amount of cell suspension was transferred to a new cell culture dish.

On a long term basis, cells were stored in liquid nitrogen. Therefore, cells were harvested and resuspended in freezing medium (70% RPMI, 20% FCS and 10% DMSO), slowly cooled to -80°C using a cryo 1°C freezing container and transferred to the vapor phase of liquid nitrogen.

2.2 Cell Biological Methods

2.2.1 Transfection Of Human Cells

Transfection Using siRNA

Cells were seeded at 70% density in 6-well plates 24 h prior to transfection. siRNA transfections were performed by using INTERFERin reagent (Polyplus, Illkirch, Frankreich). 60 pmol siRNA were diluted in 189 µl serum free medium. 5 µl INTERFERin were added and the mixture was vortexed for 10 s. After incubating for 10 min at room temperature the mixture was dropped onto the cells. The medium was changed after 4 h and the knock down of respective targets was checked 48 h after transfection.

Plasmid Transfection Using Electroporation

Cells were harvested by centrifugation at 1000 rpm for 5 min and resuspended in a concentration of $5x10^6$ cells/ml in RPMI medium. 10-50 µg of plasmid DNA was added to 400 µl cell suspension. Electroporation was performed in a 4 mm-cuvette at 300 V and 500 µF (HCT116, SW48, RKO, SW480, SW620, CaCo2, HT29), 220 V and 950 µF (SW837, LS411N, LS513, Colo201, LoVo) or 200 V and 500 µF (SK-Mel-19, SK-Mel-28, SK-Mel-103, SK-Mel-147). Cells were transferred into RPMI medium. After 6 h, cells were washed once with PBS and supplemented with fresh RPMI medium. Analyses were performed after 48 h.

Plasmid Transfection Using Polyethylenimin (PEI)

Cells were seeded at 70% density in 6-well plates 24 h prior to transfection. Before transfection, the cells were washed with PBS and supplemented with fresh culture medium. For transfection, two solutions were prepared: solution A contained 100 µl PBS mixed with 2-7 µg plasmid DNA, whereas solution B contained 95 µl PBS mixed with 5 µl PEI (0.0025% final concentration). Both solutions were mixed by pipetting and were incubated at room temperature for 15 min. The mixture was dropped onto the cells and after 4 h cells were washed three times and supplemented with fresh RPMI medium. Analyses were performed after 48 h.

Plasmid Transfection Using METAFECTENE©

Cells were seeded at 70% density in 6-well plates 24 h prior to transfection. For the generation of stable expression cell lines, METAFECTENE© (Biontex Laboratories GmbH, Martinsried, Germany) was used. Two solutions were prepared: solution A contained 100 µl PBS mixed with 2 µg plasmid DNA, solution B contained 100 µl PBS mixed with 6 µl METAFECTENE©. Both solutions were mixed and incubated at room temperature for 15 min. Afterwards, the mixture was dropped onto the cells. 6 h after transfection cells were washed twice with PBS and supplemented with fresh cell culture medium.

2.2.2 Generation Of Stable Cell Lines

For the generation of cell lines stably expressing plasmid DNA cells were transfected with METAFECTENE©. 24 h after transfection, cells were seeded in different dilutions (1:250, 1:500, 1:1000, 1:5000) into RPMI medium containing 1 µg/ml puromycin. Puromycin enables the selection of successfully transfected cells. Analyses of the single cell clones were performed after 30 generations.

2.2.3 Karyotype Analyses

Chromosome Spreading

Cells were treated with 150 nM Taxol for 4 h. After centrifugation at 2000 rpm for 5 min, cells were resuspended in 2 ml hypotonic solution (40% RPMI medium, 60% *aqua dest.*) and incubated for 20 min at room temperature. Afterwards, cells were fixed with 1 ml ice-cold Carnoy´s fixative (75% methanol, 25% glacial acetic acid) and centrifuged for 5 min at 2000 rpm. The fixation step was repeated three times. Subsequently, cells were resuspended in 500 µl 100% glacial acetic acid and dropped onto a pre-cooled, wet object slide, which was in turn incubated for 5 min at 42°C. Dried slides were stained in 8% Giemsa staining solution (Merck, Darmstadt, Germany) in H_2O for 25 min. Slides were washed and dried at room temperature and embedded in Euparal (Carl Roth, Karlsruhe, Germany). Object slides were analyzed using Zeiss Axioscope FS microscope (Zeiss, Oberkochen, Germany) equipped with a Hamamatsu C4742-95 camera and the Hokawo Launcher 2.1 software (Hamamatsu Photonics, Hamamatsu, Japan)

CEP-FISH

Asynchronously growing cells were harvested by centrifugation at 2000 rpm for 5 min, resuspended in hypotonic solution, fixed by using Carnoy´s fixative and dropped onto coverslips as described above.

Object slides were incubated in 2x SCC solution (0.3 M sodium chloride, 30 mM trisodium citrate, pH 7.0) for 2 min at room temperature. After dehydration in an alcohol series of 70%, 85% and 100% ethanol for 2 min each, object slides were air dried. 0.6 µl of each probe specific for chromosome 7 and chromosome 15 or chromosome 6 and chromosome 18 were added to the hybridization solution and pre-warmed for 5 min at 37°C. Cells were covered with the probe mixture. Sample and probe were heated for 2 min at 75°C and placed for 2 h at 37°C. Afterwards, the cover slip was immersed in 0.25x SSC at 72°C for 4 min (CRC cell lines) or 6 min (melanoma cell lines). Thereafter, the cells were incubated in 2x SSC containing 0.05% Tween-20 at room temperature for 5 min and stained with Hoechst 33342 in 2x SSC + 0.05% Tween-20 for 5 min. Object slides were washed three times with 2x SSC + 0.05% Tween-20, dried and embedded in Vectashield (Vector Laboratories, Burlingame, CA, USA). Analyses were performed on a DeltaVision Elite microscope.

2.2.4 Synchronization Of Human Cells

Cell Cycle Synchronization *via* Double Thymidine Block

Cell cycle synchronization of human cells at the G_1-/S-transition was achieved by a double thymidine block. Cells were grown in 2 mM thymidine for 16 h. After washing the cells five times with PBS, they were released into fresh culture medium for 8 h. Following, cells were seeded in 2 mM thymidine for another 16 h. Cells were washed five times with PBS and released into fresh culture medium. For the analysis of lagging chromosomes, cells were fixed 8.5 h (CRC cell lines) or 9.5 h (melanoma cell lines) after release from thymidine.

Mitotic Synchronization

Synchronization of cells in mitosis was achieved by treatment with 2 µM DME for 16 h.

2.2.5 Immunofluorescence Microscopy

Cells were fixed for immunofluorescence microscopy by using 2% paraformaldehyde in PHEM buffer (60 mM PIPES pH 7.0, 27 mM HEPES, 10 mM EGTA, 4 mM $MgCl_2$) for 5 min at room temperature followed by 5 min methanol fixation at -20°C. In order to avoid unspecific antibody binding, cells were blocked with 5% FCS in PBS for 30 min. Afterwards, cells were incubated with primary antibodies in PBS containing 2% FCS for 1.5 h at room temperature. Afterwards, cells were washed three times with PBS and incubated with fluorescence-labeled secondary antibody for 1.5 h at room temperature. After washing once with PBS, cells were incubated in Hoechst33342 (1:15000 in PBS) (Invitrogen, Carlsbad, CA, USA) for 5 min and washed three times with PBS. Object slides were dried and embedded

using VectaShield (Vector Laboratories, Burlingame, CA, USA). Cells were analyzed using a Leica DM600B fluorescence microscope equipped with an ORCA-ER camera. Images were taken in a 60x magnification with a z-optical spacing of 0.2 µm. Deconvolution and further analyses were performed using the Leica LAS-AF software. Alternatively, a DeltaVision Elite microscope (GE Healthcare, Chalfont St. Giles, Great Britain) equipped with a PCO Edge sCMOS camera (PCO, Kelheim, Germany) was used. Images were taken with an Olympus 60x 1.40 NA objective (Olympus, Tokio, Japan) with a z-optical spacing of 0.4 µm, deconvolved and further analyzed using the Softworx 5.0 software.

2.2.6 Analyses Of Spindle Orientation

Asynchronously growing cells were seeded onto fibronectin coated coverslips (BD Biosciences, Heidelberg, Germany). Cells were fixed using ice cold methanol for 6 min at -20°C, blocked by using 5% FCS in PBS for 20 min and stained for α-tubulin, ɣ-tubulin and DNA. Microscopy was performed on a DeltaVision-ELITE microscope (GE Healthcare, Chalfont St. Giles, Great Britain) equipped with a PCO Edge sCMOS camera (PCO, Kelheim, Germany). Images were acquired with an Olympus 60x 1.40 NA objective (Olympus, Tokio, Japan) with a z-optical spacing of 0.4 µm, deconvolved and analyzed using SoftWorx 5.0 software (Applied Precision Inc., Issaquah, WA, USA). Determination of spindle orientation was calculated using the following formula: spindle axis angle= (number of z-stacks*0.4 µm / distance of centrosomes) *180/ π.

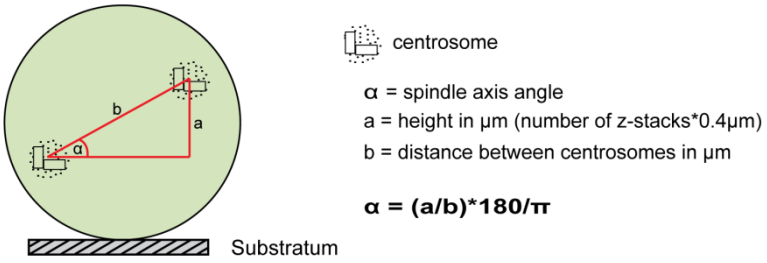

Fig. 2.1: Schematic illustration for the determination of the spindle axis angle.

2.2.7 Analyses Of Microtubule Plus-End Assembly Rates

Cells were transfected with 10 µg pEGFP-*EB3* plasmid *via* electroporation 48 h prior to live cell analysis. For analysis of microtubule polymerization rates of monopolar spindles, cells were treated with 2 µM DME in phenol red free RPMI medium for 1 h (CRC cell lines) -2 h (melanoma cell lines). Live cell analyses were performed at 37°C and 5% CO_2 using a Delta Vision Elite microscope equipped with a PCO edge sCMOS camera. Images of 4 sections

with a z-optical spacing of 0.4 µm were taken every 2 sec for 30 sec. Images were deconvolved and further analyzed using the Soft WoRX 5.0 software.

2.2.8 Chorion-Allantoic Membrane (CAM) Assay

Fertilized White Leghorn chick eggs were incubated at 37.8°C and 80% relative humidity. A small window was cut into the shell on day three of chick development. Eggs with resealed window were further incubated until day 10 of chick development. Two million HCT116 cells per CAM were resuspended in a mixture of 50% RPMI1640 medium and 50% matrigel in a total volume of 40 µl. After incubation of cell suspensions for 30 min at 37°C and 5% CO_2, cells were applied on top of the CAM. On day 17 of chick development, tumors were dissected.

2.2.9 Immunohistology

For immunohistological analyses, dissected tumors were fixed in 4% paraformaldehyde for 20 min, washed three times with PBS and transferred into 10% sucrose for 2 h at 4°C. After an overnight incubation in 30% sucrose at 4°C tumors were embedded in tissue freezing medium and stored at -80°C. Hardened tumor blocks were cut in 12 µm thick sections using a cryotome. Cryosections were transferred onto microscope slides and stored at -20°C.
For staining of the cryosections, microscope slides were thawed, dried at room temperature and blocked using blocking solution (1% BSA, 5% goat serum and 0.2% Triton X-100 in PBS) for 30 min. Afterwards, sections were covered with primary antibodies diluted in antibody solution (1% BSA and 0.5% Triton X-100 in 0.05 M TBS) over night at 4°C. The cryosections were washed two times with PBS. Subsequently, they were covered with secondary antibody and DAPI mixed in antibody solution for 1 h at room temperature. Specimens were washed three times, mounted in Fluoromount-G (Sigma-Aldrich, Taufkirchen, Germany) and analyzed with a Zeiss Axio Imager Z1 microscope (Carl Zeiss, Göttingen, Germany).

2.2.10 *In Vitro* Migration Assay

Cells were starved for 16 h in medium containing 0.5% FCS. Cells were harvested, counted and resuspended in medium containing 0.5% FCS to a final cell concentration of $2*10^5$ cells per 200 µl. ThinCert© cell culture inserts (Greiner BioOne, Frickenhausen, Germany) were placed in a 24-well plate containing 600 µl culture medium including 10% FCS. The cell suspension was added into the cell culture inserts. Cells were incubated for 24 h at 37°C and 5% CO_2 before being detached from the bottom of the cell culture insert by Trypsin/EDTA. Detached cells were resuspended in 100 µl PBS and counted.

2.2.11 *In Vitro* Invasion Assay

Matrigel coated cell culture inserts (BD Bioscience, Bedford, MA, USA) were rehydrated according to the manufacturer´s protocol. Meanwhile, cells were harvested, counted and resuspended in cell culture medium containing 0.5% FCS to a final concentration of $2*10^5$ cells per 500 µl. Cell culture inserts were placed in a 24-well containing 750 µm cell culture medium. The cell suspension was added into the cell culture inserts and incubated for 48 h at 37°C and 5% CO_2. Following, non-invasive cells were removed from the upper surface of the membrane by scrubbing using a moistened cotton swab. Cells on the lower surface of the membrane were fixed using 2% PFA for 5 min at room temperature and methanol for 5 min at -20°C. Cells were stained using Hoechst33342 for 5 min. After the membrane was dried, it was cut from the insert, placed on an object slide and embedded using VectaShield©. Invasive cells were analyzed under the microscope at 40x magnification. Ten randomly chosen pictures were taken for each assay. Cells were counted using the ImageJ Software.

2.2.12 Rac1-Activation-Assay

Rac1-Activation-Assay was performed using the RhoA/Rac1/Cdc42 Activation Combo Biochem Kit (Cytoskeleton Inc, Denver, CO, USA) according to the manufacturer´s protocol. Cell culture plates were placed on ice and the cells were washed once with ice cold PBS. Cell lysis was performed on the plate by using 400 µl ice-cold lysis buffer (50 mM Tris pH 7.5, 10 mM $MgCl_2$, 0.5 M NaCl, 2% Igepal). Cells were harvested and centrifuged for 1 min at 14800 rpm at 4°C. The supernatant was transferred to a new reaction tube and snap frozen in liquid nitrogen. 1500 µg of cell lysate were incubated with 10 µg PAK-PBD-beads for 30 min at 4°C. Beads were washed once with wash buffer (25 mM Tris pH 7.5, 30 mM $MgCl_2$, 40 mM NaCl) and resuspended in 15 µl Laemmli sample buffer. Samples were boiled for 5 min and analyzed by SDS-PAGE and western blot. Rac1 was detected using anti-Rac1 antibody (Rac1 Arc03, Cytoskeleton Inc., Denver, CO, USA) at 1:500 dilution.

2.2.13 GEF-Assay

GEF-Assay for TRIO was performed by using Rac1 G15A Agarose Beads (Cell Biolabs Inc., San Diego, CA, USA). Cell culture plates were placed on ice and the cells were washed once with ice cold PBS. Cell lysis was performed on the plate using 400 µl ice-cold lysis buffer (20 mM HEPES, pH 7.5, 150 mM NaCl, 5 mM MgCl2, 1% Triton X-100). Cells were harvested and centrifuged for 1 min at 14800 rpm at 4°C. 2000 µg of cell lysate were incubated with 10 µg Rac1 G15A agarose beads for 1 h at 4°C. Beads were washed three times with HBS buffer (20 mM HEPES, pH 7.5, 150 mM NaCl) and resuspended in 15 µl Laemmli sample buffer. Samples were boiled for 5 min and analyzed by SDS-PAGE and western blot. TRIO

was detected using anti-TRIO antibody (TRIO D20, Santa Cruz, Dallas, TX, USA) at 1:300 dilution.

2.3 Proteinbiochemistry

2.3.1 Preparation Of Protein Lysates

Cells were harvested by centrifugation at 2000 rpm for 5 min and subsequently resuspended in 70 µl lysis Buffer (50 mM Tris-HCl pH 7.4, 150 mM NaCl, 5 mM EDTA, 5 mM EGTA, 1% (v/v) Igepal©, 0.1% (w/v) SDS, 0.1% Na-Desoxycholate, 20mM Na_3VO_4, 25 mM β-Glycerophosphate, 50 mM NaF, 5 mM Na_2MoO_4) supplemented with complete protease inhibitor cocktail EDTA-free (1:25) (Roche, Switzerland), phosphatase inhibitor (1:10) and 0.5 µM microcystin-LR (Enzo Life Sciences, Lörrach, Germany). After 10 min incubation on ice, cells were centrifuged at 14800 rpm for 20 min at 4°C. The supernatant was transferred to a new reaction tube and stored at -20°C.

2.3.2 Protein Determination

Protein levels were determined by using the Bio-Rad DC Protein assay (BioRad, Hercules, CA, USA) following the manufacturer´s protocol. Photometric measurement was performed using a VICTOR© X3 microplate reader.

2.3.3 Sodiumdodecylsulfate-Polyacrylamid Gel Electrophoresis (SDS-PAGE)

A discontinuous SDS-PAGE was used for the separation of proteins according to their molecular weight. The SDS-gel composed of a 5% stacking gel (300 nM TRIS-HCl pH 6.8, 0.1% (w/v) SDS, 5% (v/v) Rotiphorese© Gel 30) and a 6-13% resolving gel (500 mM TRIS-HCl pH 8.8, 0.1% (w/v) SDS, 6-13% (v/v) Rotiphorese© Gel 30). 5 µl of PageRuler Prestained Protein Ladder (Fermentas, St. Leon-Rot, Germany) was used for the determination of the molecular weight of the detected proteins. 50 µg protein extract were supplemented with SDS sample buffer (15% (w/v) SDS, 15% (v/v) β-mercaptoethanol, 50% glycerol, 0.25% (w/v) bromophenol blue). For protein denaturation, samples were heated at 95°C for 5 min. Proteins were separated in SDS running buffer (25 mM TRIS-HCl pH 6.8, 192 mM glycine, 0.15% (w/v) SDS) for 1 h at 28 mA and 2.5-3.5 h at 38 mA.

2.3.4 Western Blot

Semi-dry Blot

After separation of proteins *via* SDS-PAGE, they were transferred onto a nitrocellulose membrane by semi dry western blot. Transfer was performed in a blotting device at 200 mA for 1.5 h using transfer buffer (0.0025% (w/v) SDS, 24.8 mM TRIS-HCl pH 8.0, 170 mM (v/v) glycine, 20% methanol).

Tank-Blotting

Proteins larger than 100 kDa were transferred onto nitrocellulose membrane *via* tank blotting. Transfer was performed in a tank blot device for 3 h at 400 mM by using blotting buffer (0.0025% (w/v) SDS, 24.8 mM TRIS-HCl pH 8.0, 170 mM (v/v) glycine, 13% methanol).

After protein transfer the membrane was blocked for 30 min using 5% milk powder in TBS (50mM TRIS-HCl pH 7.2, 160 mM NaCl). The proteins of interest were detected with specific primary antibodies diluted in 2% BSA in TBS. The primary antibody was incubated over night at 4°. After washing the membrane three times using TBS-T (0.1% Tween in TBS) it was incubated with the secondary antibody conjugated to HRP for 1 h at room temperature. Subsequently, the membrane was washed three times in TBS-T and once in TBS for 10 min each. Proteins were detected by ECL. For this, the membrane was incubated shortly in 0.1 mM TRIS-HCl pH 8.5 containing 0.4 mM β-coumaric acid, 2.5 mM luminol and 0.03% H_2O_2. Chemoluminescence was detected using Fuji Medical X-Ray Film and the OPTIMAX-X-Ray Film Processor.

2.4 Molecular Biological Methods

2.4.1 *Escherichia coli* cells

The following *E. coli* strain was used:

DH5αF$^-$ϕ80*lacZ*ΔM15 Δ(*lacZYA-argF*)U169 *deoR recA1 hsdR*17(r_k^-, m_k^+) *phoA supE*44 *thi*-1 *gyr*A96 *rel*A1λ$^-$

2.4.2 Generation Of Competent *Escherichia coli* Cells

E. coli DH5α were inoculated in 5 ml Luria Bertani medium (LB medium) (1% peptone 140, 0.5% yeast extract, 0.5% NaCl) and kept at 37°C overnight on a shaker. The preculture was transferred to 400 ml LB medium and grown to a density of OD_{600}= 0.5 at 37°C. The culture

was incubated on ice for 5 min. After centrifugation for 5 min at 2000 rpm and resuspending in 40 ml cold TfbI buffer (30 mM potassium acetate, 100 mM RbCl, 10 mM $CaCl_2$, 15 % glycerol, pH adjusted to 6.0 using 0.2 M acetic acid containing 50 mM of $MnCl_2$) the suspension was again incubated on ice for 5 min and centrifuged for 5 min at 2000 rpm. After resuspending in 4 ml cold TfbII buffer (10 mM MOPS, 75 mM $CaCl_2$, 10 mM RbCl, 15 % glycerol, pH 6.5) the cells were incubated on ice for 15 min. Aliquots of 100 µl were snap frozen in liquid nitrogen and stored at -80°C until usage.

2.4.3 Transformation Of *Escherichia coli* Cells

Transformation of *E. coli* was performed using the heat-shock protocol. 50 µl of competent *E. coli* DH5α cells were mixed with 2 µg plasmid DNA and incubated on ice for 20 min. Subsequently, cells were incubated for 40 sec at 42°C followed by an incubation on ice for 2 min. Cells were supplemented with 600 µl LB medium and incubated for 60 min at 37°C while constant shaking. Cells were transferred to 400 ml LB medium containing appropriate antibiotics for selection of the plasmid. After overnight incubation at 37°C plasmid DNA was isolated from the liquid culture.

2.4.4 Plasmid Isolation

Plasmid DNA preparation was performed using the NucleoBond© PC 100 X-TRA Midi Kit (Macherey Nagel, Düren, Germany) according to the manufacturer´s protocol.
The DNA concentration was measured using the NanoDrop© 2000 spectro-photometer (ThermoFisher, Waltham, MA, USA).

2.4.5 RNA-Isolation

RNA was isolated using the NucleoSpin© RNA Kit according to the manufacturer´s protocol (Macherey Nagel, Düren, Germany).
RNA was quantified using NanoDrop© 2000 spectrophotometer (ThermoFisher, Waltham, MA, USA) and analysed in a 1% agarose gel.

2.4.6 cDNA Synthesis And Quantitative Real Time PCR

1 µg cDNA was synthesized from RNA using 100 pmol random hexamer primer, dNTPs (0.5 mM each), 20 U RiboLock RNase inhibitor and 200 U Maxima Reverse Transcriptase (ThermoFisher, Waltham, MA, USA). Reaction components were incubated for 10 min at 25°C followed by 30 min at 50°C. The reaction was terminated by heating at 85°C for 5 min. Quantitative real time PCR reactions were performed using gene specific primers, 30 ng

cDNA and GoTaq qPCR Master Mix (Promega, Mannheim, Germany) on a Rotor Gene Q real time PCR cycler (Qiagen, Hilden, Germany) using the following program (Table 2.12).

Table 2.12: qRT-PCR Program

Denaturation	95°C 5 min	
Denaturation	95°C 5 s	
Primer Annealing	60°C 10 s	50x
Polymerization	60°C 10 s	

Transcriptional changes were calculated based on the comparative C_T method.

2.4.7 Preparation of Samples For RNA-Sequencing

HCT116 cells were seeded in 2 mM Thymidine for 16 h, released into the cell cycle for 8 h and seeded into 2 mM Thymidine. After 1 h, siRNA transfections were conducted using 60 pmol *LUCIFERASE*, *TP53* or *TP73* siRNA. Medium was changed after 2 h. After 11 h, cells were released into the cell cycle for 6.5 h and subsequently harvested. These G_2 arrested probes were further processed by the Transcriptome and Genome Analysis Laboratory (TAL) of the University of Göttingen (Göttingen, Germany). Bioinformatical analyses were performed by Silvia von der Heyde (former University of Göttingen, Germany).

3 Results

3.1 A Mechanistic Link Between Chromosomal Instability And Tumor Cell Migration

3.1.1 Increased Interphase Microtubule Plus-End Assembly Rates Correlate With Migration And Invasion

Aneuploidy is a hallmark of human cancer, which derives from an increased rate of chromosome missegregation during mitosis. This process, termed chromosomal instability (CIN), contributes to tumorigenesis, tumor progression and therapy resistance (Holland & Cleveland 2012). However, the mechanisms behind are not well understood. CIN is often associated with late tumor stages, which are associated with larger tumors, high invasiveness and infiltration of nearby tissues. Thus, we wanted to investigate a possible link between CIN and cancer cell migration and invasion.

To investigate a potential correlation between these two phenotypes, transwell migration and invasion assays were performed. A panel of CRC cells was used, which can be subdivided into chromosomally stable, but microsatellite instable (MIN/MSI) cell lines (HCT116, SW48) and chromosomally instable (CIN) cell lines (SW480, SW620, SW837, CaCo2, HT29, LS411N, LS513, Colo201, LoVo). Intriguingly, only the CIN cell lines Colo201 and LoVo exhibited increased migration and invasion (Fig 3.1a-b). In comparison to HCT116 cells, Colo201 and LoVo cells displayed an approximal 2-fold increased migration potential as well as a nearly 2-fold increased invasion potential. SW620, SW837, CaCo2, HT29, LS411N and LS513 exhibited the lowest migration and invasion potentials. Increased microtubule plus-end assembly rates in mitosis were recently elucidated as a common cause for CIN in colorectal cancer (Ertych *et al.* 2014). Microtubule plus-end assembly rates were measured during mitosis in the panel of CRC cell lines. The measurement was performed using the GFP-tagged end binding protein EB3, which binds to growing microtubule plus-ends (Stepanova *et al.* 2003). Thus, by using live cell microscopy, the growing microtubule plus-ends can be tracked over time and microtubule plus-end assembly rates can be determined. As shown before (Ertych *et al.* 2014), all investigated CIN cell lines exhibited increased microtubule plus-end assembly rates during mitosis when compared to chromosomally stable (MIN/MSI) cell lines HCT116 and SW48 (Fig 3.1c). Microtubule dynamics are known to be required for cell migration (Vasiliev *et al.* 1970). Therefore, interphase microtubule-plus-end assembly rates were measured. Interestingly, only the migratory and invasive CIN cell lines Colo201 and LoVo displayed significantly increased microtubule plus-end assembly rates during interphase compared to the other cell lines (Fig 3.1d).

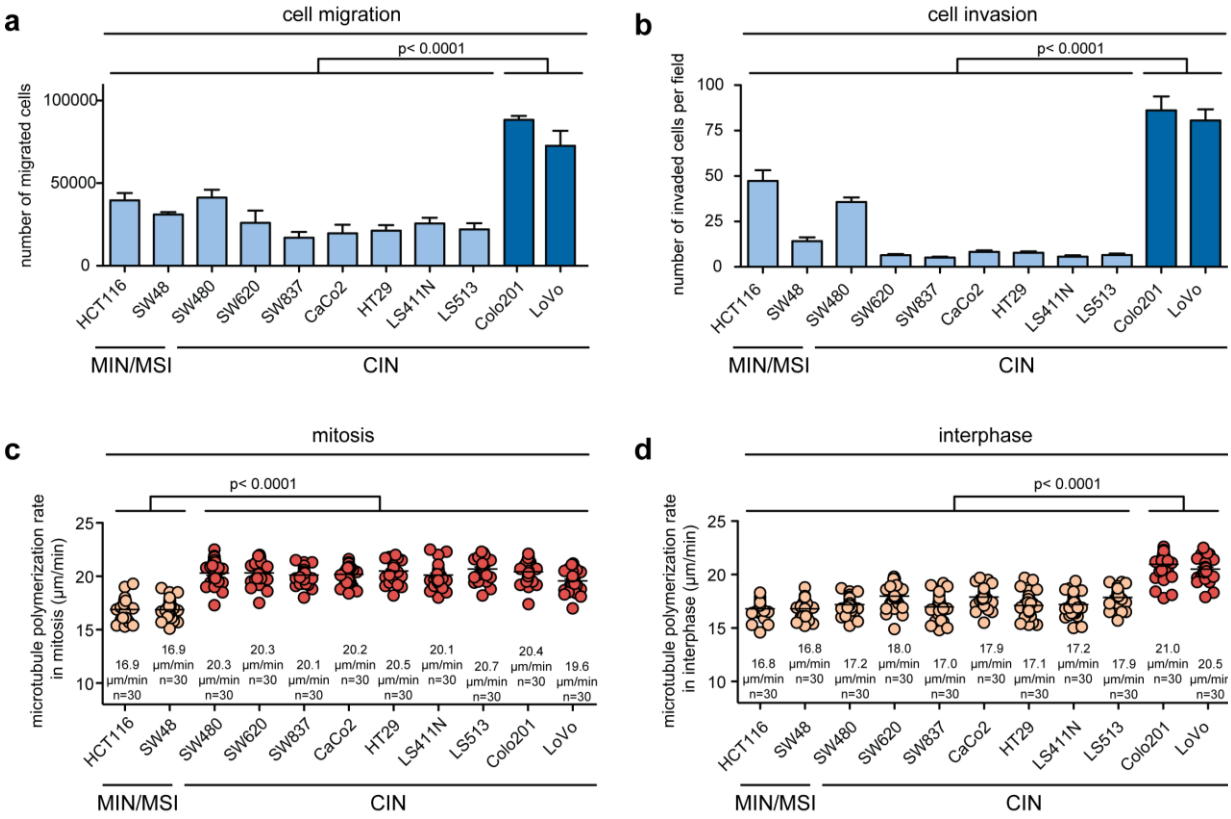

Figure 3.1: Increased interphase microtubule plus-end assembly rates correlate with a migratory and invasive phenotype. (a) Transwell migration assays of a panel of MIN/MSI and CIN CRC cell lines. 200,000 cells were seeded and bar graphs show the proportion of migrated cells after 24 h (mean ± sem, *t*-test, n=3). **(b)** Transwell invasion assays for a panel of MIN/MSI and CIN cell lines. 200,000 cells were seeded into matrigel coated cell culture inserts and bar graphs show the number of invaded cells in each picture of 30 randomly chosen pictures taken at 40x magnification from three independent experiments (*t*-test, mean ± sem, n=3). **(c)** Measurements of mitotic microtubule plus-end assembly rates in a panel of MIN/MSI and CIN CRC cell lines. Cells were treated with 2 µM DME for 1 h prior to determination of microtubule plus-end assembly rates. Scatter dot plots show the average microtubule plus-end assembly rates of 20 microtubules per cell (mean ± sem, *t*-test, n=30 cells from three independent experiments). **(d)** Measurements of interphase microtubule plus-end assembly rates using a panel of MIN/MSI and CIN CRC cell lines. Scatter dot plots show the average microtubule plus-end assembly rates of 20 microtubules per cell (mean ± sem, *t*-test, n=30 cells from three independent experiments).

These data indicate that only a subset of CIN cells acquired an abnormal increase in microtubule plus-end assembly rates in interphase, which correlates with increased cell migration and invasion.

To verify our findings, we used different melanoma cell lines that are well characterized regarding their migration and invasion potential. The melanoma cell lines SK-Mel-19 and SK-Mel-28 are known to be non-invasive, whereas the cell lines SK-Mel-103 and SK-Mel-147 are described to exhibit a highly invasive phenotype (Alla *et al.* 2010). The migration and invasion potential of these cell lines was validated by transwell migration and invasion assays. Transwell migration assays revealed 6,000 migrated SK-Mel-19 cells and 24,500

migrated SK-Mel-28, whereas for SK-Mel-103 and SK-Mel-147 migrated cells in a range from 97,000 to 100,500 were detected (Fig. 3.2a). Using transwell invasion assays, 53 and 80 invaded cells per field were observed for SK-Mel-19 and SK-Mel-28, while the highly invasive cell lines SK-Mel-103 and SK-Mel-147 exhibited 366 and 323 invaded cells per field (Fig 3.2b). These four melanoma cell lines were further analyzed with respect to their microtubule plus-end assembly rates during mitosis and interphase by EB3 tracking experiments. Interestingly, the highly migratory and invasive cell lines SK-Mel-103 and SK-Mel-147 exhibited increased microtubule plus-end assembly rates during interphase when compared to the non-invasive cell lines SK-Mel-19 and SK-Mel-28 (Fig 3.2c). Microtubule plus-end assembly rates in interphase were increased from 17.9 µm/min and 18.3 µm/min in SK-Mel-19 and SK-Mel-28, respectively, to 21.2 µm/min in both SK-Mel-103 and SK-Mel-147 cells. Apart from that, SK-Mel-19, SK-Mel-28, SK-Mel-103 and SK-Mel-147 displayed increased microtubule plus-end assembly rates during mitosis of 18.7 µm/min, 19.7 µm/min, 19.4 µm/min and 19.6 µm/min (Fig. 3.2c), when compared to chromosomal stable CRC cell lines HCT116 and SW48 (Fig. 3.1a).

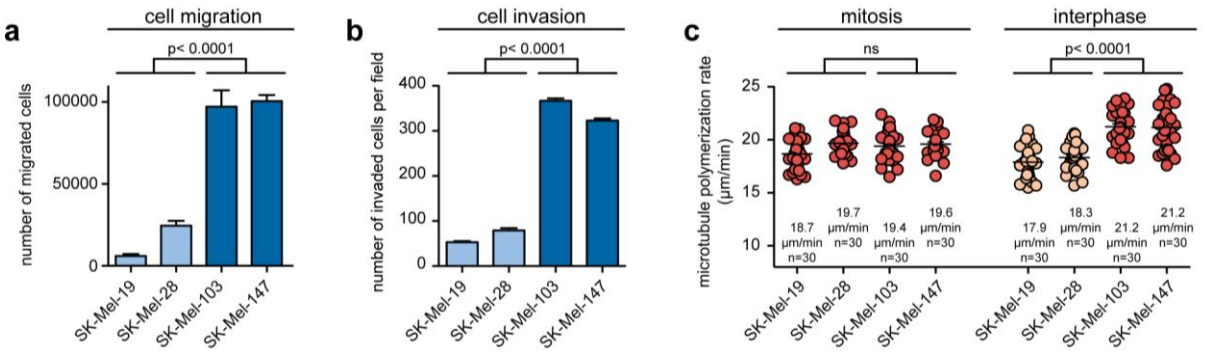

Figure 3.2: Highly migratory and invasive melanoma cell lines SK-Mel-103 and SK-Mel-147 exhibit increased interphase microtubule plus-end assembly rates. (a) Transwell migration assays using a panel of melanoma cell lines. Bar graphs show the proportion of migrated cells from 200,000 seeded cells after 24 h (mean ± sem, *t*-test, n=3). **(b)** Transwell invasion assays using a panel of four melanoma cell lines. 200,000 cells were seeded and bar graphs show the number of invaded cells in each picture of 30 randomly chosen pictures taken at 40x magnification from three independent experiments (mean ± sem, *t*-test, n=3). **(c)** Measurements of mitotic and interphase microtubule plus-end assembly rates in a panel of melanoma cell lines. Cells were treated with 2 µM DME 2 h prior to EB3 tracking experiments. Scatter dot plots show the average microtubule plus-end assembly rates of 20 microtubules per cell (mean ± sem, *t*-test, n=30 cells from three independent experiments).

In summary, a subset of the analyzed CRC and melanoma cell lines display increased microtubule plus-end assembly rates in interphase. Additionally, migration and invasion seem to be associated with CIN, but CIN is not *per se* associated with a high migration and invasion potential.

3.1.2 Alterations In Microtubule Plus-End Assembly Rates, But Not A CIN Phenotype Affect Migration And Invasion

To examine a potential interplay between increased microtubule plus-end assembly rates during interphase and increased cell migration and invasion, enhanced microtubule plus-end assembly rates were restored to normal levels by treatment with the microtubule-binding drug Taxol. Taxol inhibits dynamic microtubule properties and hence stabilizes microtubules (Jordan and Wilson 2004). 2 h prior to EB3 tracking experiments, cells were treated with 0.2 - 0.5 nM Taxol, which was previously shown to be sufficient to restore proper microtubule plus-end assembly rates in CIN cells (Ertych *et al.* 2014).

Indeed, at these sub-nanomolar concentrations, Taxol significantly suppressed increased microtubule plus-end assembly rates during mitosis as well as during interphase in both Colo201 and LoVo cells (Fig 3.3a). During mitosis, the microtubule plus-end assembly rates in Colo201 cells were reduced from 20.4 µm/min to 16.9 µm/min and in LoVo cells from 20.2 µm/min to 17.9 µm/min. During interphase, the microtubule plus-end assembly rates in Colo201 cells were decreased from 21.0 µm/min to 16.6 µm/min and in LoVo cells from 20.3 µm/min to 17.7 µm/min. These measured values are comparable to microtubule plus-end assembly rates typically seen in chromosomally stable and non-migratory HCT116 cells (Fig. 3.3a).

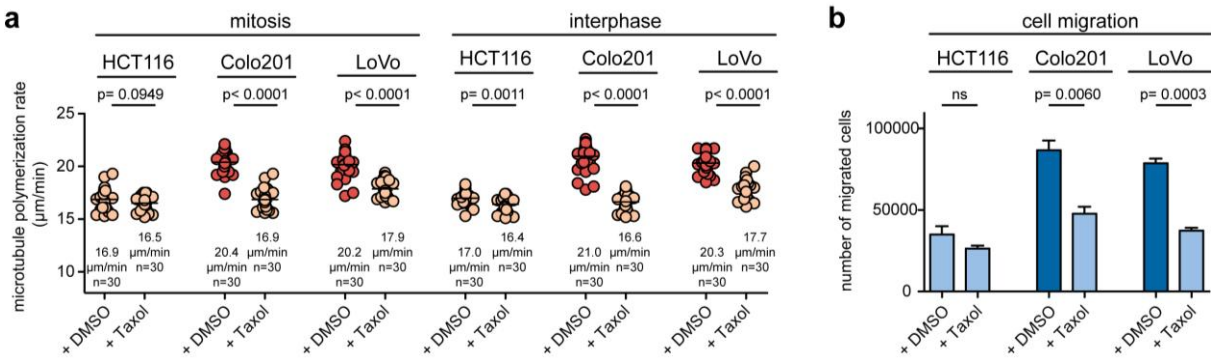

Figure 3.3: Restoration of microtubule plus-end assembly rates suppresses cell migration in CRC cell lines. (a) Measurements of mitotic and interphase microtubule plus-end assembly rates in CRC cell lines. Cells were treated with DMSO or 0.2 nM Taxol for 2 h. 1-2 h prior to EB3 tracking experiment, cells were treated with 2 µM DME. Scatter dot plots show the average microtubule plus-end assembly rates of 20 microtubules per cell (mean ± sem, *t*-test, n=30 cells from three independent experiments). **(b)** Transwell migration assays of CRC cell lines. Cells were treated with DMSO or 0.2 nM Taxol. Bar graphs show the proportion of migrated cells from 200,000 seeded cells after 24 h (mean ± sem, *t*-test, n=3).

Furthermore, transwell migration assays were performed with Taxol treated cells. The migration potential of Colo201 and LoVo cells was significantly decreased upon Taxol treatment in comparison to control DMSO treated cells (Fig 3.3b). In Colo201 cells, the

number of migrated cells was reduced by approximately 45% from 86,667 cells upon DMSO treatment to 47,667 cells upon Taxol treatment, whereas for LoVo cells the amount of migrated cells was decreased from 78,667 cells to 37,333 cells on average. In HCT116 cells, Taxol treatment did not have a significant influence on the migration potential. These results indicate an important role of microtubule plus-end assembly rates for cell migration in CRC cell lines. To further substantiate this finding, the melanoma cell lines SK-Mel-19, SK-Mel-28, SK-Mel-103 and SK Mel-147 cells were evaluated regarding their response to Taxol. EB3 tracking experiments were performed with these cell lines. 2 h prior to determination of microtubule plus-end assembly rates, cells were treated with 0.5 nM Taxol. EB3 tracking experiments revealed a significant decrease in microtubule plus-end assembly rates during both, mitosis and interphase, upon low dose Taxol treatment in all investigated cell lines (Fig 3.4a). Taxol treatment reduced the microtubule plus-end assembly rates in SK-Mel-103 and SK-Mel-147 cells to values comparable to microtubule plus-end assembly rates measured in SK-Mel-19 and SK-Mel-28 cells.

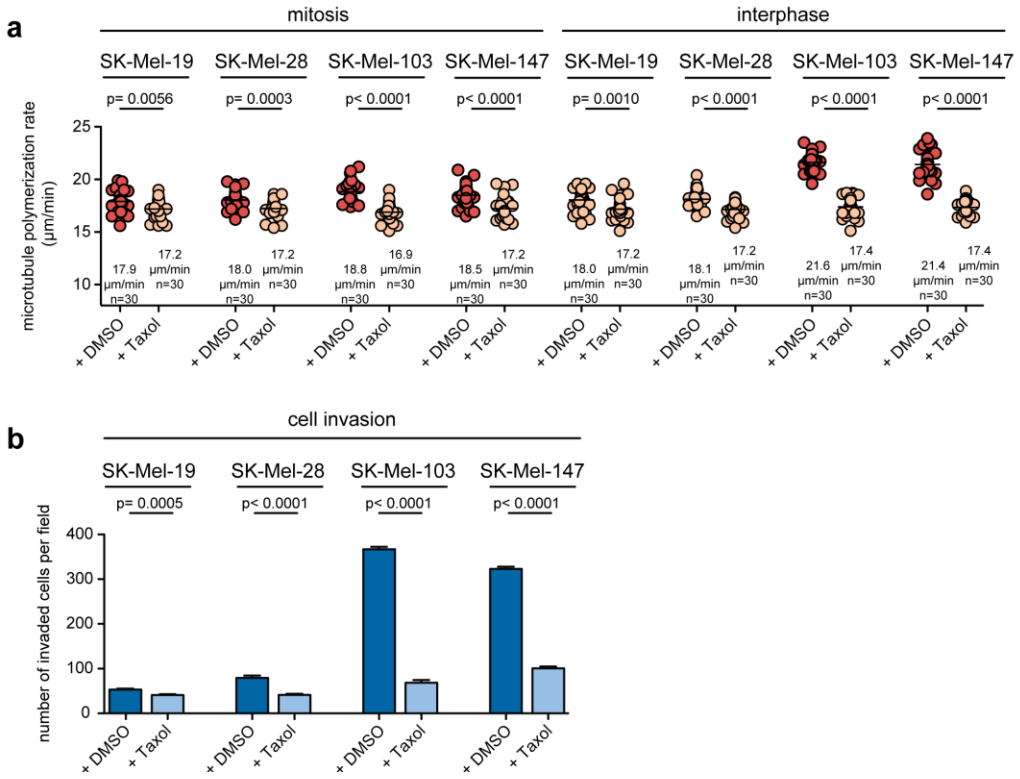

Figure 3.4: Restoration of microtubule plus-end assembly rates suppresses the invasive phenotype in melanoma cells. (a) Measurements of mitotic and interphase microtubule plus-end assembly rates in melanoma cell lines. The indicated cells were treated with DMSO or 0.5 nM Taxol for 2 h. 2 h prior to EB3 tracking experiments, cells were treated with 2 µM DME. Scatter dot plots show the average microtubule plus-end assembly rates of 20 microtubules per cell (mean ± sem, *t*-test, n=30 cells from three independent experiments). **(b)** Transwell invasion assays of the indicated melanoma cell lines. Cells were treated with DMSO or 0.5 nM Taxol. 200,000 cells were seeded and the amount of invaded cells after 48 h in each picture of 30 randomly chosen pictures taken with 40x magnification from three independent experiments was determined and illustrated as bar graphs (mean ± sem, *t*-test, n=3).

To further investigate the impact of Taxol on the invasion potential of the melanoma cells, transwell invasion assays were performed. Here, low-dose Taxol treatment significantly decreased the invasive phenotype of SK-Mel-103 and SK-Mel-147 cells. DMSO treated SK-Mel-103 and SK-Mel-147cells exhibited 366 and 323 invaded cells per field, respectively. Taxol treatment reduced the invaded cells per field to 69 cells in SK-Mel-103 and 100 cells in SK-Mel-147 (Fig 3.4b).

Increased microtubule plus-end assembly rates cause transient spindle geometry defects, which lead to merotelic microtubule-kinetochore attachments (Ertych *et al.* 2014). Merotelic attachments are erroneous microtubule-kinetochore attachments, which occur, when one kinetochore is attached to microtubules emanating from the two opposing spindle poles. Since the spindle assembly checkpoint does not detect these malattachments, cells can progress into anaphase and display so called lagging chromosomes (Cimini *et al.* 2001).

To investigate whether increases in microtubule plus-end assembly rates results in the generation of lagging chromosomes in CRC and melanoma cells, cells were synchronized at G_1/S transition by double thymidine block and released into the cell cycle and thereby treated with either DMSO or 0.2 - 0.5 nM Taxol for 8.5 h (CRC cell lines) - 9.5 h (melanoma cell lines). Cells were fixed and stained for immunofluorescence microscopy and the occurrence of lagging chromosomes during anaphase was analyzed.

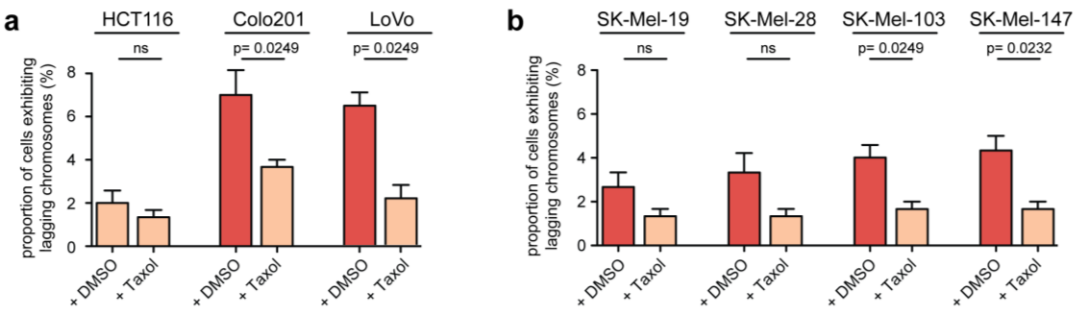

Figure 3.5: Restoration of microtubule plus-end assembly rates by low dose Taxol treatment suppresses the generation of lagging chromosomes. (a) Quantification of cells showing lagging chromosomes during anaphase. CRC cells were synchronized at G_1/S transition by a double thymidine block and released into the cell cycle thereby treating with DMSO or 0.2 nM Taxol. After 8.5 h cells were fixed and stained for immunofluorescence microscopy and the occurrence of lagging chromosomes was analyzed. Bar graphs show proportion of cells displaying at least one CREST-positive chromatid (mean ± sem, *t*-test, n=3 with a total of 300 anaphase cells). **(b)** Quantification of cells with lagging chromosomes during anaphase using melanoma cell lines. Cells were synchronized at G_1/S transition by a double thymidine block and released into the cell cycle thereby treating with DMSO or 0.5 nM Taxol. After 9.5 h cells were fixed and stained for immunofluorescence microscopy and the occurrence of lagging chromosomes was analyzed. Bar graphs show quantification of cells displaying at least one CREST-positive chromatid (mean ± sem, *t*-test, n=3 with a total of 300 anaphase cells).

The proportion of cells exhibiting lagging chromosomes in Colo201 and LoVo cells was significantly decreased after low dose Taxol treatment in comparison to DMSO treated cells.

On average 6% of DMSO treated Colo201 cells exhibited lagging chromosomes. This proportion was reduced to 3.6% upon Taxol treatment. Also in LoVo cells, the occurrence of lagging chromosomes was reduced from 6% to 2%. However, Taxol treatment had no significant influence onto the generation of lagging chromosomes in HCT116 cells (Fig 3.5a).
The melanoma cell lines investigated here have not been characterized regarding the generation of lagging chromosomes. But the increased microtubule plus-end assembly rates during mitosis (Fig 3.2c) hint to a chromosomally instable phenotype. DMSO treated melanoma cells exhibited lagging chromosomes in a range from 3% to 5%. This proportion was reduced to 1% to 2% upon low dose Taxol treatment. Thus, also in melanoma cell lines, increased microtubule plus-end assembly rates are associated with the generation of lagging chromosomes, albeit at lower frequency when compared to the CRC cell lines.
Hence, Taxol treatment decreased microtubule plus-end assembly rates in mitotic and interphase cells and reduced both the occurrence of lagging chromosomes and the migratory and invasive phenotype in CRC and melanoma cell lines. Since the generation of lagging chromosomes is tightly associated with CIN, the question arose, whether a CIN phenotype *per se* might be responsible for the increased migration and invasion potential.
The occurrence of lagging chromosomes can be specifically suppressed in the presence of increased microtubule plus-end assembly rates by overexpression of the mitotic centromere-associated kinesin *MCAK* (Ertych *et al.* 2014). MCAK is a microtubule depolymerase, which destabilizes kinetochore microtubules at the metaphase to anaphase transition, thus resolving erroneous kinetochore-microtubule-attachments (Maney *et al.* 1998; Bakhoum *et al.* 2009).
MCAK was overexpressed in the CRC cell lines HCT116 and Colo201, as well as in the melanoma cell line SK-Mel-103. The overexpression of *MCAK* was verified by western blot analyses (Fig 3.6a). Cells were synchronized at G_1/S transition, released into the cell cycle for 8.5 h (CRC cell lines) - 9.5 h (melanoma cell line) and fixed and stained for immunofluorescence microscopy. *MCAK* overexpression decreased the number of cells with lagging chromosomes in all cell lines in comparison to control vector transfected cells (Fig 3.6b). In Colo201 cells, the amount of lagging chromosomes was reduced from 6.3% to 1.6%, whereas in SK-Mel-103 cells the amount was reduced from 4% to 1.6% on average. These reductions in the occurrence of lagging chromosomes are comparable to those obtained by Taxol treatment (Fig 3.5a-b), but EB3 tracking experiments revealed no significantly altered microtubule plus-end assembly rates upon *MCAK* overexpression (Fig 3.6c).

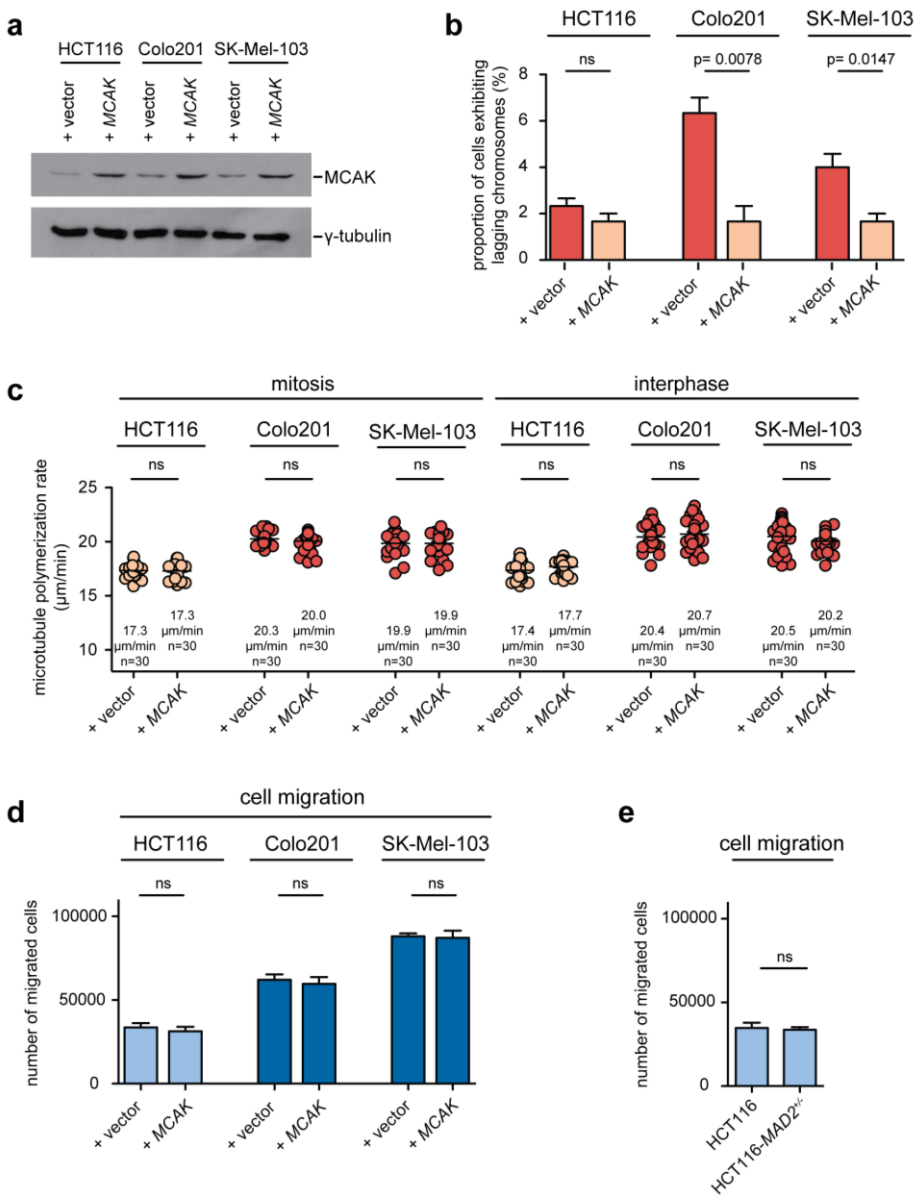

Figure 3.6: CIN does not trigger cell migration *per se*. (a) Representative western blot of HCT116, Colo201 and SK-Mel-103 cells detecting MCAK after overexpression of *MCAK*. γ-tubulin served as loading control. **(b)** The occurrence of anaphase cells with lagging chromosomes was analyzed in HCT116, Colo201 and SK-Mel-103 cells after overexpression of *MCAK*. Cells were synchronized at G_1/S transition by double thymidine block, released into the cell cycle for 8.5 h (HCT116, Colo201) or 9.5 h (SK-Mel-103) and fixed and stained for immunofluorescence microscopy. Bar graphs show proportion of cells exhibiting at least one CREST-positive chromatid (mean ± sem, *t*-test, n=3 with a total of 300 anaphase cells). **(c)** Measurements of microtubule plus-end assembly rates during mitosis and interphase after overexpression of *MCAK*. Scatter dot plots show the average microtubule plus-end assembly rates of 20 microtubules per cell (mean ± sem, *t*-test, n=30 cells from three independent experiments). **(d)** Transwell migration assays of HCT116, Colo201 and SK-Mel-103 cells were performed with or without overexpression of *MCAK*. 200,000 cells were seeded and bar graphs show the amount of migrated cells after 24 h (mean ± sem, *t*-test, n=3). **(e)** Transwell migration assay of HCT116 and HCT116 *MAD2*$^{+/-}$. 200,000 cells were seeded and bar graphs show the amount of migrated cells after 24 h (mean ± sem, *t*-test, n=3).

To investigate a potential link between CIN and migration, transwell migration assays were performed. These experiments revealed no influence of *MCAK* overexpression on the

migration potential of Colo201 and SK-Mel-103 cells (Fig 3.6d). Additionally HCT116-*MAD2*$^{+/-}$ cells were analyzed regarding their migration potential. These cells have a mitotic checkpoint defect and frequently missegregate chromosomes. But the HCT116-*MAD2*$^{+/-}$ cells did not show increased cell migration compared to parental HCT116 cells (Fig. 3.6e). Thus the occurrence of lagging chromosomes *per se* did not influence the migration potential of the highly migratory cell lines Colo201 and SK-Mel-103. Instead, abnormally increased microtubule plus-end assembly rates in mitosis and interphase are associated with the generation of lagging chromosomes and increased cell migration, respectively.

Microtubule plus-end assembly is mediated by the microtubule polymerase ch-TOG (encoded by the *CKAP5* gene) (Gard & Kirschner 1987; Brouhard *et al.* 2008). In order to further investigate the influence of increased microtubule plus-end assembly rates during migration and invasion and also to exclude unspecific effects of the Taxol treatment, *CKAP5* was repressed by siRNA in SK-Mel-103 and Colo201 cells. HCT116 was used as a control cell line. The repression of *CKAP5* was verified by western blot analyses (Fig 3.7a). Live cell microscopy experiments revealed a significant decrease of microtubule plus-end assembly rates in SK-Mel-103 and Colo201 cells to normal levels during both, mitosis and interphase, upon siRNA-mediated repression of *CKAP5* in comparison to *LUCIFERASE* siRNA transfected cells (Fig 3.7b). In HCT116 cells, microtubule plus-end assembly rates were not significantly influenced upon *CKAP5* repression (Fig. 3.7b).

Furthermore, repression of *CKAP5* also led to a significant decrease in the amount of cells exhibiting lagging chromosomes in Colo201 and SK-Mel-103 cells compared to *LUCIFERASE* siRNA transfected cells. In Colo201 cells, the number of cells showing lagging chromosomes was reduced from 6.7% to 3.6%, whereas in SK-Mel-103 cells the amount was reduced by 50% from 4% to 2%. (Fig 3.7c).

Following that, transwell migration and invasion assays were performed. Here, SK-Mel-103 and Colo201 cells displayed a significantly decreased migration and invasion potential after *CKAP5* repression in comparison to control transfected cells (Fig 3.7d-e). Upon *LUCIFERASE* siRNA transfection, Colo201 and SK-Mel-103 exhibited on average 78,333 migrated cells and 94,250 migrated cells, respectively, which were reduced to 53,417 cells and 72,250 cells upon *CKAP5* repression. Transwell invasion assays revealed on average 92 invaded Colo201 cells, which were reduced to 37 invaded cells per field upon *CKAP5* repression, and 353 invaded SK-Mel-103 cells, which were decreased to 254 cells per field after *CKAP5* repression.

The data upon repression of *CKAP5* substantiates the findings obtained upon low dose Taxol treatment: A decrease in microtubule plus-end assembly rates also decreased the migratory and invasive phenotype.

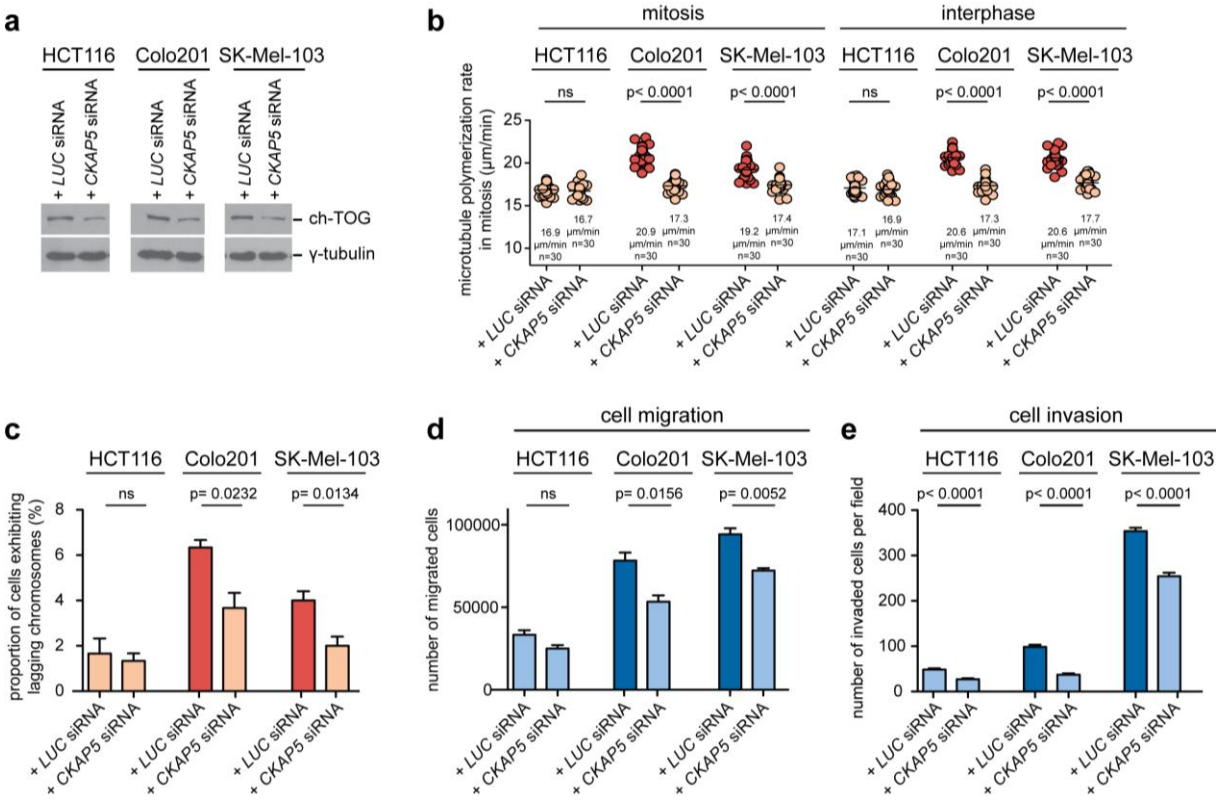

Figure 3.7: Inhibition of increased microtubule plus-end assembly rates suppresses migration and invasion. (a) Representative western blot detecting ch-TOG using HCT116, Colo201 and SK-Mel-103 cells transfected with 60 pmol *LUCIFERASE* or *CKAP5* siRNA. γ-tubulin served as loading control. **(b)** Measurements of mitotic and interphase microtubule plus-end assembly rates after repression of *CKAP5*. HCT116, Colo201 and SK-Mel-103 cells were transfected with 60 pmol *LUCIFERASE* or *CKAP5* siRNA. 1 h - 2 h prior to EB3 tracking experiments, cells were treated with 2 µM DME. Scatter dot plots show the average microtubule plus-end assembly rates of 20 microtubules per cell (mean ± sem, *t*-test, n=30 cells from three independent experiments). **(c)** Quantification of cells exhibiting lagging chromosomes after *CKAP5* or *LUCIFERASE* siRNA transfection as described in (a). Cells were synchronized at G_1/S transition by double thymidine block, released into the cell cycle for 8.5 - 9.5 h and fixed and stained for immunofluorescence microscopy. Cells displaying at least one CREST-positive chromatid were counted as positive. Bar graphs show proportion of cells with lagging chromosomes (mean ± sem, *t*-test, n=3 with a total of 300 anaphase cells). **(d)** Transwell migration assays after *CKAP5* or *LUCIFERASE* siRNA transfection as described in (a). 200,000 cells were seeded into cell culture inserts and bar graphs show the number of migrated cells after 24 h. (mean ± sem, *t*-test, n=3) **(e)** Transwell invasion assays after *CKAP5* or *LUCIFERASE* siRNA transfection as described in (a). 200,000 cells were seeded into cell culture inserts. After 48 h, the number of invaded cells in each picture of 30 randomly chosen pictures was determined. Pictures were taken with 40x magnification. Bar graphs show number of invaded cells per picture (mean ± sem, *t*-test, n=3).

Furthermore, it was of interest to investigate, whether an increase in microtubule plus-end assembly rates *per se* induces a migratory and invasive phenotype. To address this question, the microtubule polymerase ch-TOG/*CKAP5* or a control vector were overexpressed or cells were treated with low doses of Nocodazole. Our group showed recently that low concentrations of the microtubule destabilizing drug Nocodazole increased microtubule plus-end assembly rates (Ertych *et al.* 2014). HCT116 and SK-Mel-28 cells,

which neither exhibit increased microtubule plus-end assembly rates nor a migratory and invasive phenotype, were used for this approach.

The overexpression of *CKAP5* was verified by western blot analyses (Fig. 3.8a). EB3 tracking experiments were performed and revealed a significant increase in microtubule plus-end assembly rates during both, interphase and mitosis, upon *CKAP5* overexpression in comparison to control vector (Fig 3.8b). During mitosis, microtubule pus-end assembly rates were increased on average from 16.9 µm/min to 20.3 µm/min in HCT116 cells and 18.3 µm/min to 20.7 µm/min in SK-Mel-28 cells. During interphase, microtubule pus-end assembly rates were increased on average from 17.3 µm/min to 20.3 µm/min in HCT116 cells and from 17.9 µm/min to 20.6 µm/min in SK-Mel-28 cells. Under these conditions, transwell migration and invasion assays were performed to analyze the migratory and invasive phenotype after *CKAP5* overexpression (Fig 3.8c-d). Both, the migration and invasion potentials, of HCT116 and SK-Mel-28 cells were significantly increased after *CKAP5* overexpression. The migration potential was increased from 37,083 migrated HCT116 cells and 34,000 migrated SK-Mel-28 cells to 69,417 and 71,583 migrated cells, respectively. In HCT116 cells, the transwell invasion assays revealed on average 55 invaded cells per field after control vector transfection and 143 invaded cells upon *CKAP5* overexpression. In SK-Mel-28 cells, the number of invaded cells was increased from 66 invaded cells to 169 invaded cells upon *CKAP5* overexpression. As hypothesized from the induction of increased microtubule plus-end assembly rates during mitosis, HCT116 and SK-Mel-28 cells exhibited increased numbers of cells exhibiting lagging chromosomes after overexpression of *CKAP5* (Fig 3.8e). In HCT116 cells the proportion was increased from 1.6% to 4% and in SK-Mel-28 cells from 2% to 4.6% upon *CKAP5* overexpression.

In addition to *CKAP5* overexpression, cells were treated with 2 nM Nocodazole 2 h prior to the determination of microtubule plus-end assembly rates. Indeed, after Nocodazole treatment, cells exhibited increased microtubule plus-end assembly rates that were comparable to microtubule plus-end assembly rates measured upon *CKAP5* overexpression (Fig 3.8b). Transwell migration and invasion assays revealed a significantly increased migration and invasion potential (Fig 3.8bc-d), which was also comparable to the effects obtained upon *CKAP5* overexpression. Analyses of cells displaying lagging chromosomes revealed a slight increase in their occurrenc. In HCT116 cells, low dose Nocodazole treatment increased the number of lagging chromosomes from 1.5% to 3.25% on average, whereas in SK-Mel-28 cells this amount was increased from 1.6% to 3.3% in comparison to DMSO treated cells (Fig. 3.8e).

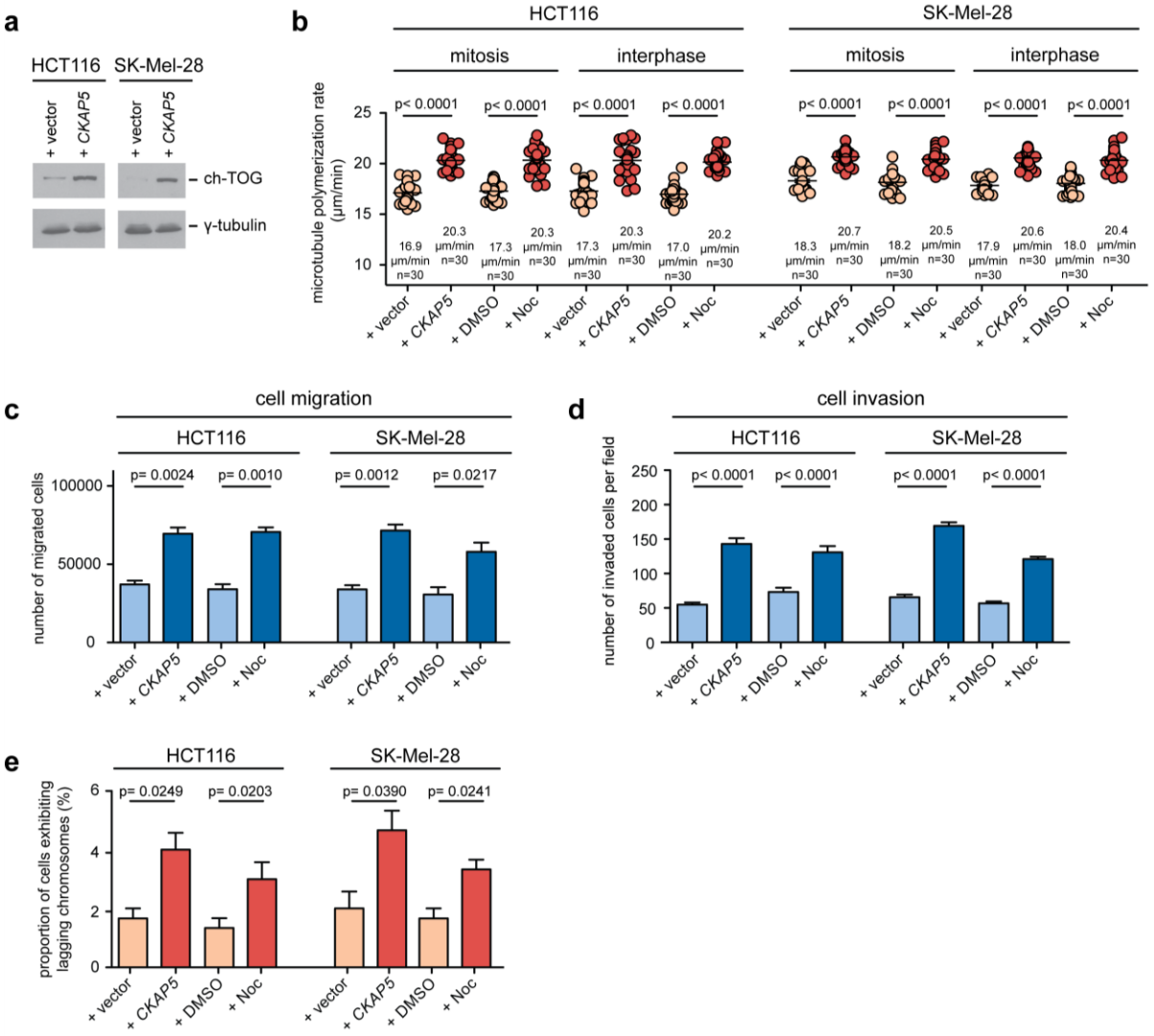

Figure 3.8: Induction of increased microtubule plus-end assembly rates triggers migration and invasion. (a) Representative western blot of HCT116 and SK-Mel-28 cells after overexpression of *CKAP5*. γ-tubulin served as loading control. **(b)** Measurements of mitotic and interphase microtubule plus-end assembly rates after overexpression of *CKAP5* or treatment with 2 nM Nocodazole for 2 h. Cells were treated with 2 µM DME 1 h - 2 h prior to EB3 tracking experiments. Scatter dot plots show the average microtubule plus-end assembly rates of 20 microtubules per cell (mean ± sem, *t*-test, n=30 cells from three independent experiments). **(c)** Transwell migration assays after overexpression of *CKAP5* or treatment with 2 nM Nocodazole. 200,000 cells were seeded into cell culture inserts. Bar graphs show number of migrated cells after 24 h (mean ± sem, *t*-test, n=3) **(d)** Transwell invasion assays after overexpression of *CKAP5* or treatment with 2 nM Nocodazole. 200,000 cells were seeded into cell culture inserts. Bar graphs show the number of invaded cells in every picture of 30 randomly chosen pictures from three independent experiments (mean ± sem, *t*-test, n=3). **(e)** Quantification of cells with lagging chromosomes after over expression of *CKAP5* or treatment with 2 nM Nocodazole. Cells were synchronized at G_1-S-transition by double thymidine block, released into the cell cycle for 8.5 h - 9.5 h and fixed and stained for immunofluorescence microscopy. Cells displaying at least one CREST-positive chromatid were quantified. Bar graphs show the proportion of cells with lagging chromosomes (mean ± sem, *t*-test, n=3-4 with a total of 300-400 anaphase cells).

3.1.3 Metastasis Associated Alterations In Human Cancer Induce Increased Microtubule Plus-End Assembly Rates

In human cancers, various alterations in gene expression are associated with a highly migratory and invasive phenotype. To address the question, whether the correlation between migration and invasion and altered microtubule dynamics can be detected also in cancer associated settings different gene alterations with prognostic significance were tested for their influence on microtubule dynamics. Thereby, inactivation of the retinoblastoma protein Rb is associated with the development of invasive cancers (Labrecque *et al.* 2016). In addition, overexpression of *E1A* and *E7* leads to inactivation of Rb. Furthermore, the overexpression of the receptor for hyaluronan-mediated motility (Rhamm/*HMMR*) is known to promote cellular motility and invasion (Maxwell *et al.* 2008; Crainie *et al.* 1999). Additionally, increased TGF-β signaling is highly correlated with metastasis in several cancer entities and known to induce EMT and to increase cell migration (Dalal *et al.* 1993; Meulmeester & Ten Dijke 2010).

HCT116 and SK-Mel-28 cells were used for siRNA-mediated repression of *RB*, for overexpression of *E7*, *E1A* and *HMMR* or for treatment with TGF-β. Transwell migration and invasion assays were conducted and confirmed the highly migratory and invasive potential after these treatments (Fig. 3.9a-b). Interestingly, in EB3 tracking experiments, *RB* repression, *E7*, *E1A* and *HMMR* overexpression or treatment with 10 ng/ml TGF-β for 3 h significantly increased microtubule plus-end assembly rates in mitosis and interphase in both cell lines (Fig. 3.9c-d). In HCT116 cells, the indicated treatments increased microtubule plus-end assembly rates in mitosis from 16.7-16.8 µm/min in control cells to 19.5-20.2 µm/min and in interphase from a range of 16.7-16.8 µm/min to 20.2-20.3 µm/min. In mitotic SK-Mel-28 cells, elevated microtubule polymerization rates of 19.5-20.5 µm/min were measured compared to 18.4-19.3 µm/min on average in control cells. During interphase, the indicated treatments increased microtubule plus-end assembly rates from 18.3-18.4 µm/min to polymerization rates ranging from 20.3-20.6 µm/min.

Thus, cancer relevant alterations, which are described to be associated with a highly invasive phenotype are accompanied by increased mitotic and interphase microtubule plus-end assembly rates.

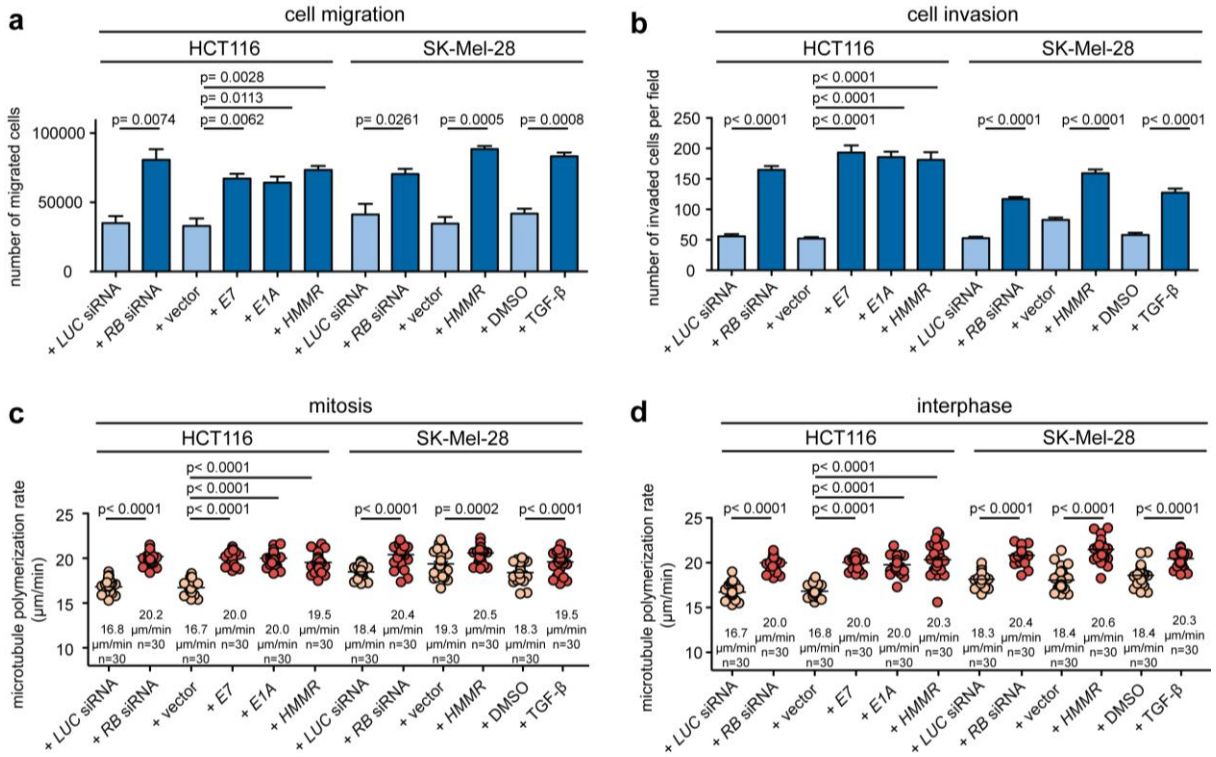

Figure 3.9: Invasion-associated alterations in cancer correlate with increased microtubule plus-end assembly rates. (a) Transwell migration assays of HCT116 and SK-Mel-28 cells after transfection with 60 pmol *LUCIFERASE* or *RB* siRNA, or overexpression of *E7*, *E1A* or *HMMR*, or after treatment with 10 ng/ml TGF-β. 200,000 cells were seeded and bar graphs show the amount of migrated cells after 24 h (mean ± sem, *t*-test, n=3). **(b)** Transwell invasion assays of HCT116 and SK-Mel-28 cells after the indicated treatments. 200,000 cells were seeded. Bar graphs show the number of invaded cells in every picture of 30 randomly chosen pictures from three independent experiments (mean ± sem, *t*-test, n=3). **(c)** EB3 tacking experiments of HCT116 and SK-Mel-28 cells in mitosis after the indicated treatments. Scatter dot plots show the average microtubule plus-end assembly rates of 20 microtubules per cell (mean ± sem, *t*-test, n=30 cells from three independent experiments). **(d)** EB3 tracking experiment of HCT116 and SK-Mel-28 cells in interphase after the indicated treatments. Scatter dot plots show the average microtubule plus-end assembly rates of 20 microtubules per cell (mean ± sem, *t*-test, n=30 cells from three independent experiments).

3.1.4 The Microtubule Plus-End Binding Protein EB1 Is Important For Microtubule-Dependent Signaling

The previous observations indicate a strong correlation between abnormally increased microtubule plus-end assembly rates and a migratory and invasive phenotype. Migration and invasion is mainly driven by different actin filament structures and their remodeling. But also microtubules are described to play a role during cell motility (Waterman-Storer & Salmon 1999). Still the question arises, how changes in microtubule dynamics affect cellular motility. An interesting hypothesis is that microtubule plus-ends might form moving signaling platforms, in which the end-binding protein EB1 plays an important role. Thus, it was of interest to investigate, whether the repression of *EB1* in human cancer cells would affect CIN and cell migration. Therefore, *EB1* was partially repressed by the use of siRNA in SW620

and SK-Mel-103 cells. Repression of *EB1* was verified by western blot analyses (Fig. 3.10a). Interestingly, *EB1* knock down did not affect microtubule plus-end assembly rates neither in mitosis nor in interphase (Fig 3.10b). However, the occurrence of cells with lagging chromosomes was significantly decreased (Fig 3.10c). Moreover, SK-Mel-103 cells showed a significant decreased migration potential upon *EB1* repression in transwell migration assays (Fig. 3.10d).

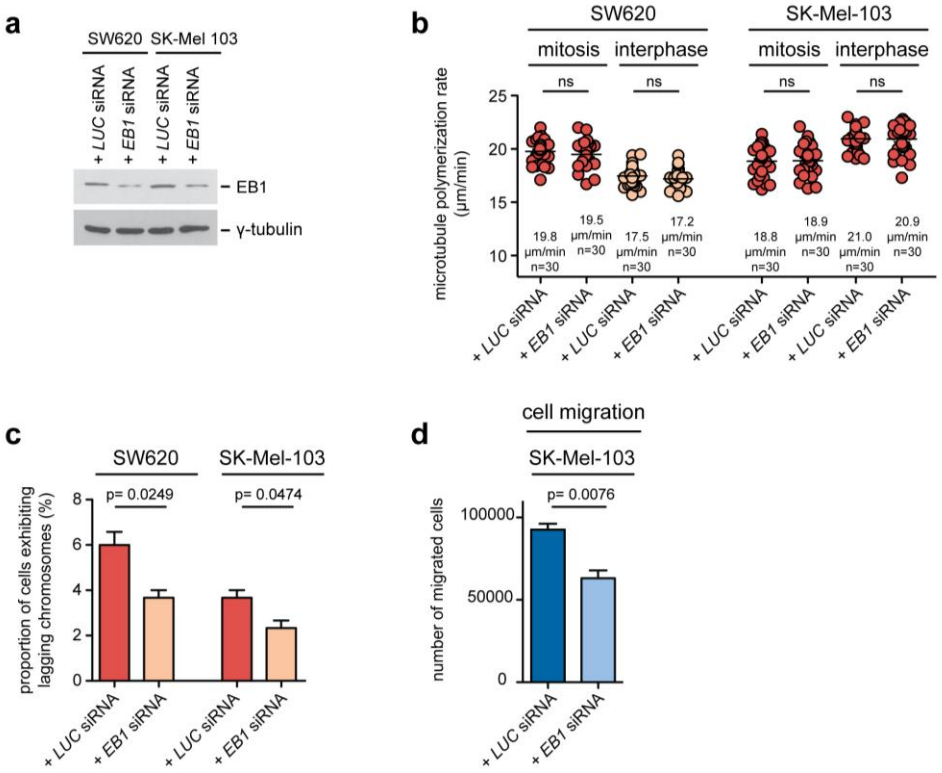

Figure 3.10: Repression of *EB1* reduces the migratory and CIN phenotype while having no impact on microtubule plus-end assembly rates. (a) Representative western blot of SW620 and SK-Mel-103 cells after repression of *EB1*. Cells were transfected with 80 pmol *LUCIFERASE* or *EB1* siRNA. γ-tubulin served as loading control **(b)** Measurements of microtubule plus-end assembly rates in mitosis and interphase after repression of *EB1*. SW620 and SK-Mel-103 cells were transfected with 80 pmol *LUCIFERASE* or *EB1* siRNA. Scatter dot plots show the average microtubule plus-end assembly rates of 20 microtubules per cell (mean ± sem, *t*-test, n=30 cells from three independent experiments). **(c)** Quantification of cells exhibiting lagging chromosomes after repression of *EB1*. Cells were synchronized at G_1/S transition by double thymidine block, released into the cell cycle for 8.5 h - 9.5 h and fixed and stained for immunofluorescence microscopy. Cells displaying at least one CREST-positive chromatid were counted as positive. Bar graphs show the proportion of cells displaying lagging chromosomes (mean ± sem, *t*-test, n=3 with a total of 300 anaphase cells). **(d)** Transwell migration assays after repression of *EB1*. 200,000 cells were seeded and bar graphs show the number of migrated cells after 24 h (mean ± sem, *t*-test, n=3)..

These results revealed that EB1 is involved in triggering enhanced migration and CIN in SK-Mel-103 and SW620 cells in response to increased microtubule plus-end assembly rates. Since partial *EB1* repression did not alter the microtubule plus-end assembly rates itself, the results suggest, that EB1 acts downstream of microtubules.

3.1.5 SW620 And SK-Mel-103 Cells Exhibit Elevated Levels Of Active TRIO

The repression of *EB1* seems to disrupt a signaling pathway, which is important for migration and invasion downstream of microtubule dynamics. Therefore, it was of utmost interest to investigate, how EB1-derived signaling affect cellular motility. Recently, the binding of EB1 to TRIO was described (Van Haren *et al.* 2014). TRIO is a guanine nucleotide exchange factor (GEF) for Rac1 and is part of a gene signature of genes implicated in cell migration (referred to as HCCS24) as well as of the HET70 signature of genes associated with aneuploidy (Kohn *et al.* 2012, Sheltzer 2013;). Therefore, TRIO represents an interesting candidate that may link microtubule dynamics to CIN and cell migration.

To test for an involvement of TRIO in CIN and migration, GEF assays were performed to analyze TRIO activity in chromosomally instable SW620 and highly migratory SK-Mel-103 cells. For this, an agarose bead coupled nucleotide-free Rac1 mutant (Rac1 G15A) that binds to activated GEFs with increased affinity was used to pull down active TRIO.

TRIO activity in chromosomal instable SW620 cells was compared to chromosomal stable HCT116 cells during mitosis. Cells were arrested in mitosis by treatment with 2 µM DME for 16 h. Additionally, cells were treated with DMSO or 0.2 nM Taxol. Treatment with the TRIO specific inhibitor ITX3 (Bouquier *et al.* 2009) served as a control. Western blot analyses revealed similar levels of endogenous TRIO in HCT116 and SW620 cells, which were not altered upon Taxol or ITX3 treatment (depicted as input) (Fig 3.11a). However, an increased proportion of active TRIO was immunoprecipitated using the GST-Rac1 G15A agarose beads in DMSO treated SW620 cells compared to DMSO treated HCT116 cells. Importantly, the amount of active TRIO was reduced upon low dose Taxol treatment. ITX3 treated cells exhibited the lowest proportion of active TRIO, demonstrating a significant inhibition of TRIO activity (Fig 3.11a).

GEF-assays were also performed using the melanoma cell lines SK-Mel-28 and SK-Mel-103. Here, it was distinguished between mitotic and interphase cells. Mitotic cells were obtained by treatment with 2 µM DME for 16 h. Additionally, cells were treated with DMSO, 0.5 nM Taxol or 15 µM ITX3. Interestingly, SK-Mel-103 cells displayed elevated levels of endogenous TRIO in comparison to SK-Mel-28 (depicted as input). These increased levels of endogenous TRIO were not altered upon Taxol or ITX3 treatment (Fig 3.11b). After immunoprecipitation using GST-Rac1 G15A agarose beads a higher proportion of active TRIO was detected in DMSO treated SK-Mel-103 when compared to DMSO treated SK-Mel-28 cells. This increased level of active TRIO was reduced by treatment with 0.5 nM Taxol. ITX3 treated cells exhibited very low proportions of active TRIO (Fig 3.11b).

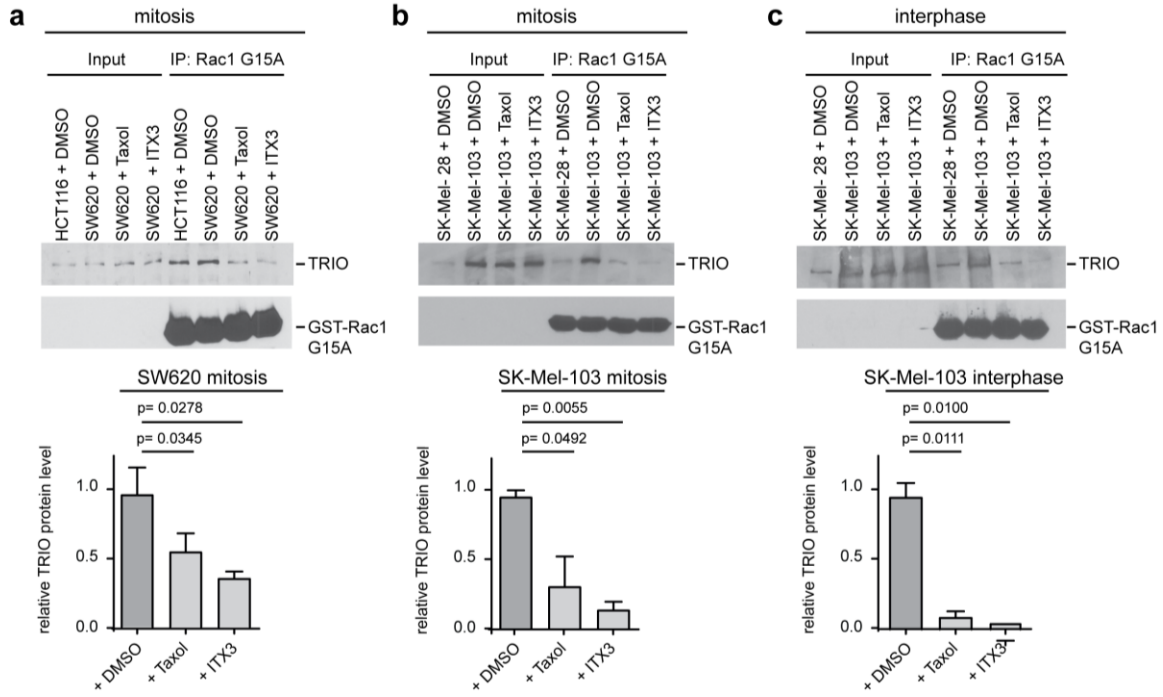

Figure 3.11: Elevated levels of active TRIO in SW620 and SK-Mel-103 cells depend on increased microtubule plus-end assembly rates. (a) HCT116 cells and SW620 cells were treated with 2 µM DME for 16 h in combination with DMSO, 0.2 nM Taxol or 15 µM ITX3. GEF assays were performed using 2 mg lysate and 10 µg GST-Rac1 G15A agarose beads for 1 h at 4°C. A representative western blot detecting TRIO is shown and quantifications of relative TRIO protein levels from three independent experiments are given. Bar graphs show amounts of active TRIO normalized to control treated cells (mean ± sem, *t*-test, n=3). **(b)** SK-Mel-28 and SK-Mel-103 cells were treated with 2 µM DME for 16 h in combination with DMSO, 0.5 nM Taxol or 15 µM ITX3. GEF assays were performed with 2 mg lysate and 10 µg GST-Rac1 G15A agarose beads for 1 h at 4°C. A representative western blot detecting TRIO is shown and quantifications of relative TRIO protein levels from three independent experiments are given. Bar graphs show amounts of active TRIO normalized to control treated cells (mean ± sem, *t*-test, n=3). **(c)** Asynchronously growing SK-Mel-28 and SK-Mel-103 cells were treated with DMSO, 0.5 nM Taxol or 15 µM ITX3 for 16 h. GEF assays were performed using 2 mg lysate and 10 µg GST-Rac1 G15A agarose beads for 1 h at 4°C. A representative western blot detecting TRIO is shown and quantifications of relative TRIO protein levels from three independent experiments are given. Bar graphs show proportions of active TRIO normalized to control treated cells (mean ± sem, *t*-test, n=3).

SK-Mel-103 and SK-Mel-28 cells were also analyzed during interphase. Asynchronously growing cells were treated with DMSO, 0.5 nM Taxol or 15 µM ITX3 for 16 h. Also during interphase, SK-Mel-103 cells exhibited increased proportions of endogenous TRIO as opposed to SK-Mel-28 cells (depicted as input) (Fig 3.11c). Higher proportions of active TRIO were immunoprecipitated using GST-Rac1 G15A agarose beads in DMSO treated SK-Mel-103 as opposed to DMSO treated SK-Mel-28 cells. These elevated proportions were reduced upon low dose Taxol and ITX3 treatment.

In summary, GEF assays revealed elevated levels of active TRIO in the CIN cell line SW620 during mitosis as well as in the highly migratory and invasive and cell line SK-Mel-103 in interphase and mitosis. GEF activity depended on increased microtubule plus-end assembly rates, since Taxol treatment decreased the proportion of active TRIO.

TRIO was shown to bind to microtubule plus-ends *via* Nav1/EB1-complex or directly *via* EB1 (Van Haren *et al.* 2014). Therefore, it was tested, whether GEF activity of TRIO depends on its microtubule plus-end localization *via* EB1. SW620 and SK-Mel-103 cells were transfected with 80 pmol *LUCIFERASE* or *EB1* siRNA. To investigate active TRIO levels in mitotic SW620 cells, cells were treated with 2 µM DME for 16 h. GEF assays were performed and revealed decreased proportions of active TRIO upon *EB1* repression in comparison to cells transfected with *LUCIFEARSE* siRNA (Fig. 3.12a). SK-Mel-103 cells were analyzed during mitosis and interphase. Mitotic cells were obtained by treatment with 2 µM DME for 16 h. During both, mitosis and interphase, SK-Mel-103 cells exhibited decreased proportions of active TRIO upon repression of *EB1* (Fig. 3.12b-c), revealing an EB1-dependent activation of TRIO.

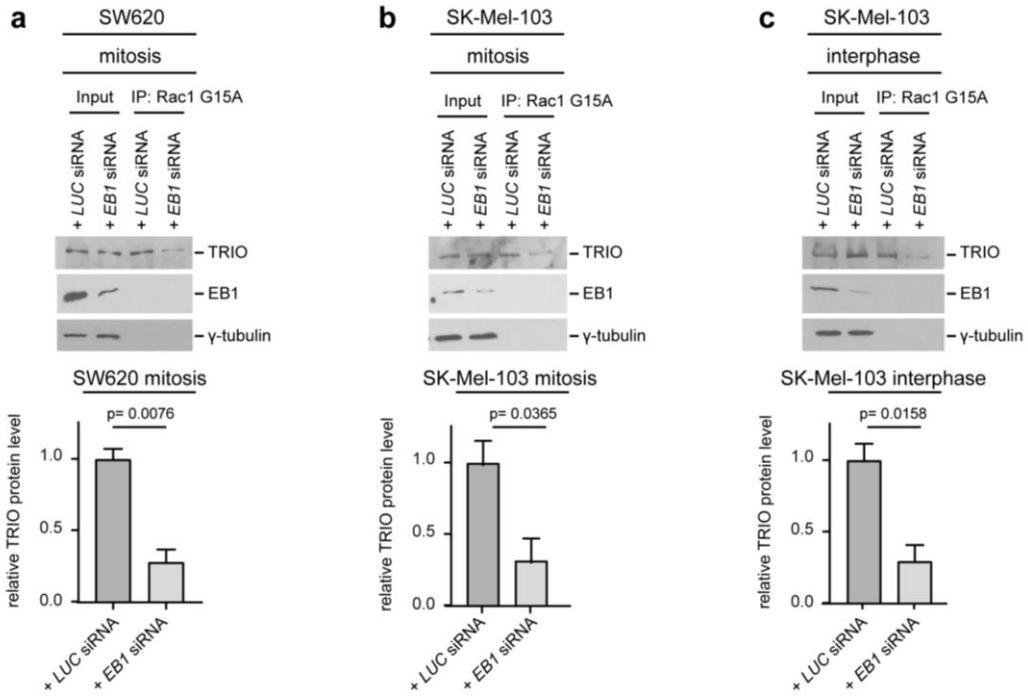

Figure 3.12: TRIO activity depends on its microtubule plus-end localization *via* EB1. (a) SW620 cells were transfected with 80 pmol *LUCIFERASE* or *EB1* siRNA. Cells were treated with 2 µM DME for 16 h. GEF assays were performed using 2 mg lysate and 10 µg GST-Rac1 G15A agarose beads for 1 h at 4°C. A representative western blot and quantifications of active TRIO protein levels are given. Bar graphs show proportions of active TRIO normalized to *LUCIFERASE* transfected cells (mean ± sem, *t*-test, n=3). **(b)** SK-Mel-103 cells were transfected with 80 pmol *LUCIFERASE* or *EB1* siRNA. Cells were treated with 2 µM DME for 16 h. GEF assays were performed using 2 mg lysate and 10 µg GST-Rac1 G15A agarose beads for 1 h at 4°C. A representative western blot and quantifications of active TRIO protein levels are given. Bar graphs show proportions of active TRIO normalized to *LUCIFERASE* transfected cells (mean ± sem, *t*-test, n=3). **(c)** SK-Mel-103 cells were transfected with 80 pmol *LUCIFERASE* or *EB1* siRNA. GEF assays were performed using 2 mg lysate and 10 µg GST-Rac1 G15A agarose beads for 1 h at 4°C. A representative western blot and quantifications of active TRIO protein levels are shown. Bar graphs show proportions of active TRIO normalized to *LUCIFERASE* transfected cells (mean ± sem, *t*-test, n=3).

3.1.6 Inhibition Of TRIO Decreases CIN And Migration in SW620 and SK-Mel-103 Cells

In order to analyze whether increased TRIO activity as detected in the GEF assays influence the migratory and the CIN phenotype, SK-Mel-103 and SW620 cells were treated with the TRIO specific inhibitor ITX3. ITX3 treatment did not alter the microtubule plus-end assembly rates during mitosis and interphase in neither SW620 nor SK-Mel-103 cells (Fig. 3.13a).

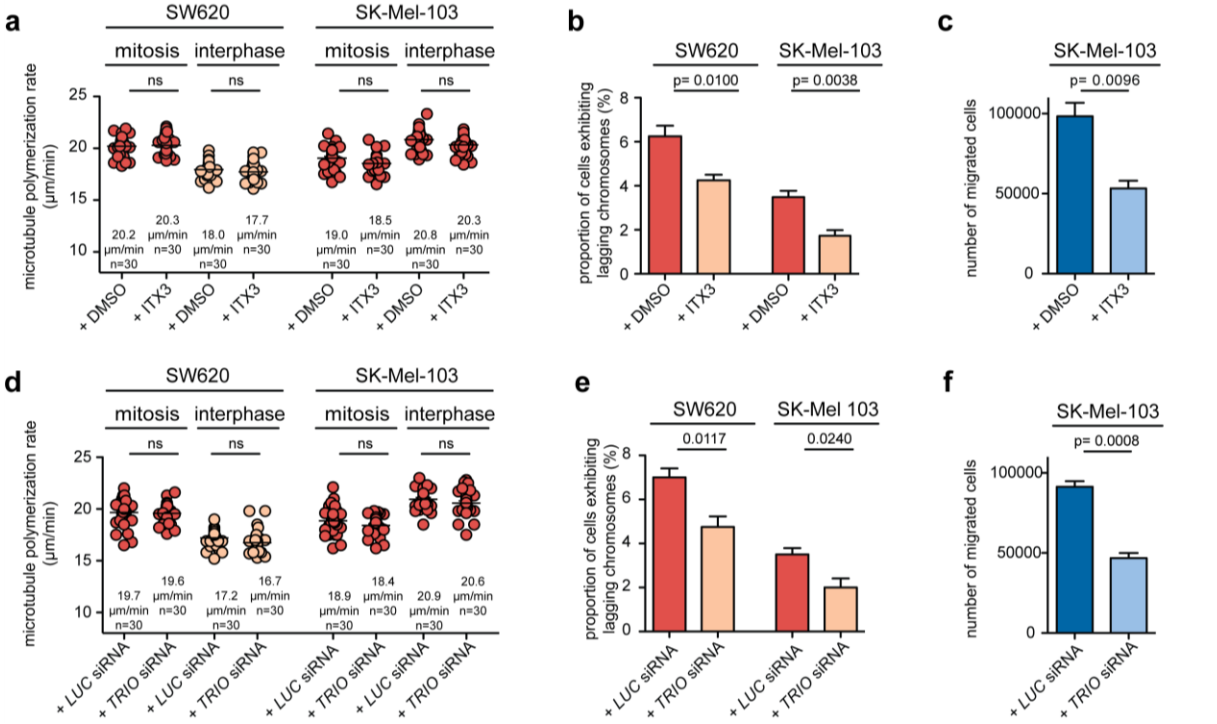

Figure 3.13: Inhibition of TRIO suppresses the generation of lagging chromosomes and inhibits cell migration. (a) Measurements of mitotic and interphase microtubule plus-end assembly rates in SW620 and SK-Mel-103 cells treated with DMSO or 15 µM ITX3. Scatter dot plots show the average microtubule plus-end assembly rates of 20 microtubules per cell (mean ± sem, *t*-test, n=30 cells from three independent experiments). **(b)** Quantification of cells exhibiting lagging chromosomes during anaphase. SW620 and SK-Mel-103 cells were treated with DMSO or 15 µM ITX3. Cells were synchronized at the G_1/S transition by double thymidine block and released into the cell cycle. After 8.5 h - 9.5 h cells were fixed and stained for immunofluorescence microscopy. Bar graphs show quantification of cells showing at least one CREST-positive chromatid (mean values ± sem, *t*-test, n=4 with a total of 400 anaphase cells). **(c)** Transwell migration assays of SK-Mel-103 cells. Cells were treated with DMSO or 15 µM ITX3. 200,000 cells were seeded into cell culture inserts. Bar graphs show the number of migrated cells after 24 h (mean ± sem, *t*-test, n=3). **(d)** Measurements of mitotic and interphase microtubule plus-end assembly rates in SW620 and SK-Mel-103 cells transfected with 60 pmol *LUCIFERASE* or *TRIO* siRNA. Scatter dot plots show the average microtubule plus-end assembly rates of 20 microtubules per cell (mean ± sem, *t*-test, n=30 cells from three independent experiments). **(e)** Quantification of cells showing lagging chromosomes during anaphase. SW620 and SK-Mel-103 cells were transfected with 60 pmol *LUCIFERASE* or *TRIO* siRNA. Cells were synchronized at the G_1/S transition and released into the cell cycle. After 8.5 h - 9.5 h cells were fixed and stained for immunofluorescence microscopy and the occurrence of lagging chromosomes was analyzed. Bar graphs show the amount of cells exhibiting at least one CREST-positive chromatid (mean values ± sem, *t*-test, n=4 with a total of 400 anaphase cells). **(f)** Transwell migration assays of SK-Mel-103 cells. Cells were transfected with 60 pmol *LUCIFERASE* or *TRIO* siRNA. 200,000 cells were seeded and bar graphs show the proportion of migrated cells after 24 h (mean ± sem, *t*-test, n=3).

However, the proportion of cells showing lagging chromosomes was significantly reduced in both cell lines. In SW620 cells, the occurrence of lagging chromosomes was reduced from 6.25% to 4.25% on average, whereas in SK-Mel-103 cells the amount was decreased from 3.5% to 1.75% on average (Fig. 3.13b). Transwell migration assays of SK-Mel-103 cells also revealed a decreased cell migration activity. Upon ITX3 treatment, the number of migrated cells was reduced from 98,333 cells to 53,333 cells (Fig. 3.13c).

To exclude unspecific effects of the TRIO inhibitor, siRNA-mediated repression of *TRIO* was conducted. These experiments confirmed the results obtained by ITX3 treatment. Although the microtubule plus-end assembly rates were not significantly altered during mitosis and interphase (Fig. 3.13d), a significant decrease in the occurrence of lagging chromosomes was detected in both SW620 and SK-Mel-103 cells upon *TRIO* repression. SW620 cells exhibited on average 4.75% lagging chromosomes, whereas *LUCIFERASE* transfected cells exhibited 7%. In SK-Mel-103 cells, the amount of cells displaying lagging chromosomes was reduced from 3.5% to 2% on average (Fig. 3.13e). In addition, SK-Mel-103 cells exhibited a reduced migration behavior upon *TRIO* repression compared to *LUCIFERASE* transfected cells. The amount of migrated cells was reduced from 91,333 cells to 46,667 cells (Fig. 3.13f). These results might indicate that increased TRIO activity can account for the induction of lagging chromosomes and increased cell migration.

3.1.7 Elevated Rac1 Activity Affects CIN And Migration In SW620 And SK-Mel-103 Cells

The previous experiments revealed an increased level of active TRIO in the CIN cell line SW620 during mitosis and in the highly migratory and invasive cell line SK-Mel-103. Since TRIO functions as a GEF for Rac1 (Blangy *et al.* 2000; Cannet *et al.* 2014), it was of interest to investigate whether Rac1 activity was increased in these cells. To test this, PAK-PBD agarose beads were used for pull down assays to isolate GTP-bound Rac1 from cell lysates derived from mitotic HCT116 and SW620 cells and from mitotic and interphase SK-Mel-28 and SK-Mel-103 cells.

HCT116 and SW620 cells were synchronized in mitosis by treatment with 2 µM DME for 16 h. The treatment was combined with DMSO, 0.2 nM Taxol, 15 µM ITX3 or 40 µM of the Rac1 inhibitor NSC23766. While the overall Rac1 levels did not vary significantly between the two cell lines, DMSO treated SW620 cells displayed nearly 1.5 fold higher levels of active Rac1 as opposed to DMSO treated HCT116 cells. Importantly, Taxol treatment of SW620 cells reduced Rac1 activity to levels similar to HCT116 cells. The inhibition of Rac1 by using its specific inhibitor NSC23766 served as a control and revealed a significant inhibition of

Rac1, whereas treatment with the TRIO inhibitor ITX3 revealed the dependency of Rac1 on TRIO (Fig. 3.14a).

Rac1 pull down assays were also performed with mitotic and interphase SK-Mel-28 and SK-Mel-103 cells. To obtain mitotic lysates, SK-Mel-28 and SK-Mel-103 cells were treated with 2 µM DME for 16 h in combination with DMSO, 0.5 nM Taxol, 40 µM NSC23766 or 15 µM ITX3. Rac1 activity assays using mitotic cell lysates revealed nearly 1.5-fold increased levels of active Rac1 in DMSO treated SK-Mel-103 cells compared to DMSO treated SK-Mel-28 cells, whereas the overall Rac1 levels did not vary between the two cell lines. Similar to the experiment using SW620 cells, treatment with low doses Taxol, NSC23766 and ITX3 reduced the proportion of active Rac1 also in the melanoma cells (Fig. 3.14b).

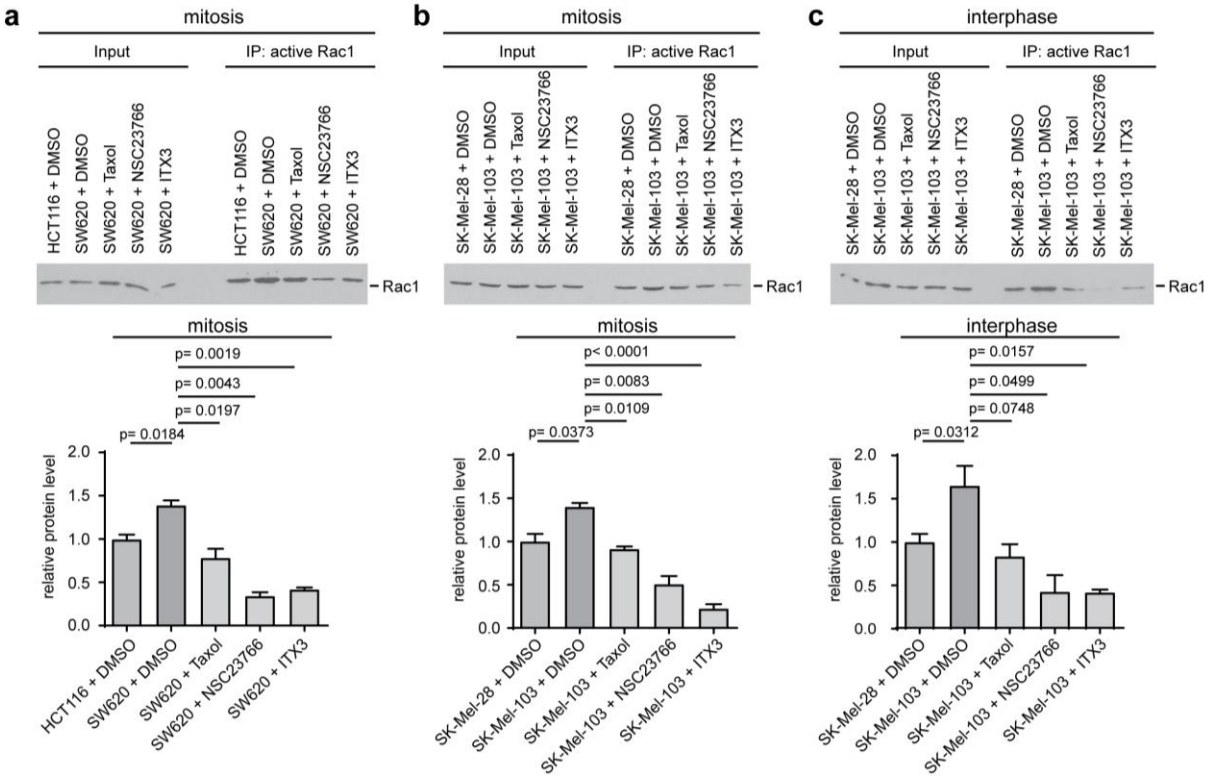

Figure 3.14: Elevated levels of active Rac1 are dependent on increased microtubule plus-end assembly rates. (a) HCT116 cells were treated with DMSO and SW620 cells were treated with DMSO, 0.2 nM Taxol, 40 µM NSC23766 or 15 µM ITX3 for 16 h combined with 2 µM DME to synchronize cells in mitosis. 1.5 mg of cell lysates were incubated with 10 µg PAK-PBD agarose beads for 30 min at 4°C and active Rac1 was precipitated and detected on western blot using Rac1 specific antibodies. A representative western blot is shown. Western blot quantifications of active Rac1 protein levels normalized to DMSO treated control cells are represented as bar graphs (mean ± sem, *t*-test, n=3). **(b)** SK-Mel-28 and SK-Mel-103 cells were treated with 2 µM for 16 h combined with DMSO, 0.5 nM Taxol, 40 µM NSC23766 or 15 µM ITX3 and processed as HCT116 and SW620 described in (a). A representative western blot is shown. Western blot quantifications of active Rac1 protein levels normalized to DMSO treated control cells are represented as bar graphs (mean ± sem, *t*-test, n=3). **(c)** Asynchronously growing SK-Mel-28 cells were treated with DMSO and SK-Mel-103 cells were treated with DMSO, 0.5 nM Taxol, 40 µM NSC23766 or 15 µM ITX3 for 16 h. Interphase cell lysates were processed as described in (a). A representative western blot is shown. Western blot quantifications of active Rac1 protein levels normalized to DMSO treated control cells are represented as bar graphs (mean ± sem, *t*-test, n=3).

SK-Mel-28 and SK-Mel-103 cells were also analyzed regarding their proportions of active Rac1 during interphase. Similar to mitotic cells, DMSO treated interphase SK-Mel-103 cells exhibited higher levels of active Rac1 as opposed to DMSO treated SK-Mel-28 cells. Here, the level of active Rac1 was increased approximately 1.75-fold. Also in interphase, these elevated Rac1 levels could be reduced by Taxol, as well as by NSC23766 and ITX3 treatment (Fig 3.14c).

Active Rac1 pull-down assays revealed elevated levels of active Rac1 in SW620 cells during mitosis and in SK-Mel-103 cells during both, mitosis and interphase. Since ITX3 treatment reduced the levels of active Rac1, Rac1 was verified as a downstream target of TRIO.

In order to further evaluate the relevance of active Rac1 for the migrating and invasive phenotype as well as for the generation of lagging chromosomes, a constitutively active mutant of Rac1 (Rac1 Q61L) was overexpressed in HCT116 cells. HCT116 cells exhibit neither a migratory phenotype nor elevated amounts of cells with lagging chromosomes. However, after overexpression of *Rac1* Q61L, the migration potential of HCT116 cells was enhanced from 35,667 cells to 69,000 cells on average. Treatment with the Rac1 inhibitor NSC23766 reduced cell migration observed upon *Rac* Q61L overexpression to a level comparable to the control transfected cells, showing the specificity of the *Rac1* Q61L overexpression (Fig. 3.15a).

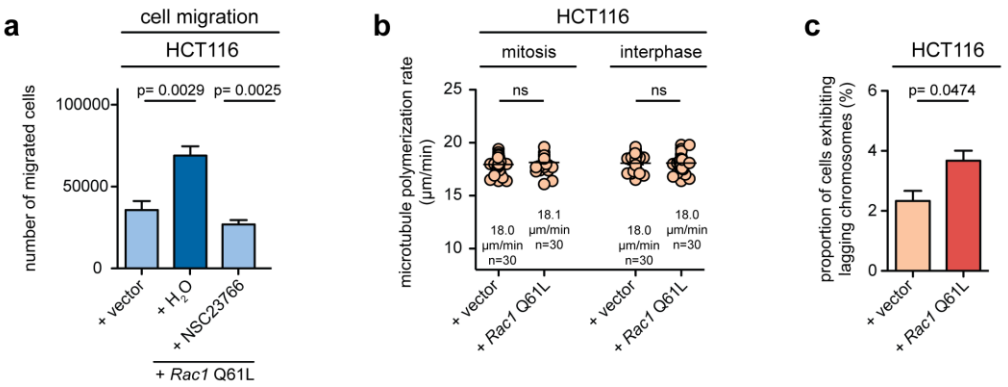

Figure 3.15: Overexpression of a constitutively active Rac1 mutant protein induces migration and the generation of lagging chromosomes. (a) Transwell migration assays of HCT116 cells transfected with a constitutively active mutant of Rac1 (Rac1 Q61L).10 µg *Rac1* Q61L were overexpressed and cells were treated with H_2O or 40 µM NSC23766. 200,000 cells were seeded for the migration assay. Bar graphs show the number of migrated cells after 24 h (mean ± sem, *t*-test, n=3). **(b)** Measurements of mitotic and interphase microtubule plus-end assembly rates in HCT116 cells with an overexpression of *Rac1* Q61L. 1 h prior to EB3 tracking experiments, cells were treated with 2 µM DME. Scatter dot plots show the average microtubule plus-end assembly rates of 20 microtubules per cell (mean ± sem, *t*-test, n=30 cells from three independent experiments). **(c)** Quantification of HCT116 cells displaying lagging chromosomes during anaphase after overexpression of *Rac1* Q61L. Cells were synchronized at G_1/S transition by double thymidine block and released into the cell cycle. After 8.5 h cells were fixed and stained for immunofluorescence microscopy and cells with lagging chromosomes were quantified. Bar graphs show the amount of HCT116 cells exhibiting at least one CREST-positive chromatid (mean values ± sem, *t*-test, n=3 with a total of 300 anaphase cells).

Interestingly, EB3 tracking experiments revealed that the overexpression of *Rac1* Q61L did not affect microtubule plus-end assembly rates (Fig. 3.15b). However, the quantification of cells with lagging chromosomes during anaphase showed increased amounts from 2.3% in control vector transfected cells to 3.6% in *Rac1* Q61L expressing cells (Fig. 3.15c).

Since the overexpression of a constitutively active Rac1 mutant induced a migratory phenotype and the generation of lagging chromosomes, the question arose whether a dominant negative mutant of Rac1 would reduce migration and the amount of cells showing lagging chromosomes in migratory and CIN cells. To test this, a dominant negative mutant of Rac1 (Rac1 T17N), which is described to inhibit Rac1´s function (Ridley *et al.* 1992), was overexpressed in SK-Mel-103 and SW620 cells. In transwell migration assays, the overexpression of *Rac1* T17N indeed led to a decrease of the migration potential. Upon control vector transfection, 95,417 migrating cells were detected on average, which were reduced to 51,667 cells upon overexpression of *Rac1* T17N (Fig. 3.16a). While having no significant influence onto the microtubule plus-end assembly rates of SW620 and SK-Mel-103 cells (Fig. 3.16b), the amount of cells exhibiting lagging chromosomes was significantly decreased (Fig. 3.16c). Control transfected SK-Mel-103 cells exhibited 4% lagging chromosomes on average, which were reduced to 2.25% upon overexpression of *Rac1* T17N. In SW620 cells, the occurrence of lagging chromosomes was reduced from 6.7% to 3.3%.

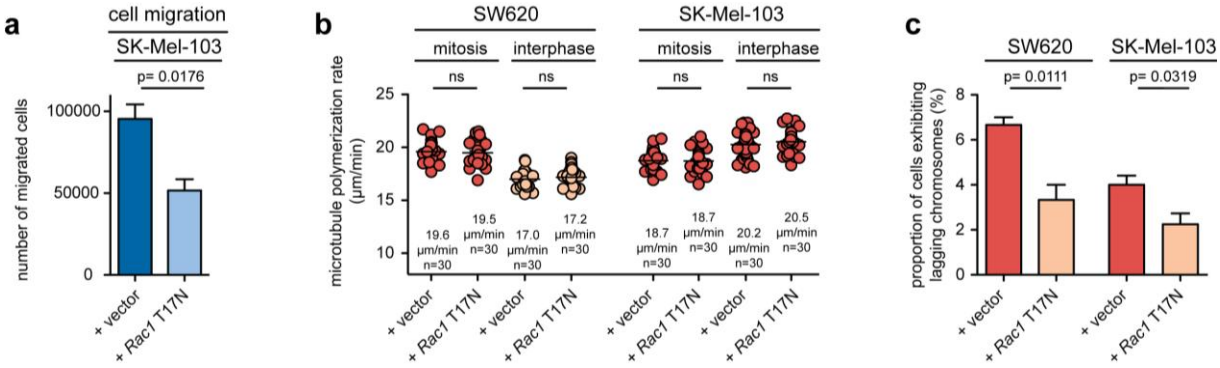

Figure 3.16: Overexpression of a dominant negative mutant protein of Rac1 reduces migration and the generation of lagging chromosomes in SW620 and SK-Mel-103 cells. (a) Transwell migration assays of SK-Mel-103 cells transfected with *Rac1* T17N.10 µg *Rac1* T17N or control vector were overexpressed. 200,000 cells were seeded in cell culture inserts for migration assay. Bar graphs show the amount of migrated cells after 24 h (mean ± sem, *t*-test, n=3). **(b)** Measurements of mitotic and interphase microtubule plus-end assembly rates in SW620 and SK-Mel-103 cells with an overexpression of *Rac1* T17N. 1 h - 2 h prior to EB3 tracking experiments, cells were treated with 2 µM DME. Scatter dot plots show the average microtubule plus-end assembly rates of 20 microtubules per cell (mean ± sem, *t*-test, n=30 cells from three independent experiments). **(c)** Quantification of cells showing lagging chromosomes during anaphase in SW620 and SK-Mel-103 cells with an overexpression of *Rac1* T17N. Cells were synchronized at G_1/S transition by double thymidine block and released into the cell cycle. After 8.5 h - 9.5 h cells were fixed and stained for immunofluorescence microscopy. Bar graphs show the amount of cells exhibiting at least one CREST-positive signal (mean ± sem, *t*-test, n=3 (SW620) - 4 (SK-Mel-103) with a total of 300-400 anaphase cells).

To further substantiate the role of Rac1 in cell migration and in the generation of lagging chromosomes, Rac1 activity was inhibited in SW620 and SK-Mel-103 cells by treatment with the Rac1 specific inhibitor NSC23766. In transwell migration assays, NSC23766 treatment led to a significant decrease of migrating SK-Mel-103 cells. In comparison to control treated cells, the amount of migrated cells was reduced from 93,250 cells to 44,333 cells on average upon NSC23766 treatment (Fig. 3.17a). In addition, analyses of lagging chromosomes in SW620 and SK-Mel-103 cells revealed a decreased number of cells displaying lagging chromosomes after treatment with NSC23766. The occurrence of lagging chromosomes was reduced from 6.3% to 3.3% and 4.3% to 2% in SW620 and SK-Mel-103 cells, respectively (Fig. 3.17b). However, microtubule plus-end assembly rates were neither altered in interphase nor in mitosis in both cell lines (Fig. 3.17c).

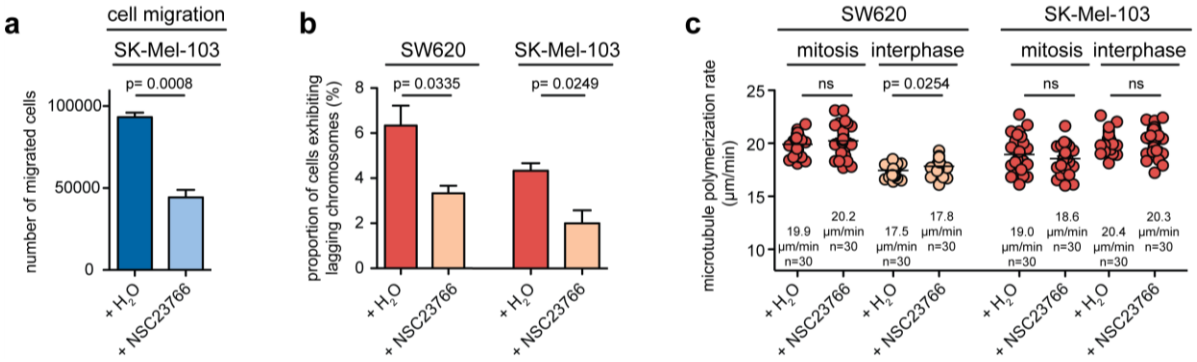

Figure 3.17: Inhibition of Rac1 by its specific inhibitor decreases migration and the generation of lagging chromosomes. (a) Transwell migration assays of SK-Mel-103 cells treated with H_2O or 40 µM NSC23766. 200,000 cells were seeded for the migration assay. Bar graphs show the number of migrated cells after 24 h (mean ± sem, *t*-test, n=3). **(b)** Quantification of cells showing lagging chromosomes during anaphase in SW620 and SK-Mel-103 cells treated with H_2O or 40 µM NSC23766. Cells were synchronized by double thymidine block and released into the cell cycle. After 8.5 h - 9.5 h, cells were fixed and stained for immunofluorescence microscopy. Bar graphs show the proportion of cells exhibiting at least one CREST-positive chromatid (mean ± sem, *t*-test, n=3 with a total of 300 anaphase cells). **(c)** Measurements of mitotic and interphase microtubule plus-end assembly rates in SW620 and SK-Mel-103 cells. Cells were treated with H_2O or 40 µM NSC23766 for 2 h. 1-2 h prior to EB3 tracking experiments, cells were treated with 2 µM DME. Scatter dot plots show the average microtubule plus-end assembly rates of 20 microtubules per cell (mean ± sem, *t*-test, n=30 cells from three independent experiments).

These results substantiate the hypothesis, that elevated levels of Rac1 contribute to both, a migratory phenotype and the generation of lagging chromosomes, in highly migratory cells exhibiting CIN.

3.1.8 The Arp2/3 Complex Acts Downstream Of Rac1 During Migration And The Development Of CIN

Rac1 is well described for its role in lamellipodia formation during cell motility. In the lamellipodium, actin branching is achieved by Rac1-mediated activation of the Arp2/3 complex (Ridley *et al.* 2003). Therefore, it was of interest to investigate whether the Arp2/3 complex acts as a downstream effector of Rac1 during migration and chromosome segregation.

To address this, inhibition of Arp2/3 was achieved by using the specific Arp2/3 inhibitor CK666 in SW620 and SK-Mel-103 cells. Transwell migration assays using SK-Mel-103 cells were performed and revealed a significantly decreased amount of migrated cells upon CK666 treatment. The number of migrated SK-Mel-103 cells was reduced from 89,667 cells on average in control experiments to 58,167 migrated cells upon CK666 treatment (Fig. 3.18a). Analyses of cells displaying lagging chromosomes revealed a significant decrease of chromosome missegregation in both cell lines. In CK666 treated SW620 cells, the amount of cells showing lagging chromosomes was reduced from 6% to 3.6% on average, whereas CK666 treatment in SK-Mel-103 cells decreased the number from 4.3% to 2.3% (Fig. 3.18b). Similar to treatments with NSC23766 and ITX3, CK666 treatment had no significant influence on the microtubule plus-end assembly rates during mitosis and interphase in SW620 and SK-Mel-103 cells (Fig. 3.18c).

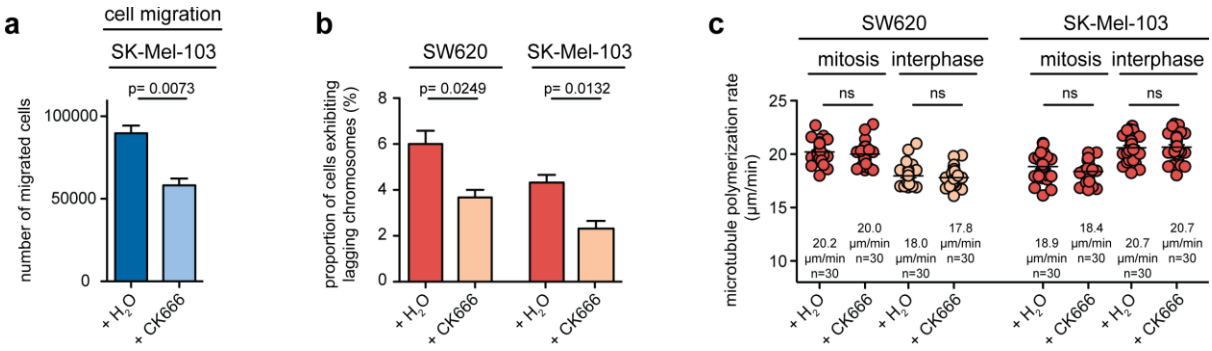

Figure 3.18: Inhibition of the Arp2/3 complex decreases migration and the generation of lagging chromosomes. (a) Transwell migration assays of SK-Mel-103 cells treated with H_2O or 20 µM CK666. 200,000 cells were seeded in cell culture inserts for the migration assay. Bar graphs show the number of migrated cells after 24 h (mean ± sem, *t*-test, n=3). **(b)** Quantification of cells exhibiting lagging chromosomes during anaphase in SW620 and SK-Mel-103 cells treated with H_2O or 20 µM CK666. Cells were synchronized by double thymidine block and released into the cell cycle. After 8.5 h - 9.5 h, cells were fixed and stained for immunofluorescence microscopy. Bar graphs show the proportion of cells exhibiting at least one CREST-positive chromatid (mean ± sem, *t*-test, n=3 with a total of 300 anaphase cells). **(c)** Measurements of mitotic and interphase microtubule plus-end assembly rates in SW620 and SK-Mel-103 cells. Cells were treated with DMSO or 20 µM CK666 for 2 h. 1-2 h prior to EB3 tracking experiments, cells were treated with 2 µM DME. Scatter dot plots show the average microtubule plus-end assembly rates of 20 microtubules per cell (mean ± sem, *t*-test, n=30 cells from three independent experiments).

Since the inhibition of the Arp2/3 complex revealed similar results as previously obtained by Rac1 and TRIO inhibition, it seems likely, that TRIO, Rac1 and the Arp2/3 complex act in the same pathway. All three proteins seem to be important players for the development of a highly migratory phenotype and for the generation of lagging chromosomes. On the other hand, inhibition of any component of the TRIO-Rac1-Arp2/3 pathway resulted in decreased migration and decreased chromosome missegregation in highly migratory and invasive cancer cells exhibiting CIN.

3.1.9 Inhibition Of TRIO, Rac1 And The Arp2/3 Complex Affects Spindle Orientation In SW620 Cells

Ertych *et al.* described the phenotype of increased microtubule plus-end assembly rates and showed that these increased microtubule plus-end assembly rates are associated with transient mitotic spindle orientation defects, which, in turn, result in the induction of lagging chromosomes (Ertych *et al.* 2014). Since inhibition of TRIO, Rac1 and the Arp2/3 complex reduced the amounts of lagging chromosomes, I investigated, whether spindle orientation is influenced by the TRIO-Rac1-Arp2/3 pathway. To address this question, SW620 cells were seeded onto fibronectin coated slides and treated with DMSO, 0.2 nM Taxol, 15 µM ITX3, 40 µM NSC23766 or 20 µM CK666 for 16 h. Afterwards, cells were fixed for immuno-fluorescence microscopy and the spindle axis angle was determined. Staining for α-tubulin, γ-tubulin and DAPI marked the mitotic spindle and the centrosomes and allowed the discrimination between cells in prometaphase and cells in metaphase due to positioning of the centrosomes with respect to the chromosomes (Fig. 3.19a). Images with a z-optical spacing of 0.4 µm were taken and the spindle axis angle was determined by the formula: spindle axis angle= (number of z-stacks*0.4 µm / distance of centrosomes) *180/ π (Fig. 3.19b).

During prometaphase, DMSO treated SW620 cells exhibited a mean spindle axis angle of 22.8°, which was significantly reduced to 9.2° upon treatment with 0.2 nM Taxol. Similarly, inhibition of TRIO, Rac1 or the Arp2/3 complex significantly decreased the spindle axis angle. Upon drug treatment, mean spindle axis angles were reduced to values ranging from 10.1° to 10.9° (Fig. 3.19c). During metaphase, the spindle axis angle in DMSO treated SW620 cells was not as variable as observed in prometaphase cells. While prometaphase cells exhibited 22.8°, the analyses of metaphase cells revealed a mean spindle axis angle of 8.5°. However, a reduction of the mean spindle axis angle in metaphases was also detected upon inhibitor treatment. Taxol treatment reduced the angle in metaphase to 4.6°. Upon ITX3, NSC23766 and CK666 treatment, the spindle axis angles were reduced to 4.4°, 5.4° and 4.2°, respectively (Fig. 3.19d).

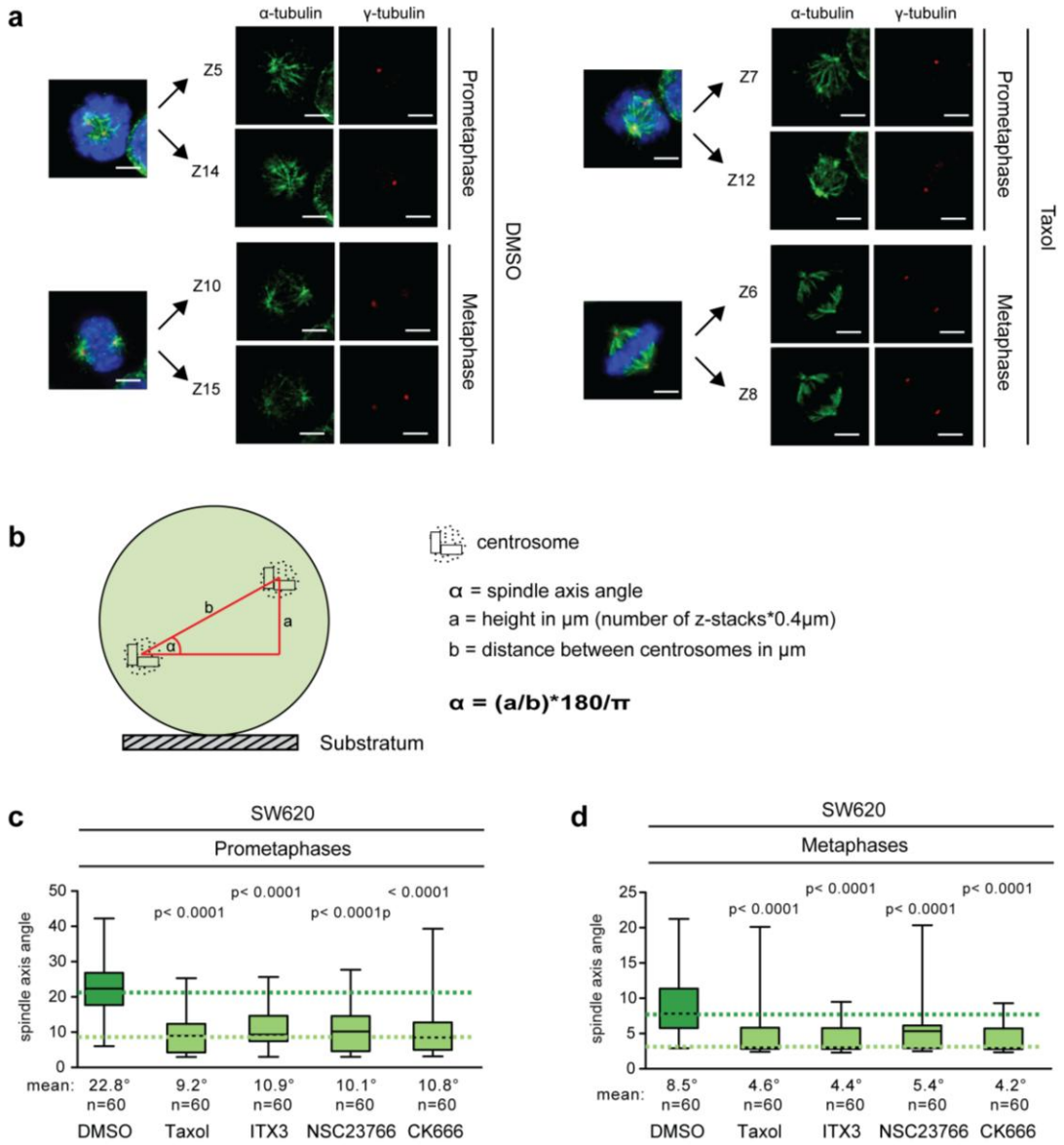

Figure 3.19: Analyses of spindle orientation in SW620 cells during prometaphase or metaphase. (a) Representative immunofluorescence images of DMSO or Taxol treated prometaphase or metaphase SW620 cells. Cells were stained for α-tubulin, γ-tubulin and DAPI. A maximum intensity projection as well as pictures with focused centrosomes are shown. Z refers to the respective z-stack with focused centrosome. Scale bar 10 µM. **(b)** Schematic illustration for the determination of the spindle axis angle. **(c)** Measurements of spindle axis angle in prometaphase. SW620 cells were seeded onto fibronectin coated slides and treated with DMSO, 0.2 nM Taxol, 15 µM ITX3, 40 µM NSC23766 or 20 µM CK666 for 16 h. Afterwards, cells were fixed and stained for immunofluorescence microscopy. Pictures of cells in prometaphase were taken and the angle between centrosomes and substratum was analyzed. The box and whisker plots show the range, median and quartile of the measurements (*t*-test, n= 60 cells from three independent experiments). Additionally, mean values are given. **(d)** Measurements of spindle axis angle in metaphase. SW620 cells were treated as described in (a). Pictures of cells in metaphase were taken and the angle between centrosomes and substratum was determined. The box and whisker plots show the range, mean and quartile of the measurements (*t*-test, n= 60 cells from three independent experiments). Additionally, mean values are given.

These results indicate an important role for TRIO, Rac1 and the Arp2/3 complex in spindle positioning during mitosis, in addition to their well established role in cell motility.

3.1.10 Inhibition Of TRIO, Rac1 Or The Arp2/3 Complex Suppresses CIN In SW620 And SK-Mel-103 Cells

SK-Mel-103 and SW620 cells exhibited an increased amount of cells displaying lagging chromosomes, which were reduced by treatment with the TRIO inhibitor ITX3, the Rac1 inhibitor NSC23766 and the Arp2/3 complex inhibitor CK666. Since the occurrence of lagging chromosomes is a widely recognized mechanism for the appearance of CIN (Cimini *et al.* 2001), it was of interest to investigate whether the inhibition of TRIO, Rac1 and the Arp2/3 complex would also affect the CIN phenotype present in SK-Mel-103 and SW620 cells. To evaluate CIN, single cell clones of both cell lines were generated in the presence or absence of the different inhibitors. As a control, cells were treated with low doses of Taxol, because Taxol was already proven to suppress CIN (Ertych *et al.* 2014). Cell clones were grown for 30 generations and their chromosome number deviation was analyzed by chromosome counting in metaphase spreads and by CEP-FISH analyses. SW620 cell clones were analyzed by individual chromosome counting. Upon Taxol treatment, the amount of cells with a chromosome numbers deviating from modal was highly decreased (Fig. 3.20a).

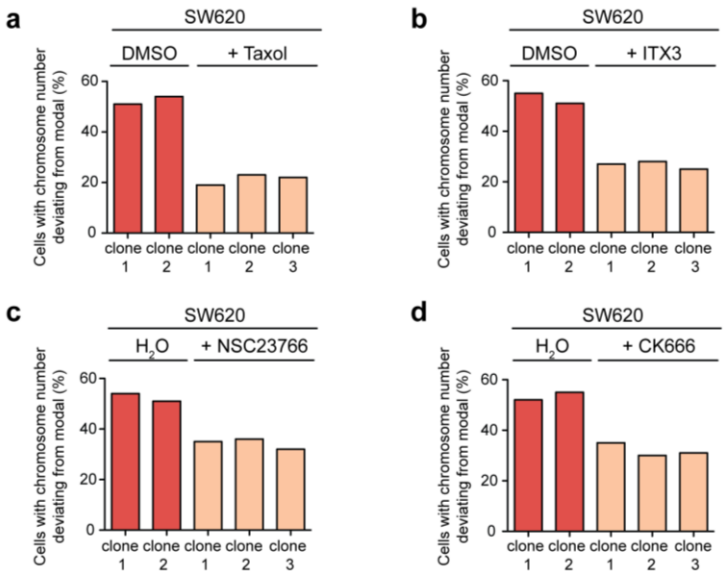

Figure 3.20: Inhibition of TRIO, Rac1 or the Arp2/3 complex suppresses CIN in SW620 cells. **(a)** Karyotype analyses by chromosome counting in metaphase spreads of single cell clones derived from SW620 cells treated with DMSO or 0.2 nM Taxol for 30 generations. The percentage of cells with a chromosome number deviating from modal was determined (n=100 cells). **(b)** Karyotype analyses by chromosome counting in metaphase spreads of single cell clones derived from SW620 cells treated with DMSO or 15 µM ITX3 for 30 generations. The percentage of cells with a chromosome number deviating from modal was determined (n=100 cells). **(c)** Karyotype analyses by chromosome counting in metaphase spreads of single cell clones treated with H_2O or 40 µM NSC23766 for 30 generations. The percentage of cells with a chromosome number deviating from modal was determined (n=100 cells). **(d)** Karyotype analyses by chromosome counting in metaphase spreads of single cell clones derived from SW620 cells treated with H_2O or 20 µM CK666 for 30 generations. The percentage of cells with a chromosome number deviating from modal was determined (n=100 cells).

Also ITX3, NSC23677 and CK666 treated single cell clones showed decreased numbers of aneuploid cells when compared to the respective control treated cells (Fig. 3.20b-d). Thereby, inhibition of TRIO by ITX3 revealed the strongest reduction in cells with chromosome numbers deviating from modal.

SW620 single cell clones were further studied by CEP-FISH analyses. Therefore, α-satellite probes specific for chromosome 7 and chromosome 15 were used.

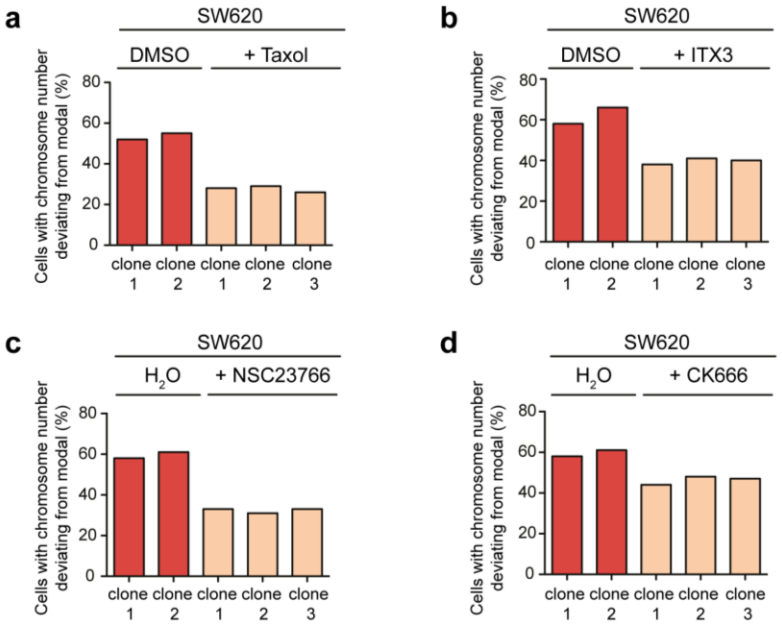

Fig. 3.21: CEP-FISH analyses of SW620 derived single cell clones treated with TRIO, Rac1 or Arp2/3 complex inhibitor. (a) CEP-FISH analyses detecting chromosome 7 and chromosome 15 in single cell clones derived from SW620 cells treated with DMSO or 0.2 nM Taxol for 30 generations. The percentage of cells with a chromosome number deviating from modal was calculated (n=100 cells). **(b)** CEP-FISH analyses of single cell clones derived from SW620 cells treated with DMSO or 15 µM ITX3 for 30 generations. The percentage of cells with a chromosome number deviating from modal was calculated (n=100 cells). **(c)** CEP-FISH analyses of single cell clones derived from SW620 cells treated with H_2O or 40 µM NSC23766 for 30 generations. The percentage of cells with a chromosome number deviating from modal was calculated (n=100 cells). **(d)** CEP-FISH analyses of single cell clones derived from SW620 cells treated with H_2O or 20 µM CK666 for 30 generations. The percentage of cells with a chromosome number deviating from modal was calculated (n=100 cells).

In order to verify the results obtained in SW620 cells, also SK-Mel-103 cells were analyzed after treatment with the different inhibitors by CEP-FISH analyses. Here, α-satellite probes specific for chromosome 6 and chromosome 18 were used. Also in this cell line, the different treatments reduced the amount of cells with chromosome numbers deviating from modal. Treatment with Taxol, ITX3 and NSC23766 had a stronger effect than treatment with CK666. Whereas upon Taxol, ITX3 and NSC23766 treatment the amount of aneuploid cells was reduced by 18-24%, CK666 treatment led to a reduction in aneuploid cells by 9-11% in the different single cell clones (Fig. 3.22a-d).

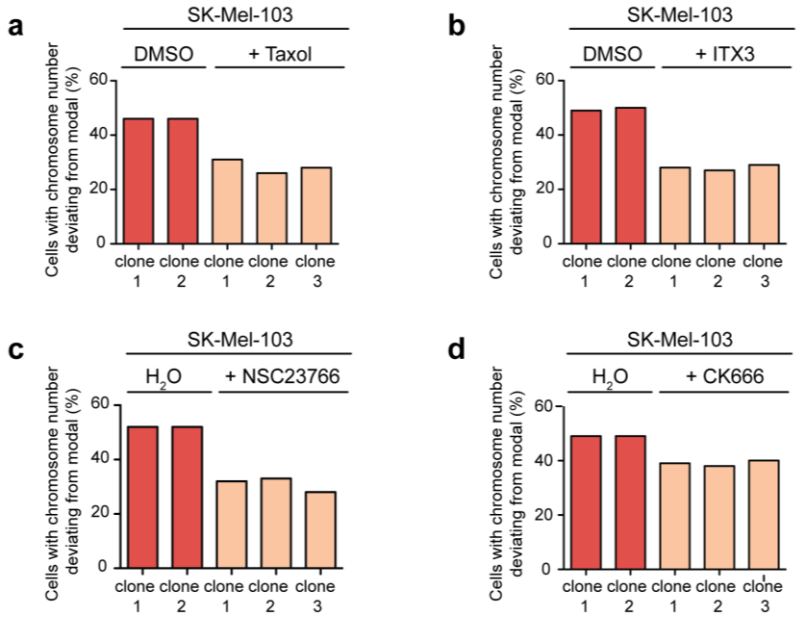

Figure 3.22: Inhibition of TRIO, Rac1 and Arp2/3 complex suppresses CIN in SK-Mel-103 cells. **(a)** CEP-FISH analyses detecting chromosome 6 and chromosome 18 in single cell clones derived from SK-Mel-103 cells treated with DMSO or 0.5 nM Taxol for 30 generations. The percentage of cells with a chromosome number deviating from modal was calculated (n=100 cells). **(b)** CEP-FISH analyses of single cell clones derived from SK-Mel-103 cells treated with DMSO or 15 µM ITX3 for 30 generations. The percentage of cells with a chromosome number deviating from modal was calculated (n=100 cells). **(c)** CEP-FISH analyses of single cell clones derived from SK-Mel-103 cells treated with H_2O or 40 µM NSC23766 for 30 generations. The percentage of cells with a chromosome number deviating from modal was calculated (n=100 cells). **(d)** CEP-FISH analyses of single cell clones derived from SK-Mel-103 cells treated with H_2O or 20 µM CK666 for 30 generations. The percentage of cells with a chromosome number deviating from modal was calculated (n=100 cells).

In order to test whether long-term treatment of cells with the different inhibitors has an effect on cell migration and microtubule plus-end assembly rates, one single cell clone derived from Taxol, ITX3, NSC23766 and CK666 treated SW620 or SK-Mel-103 cells was analyzed. As expected, Taxol treatment reduced the microtubule plus-end assembly rates during mitosis and interphase in single cell clones (Fig. 3.23a). In contrast, treatment with ITX3, NSC23766 or CK666 did not alter microtubule plus-end assembly rates. Transwell migration assays were performed with a single cell clone derived from SK-Mel-103 cells treated with 0.5 nM Taxol, 15 µM ITX3, 40 µM NSC23766 or 20 µM CK666. Here, prolonged treatment with the different inhibitors reduced cell migration robustly (Fig. 3.23b).

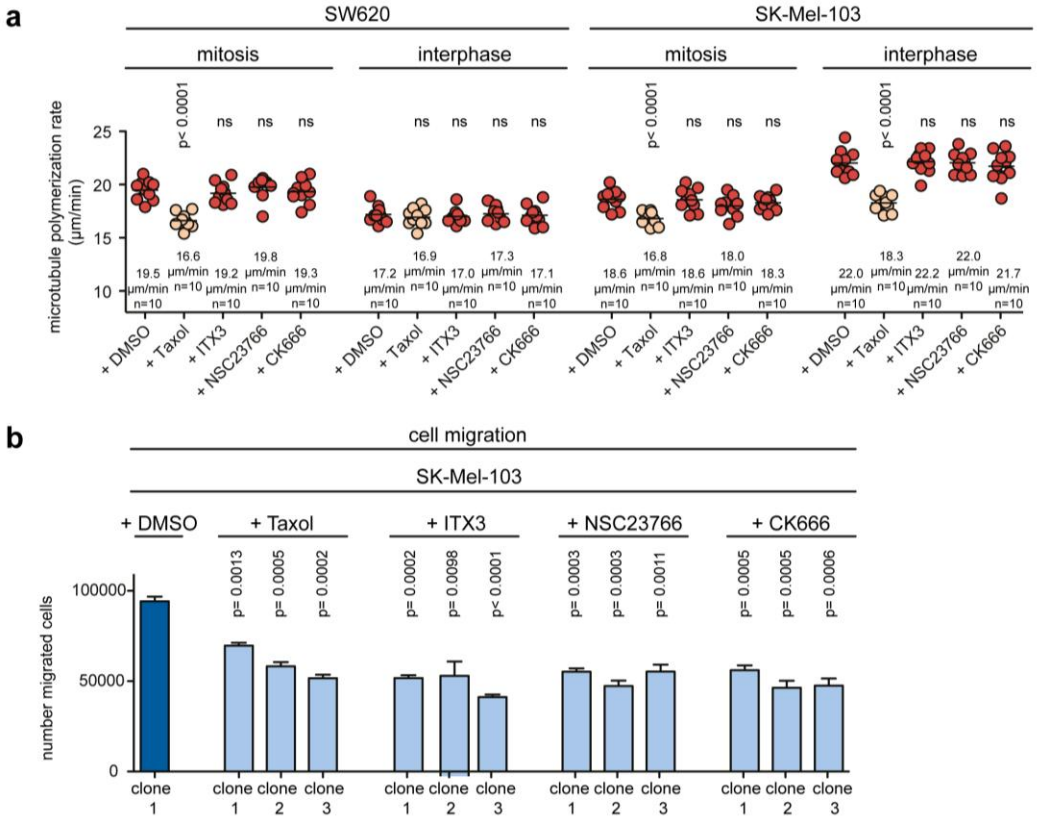

Figure 3.23: Single cell clones treated with inhibitor of TRIO, Rac1 or the Arp2/3 complex show no alterations in microtubule plus-end assembly rates but a reduce migratory phenotype. (a) Measurements of microtubule plus-end assembly rates during mitosis and interphase. Single cell clone 1 of SW620 (Fig. 3.20, Fig 3.21) and clone 1 of SK-Mel-103 (Fig. 3.22) generated over 30 generations in the presence of DMSO, 0.2 nM (SW620) or 0.5 nM (SK-Mel-103) Taxol, 15 µM ITX3, 40 µM NSC23766 and 20 µM CK666 were treated with 2 µM DME for 1 h - 2 h prior to EB3 tracking experiments. Scatter dot plots show the average microtubule plus-end assembly rates of 20 microtubules per cell (mean ± sem, *t*-test, n=10 cells). **(b)** Transwell migration assays of SK-Mel-103 single cell clones treated as described in (a). 200,000 cells were seeded in cell culture inserts. Bar graphs show the number of migrated cells after 24 h (mean ± sem, *t*-test, n=3).

To further verify that the observed reduction in aneuploidy depends on the used drugs, the generated single cell clones were cultivated for further 30 generations in the absence of drugs. Afterwards, the chromosome numbers were determined by CEP-FISH analyses and compared to the chromosome copy numbers obtained before removal of the drug. These analyses revealed an increase in aneuploid cells in all SW620 and SK-Mel-103 cell clones after removal of the different drugs (Fig. 3.24a-b). Thus, CIN is re-introduced after re-activation of the TRIO-Rac1-Arp2/3 pathway.

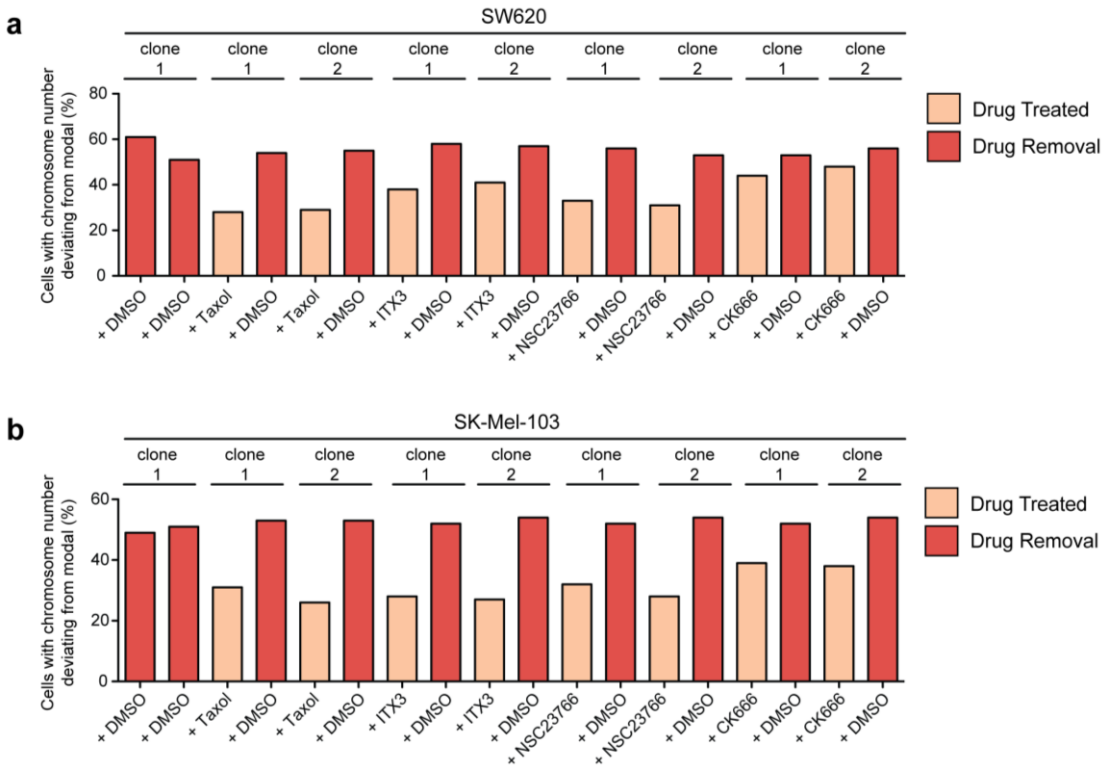

Figure 3.24: Drug removal re-induces CIN. (a) CEP-FISH analyses of SW620 cells before and after drug removal. After treatment with Taxol, ITX3, NSC23766 and CK666 for 30 generations, SW620 derived single cell clones were treated with DMSO for additional 30 generations. The percentage of cells with a chromosome number deviating from modal was determined (n=100 cells). **(b)** CEP-FISH analyses of SK-Mel-103 cells before and after drug removal. After treatment with Taxol, ITX3, NSC23766 and CK666 for 30 generations, SK-Mel-103 derived single cell clones were treated with DMSO for additional 30 generations. The proportion of cells with a chromosome number deviating from modal was calculated (n=100 cells).

3.2 The Role Of p53 And p73 In Chromosomal Instability And Migration

3.2.1 Loss Of *TP53* And *TP73* Increases Microtubule Plus-End Assembly Rates And Induces CIN

A frequent lesion in the vast majority of human cancer types is a loss of function of the tumor suppressor p53. However, the loss of *TP53* is not sufficient to induce aneuploidy in human cells (Bunz *et al.* 2002). The p53 homolog *TP73* is located on chromosome arm 1p36, which is frequently deleted in various cancer types. This loss was shown to be associated with cancer (Kaghad *et al.* 1997). Furthermore, p73 suppresses polyploidy in the absence of p53 (Talos *et al.* 2007). Therefore, we were interested to investigate whether p53 and p73 might cooperate to suppress CIN in cancer cells.

To address this hypothesis, *TP53* and *TP73* were either separately or concomitantly repressed by siRNA in the chromosomal stable cell line HCT116 and microtubule plus-end assembly rates were measured. The knock down efficiency of *TP53* and *TP73* was confirmed by western blot (Fig. 3.25a).

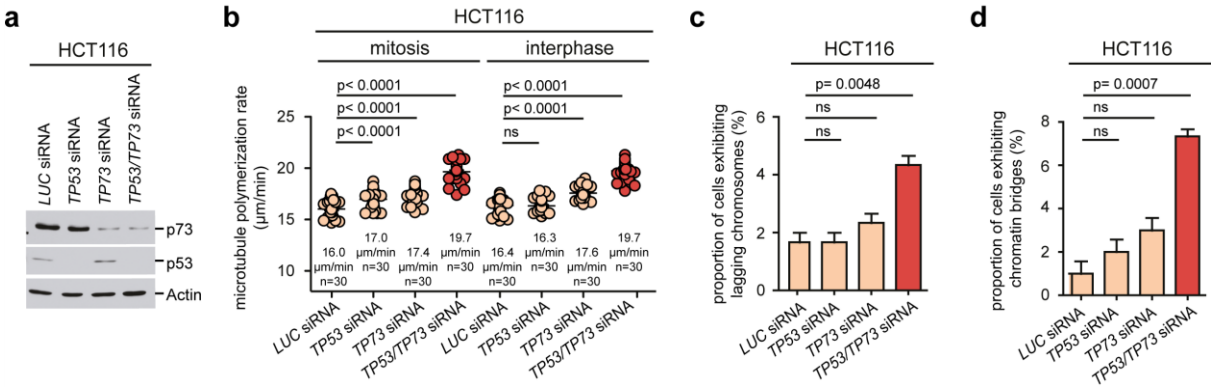

Figure 3.25: Concomitant repression of *TP53* and *TP73* leads to increased microtubule plus-end assembly rates and induces the generation of lagging chromosomes. (a) Representative western blot showing the downregulation of *TP53* and *TP73* in response to siRNA transfection. β-actin was used as loading control. **(b)** Determination of microtubule plus-end assembly rates after repression of *TP53*, *TP73* or both concomitantly. HCT116 cells were transfected with 60 pmol *TP53*, *TP73* or *LUCIFEARSE* siRNA. For EB3 tracking experiments, cells were treated with 2 µM DME for 1 h. Scatter dot plots show the average microtubule plus-end assembly rates of 20 microtubules per cell (mean ± sem, *t*-test, n=30 cells from three independent experiments). **(c)** Quantification of cells showing lagging chromosomes during anaphase in HCT116 cells after separate or concomitant repression of *TP53* and *TP73*. Cells were synchronized at G_1/S by double thymidine block and released into the cell cycle for 8.5 h. Cells were fixed and stained for immunofluorescence microscopy. Bar graphs show the number of cells exhibiting at least one CREST-positive chromatid (mean ± sem, *t*-test, n=3 with a total of 300 anaphase cells). **(d)** Quantification of cells exhibiting chromatin bridges. Cells were processed as described in (c). Bar graphs show the number of cells displaying chromatin bridges (mean ± sem, *t*-test, n=3 with a total of 300 anaphase cells).

The knock down of either *TP53* or *TP73* revealed only a slight increase in microtubule plus-end assembly rates, whereas the simultaneous repression of both transcription factors greatly increased the microtubule plus-end assembly rates during mitosis and interphase when compared to *LUCIFERASE* siRNA transfected cells (Fig. 3.25b). During mitosis, the microtubule plus-end assembly rates were increased from 16.0 µm/min upon *LUCIFERASE* siRNA to 19.7 µm/min upon repression of both *TP53* and *TP73*. During interphase, microtubule plus-end assembly rates were enhanced from 16.4 µm/min to 19.7 µm/min.

Since increased microtubule plus-end assembly rates cause the generation of lagging chromosomes, the role of p53 and p73 during chromosome segregation was investigated. Cells were synchronized at G_1/S transition by a double thymidine block and released into the cell cycle. Cells were fixed and stained after 8.5 h and cells in anaphase displaying lagging chromosomes were quantified. Importantly, the concomitant repression of *TP53* and *TP73* in chromosomal stable HCT116 cells induced the appearance of cells exhibiting lagging chromosomes from 1.6% to 4.3%. The repression of either *TP53* or *TP73* alone did not significantly increase the proportion of cells with lagging chromosomes (Fig. 3.25c). Apart from the occurrence of lagging chromosomes, depletion of *TP53* and *TP73* led to highly increased numbers of cells showing chromatin bridges during anaphase (Fig. 3.25d).

Lagging chromosomes underlie CIN in cancer cells (Cimini *et al.* 2001). In order to further evaluate the impact of *TP53* and *TP73* on chromosomal stability, HCT116-*TP53*$^{-/-}$ cells were used for the generation of stable single cell clones repressed of *TP73* by using a *TP73* shRNA expression plasmid. Furthermore, HCT116-*TP53*$^{-/-}$ cells were transfected with a control shRNA expression plasmid. HCT116-*TP73* shRNA expression cells were available in our lab. *TP73* repression was verified by western blot analyses (Fig. 3.26a). Stable cell clones with a significant repression of *TP73* (*TP73sh* clones) were further analyzed regarding their microtubule plus-end assembly rates by EB3 tracking experiments. Here, cells with a repression of both transcription factors showed significantly increased microtubule plus-end assembly rates in mitosis and in interphase when compared to the single knock down cells HCT116-*TP53*$^{-/-}$ and HCT116-*TP73sh* (Fig. 3.26b). The increased microtubule plus-end assembly rates also correlated with elevated amounts of cells with lagging chromosomes. Upon repression of both transcription factors, the amount of cells displaying lagging chromosomes was increased more than 3-fold compared to single knock down cells (Fig. 3.26c). Karyotype analyses of three individual single cell clones by individual chromosome counting in metaphase spreads revealed an increased amount of cells with chromosome numbers deviating from modal number of 45 after concomitant loss of *TP53* and *TP73* (Fig. 3.26d). The amount of aneuploid cells was increased from 12% in both control transfected HCT116-*TP53*$^{-/-}$ cell clones to 32%-44% in the three cell clones repressed of both transcription factors, indicating a chromosomal instability phenotype.

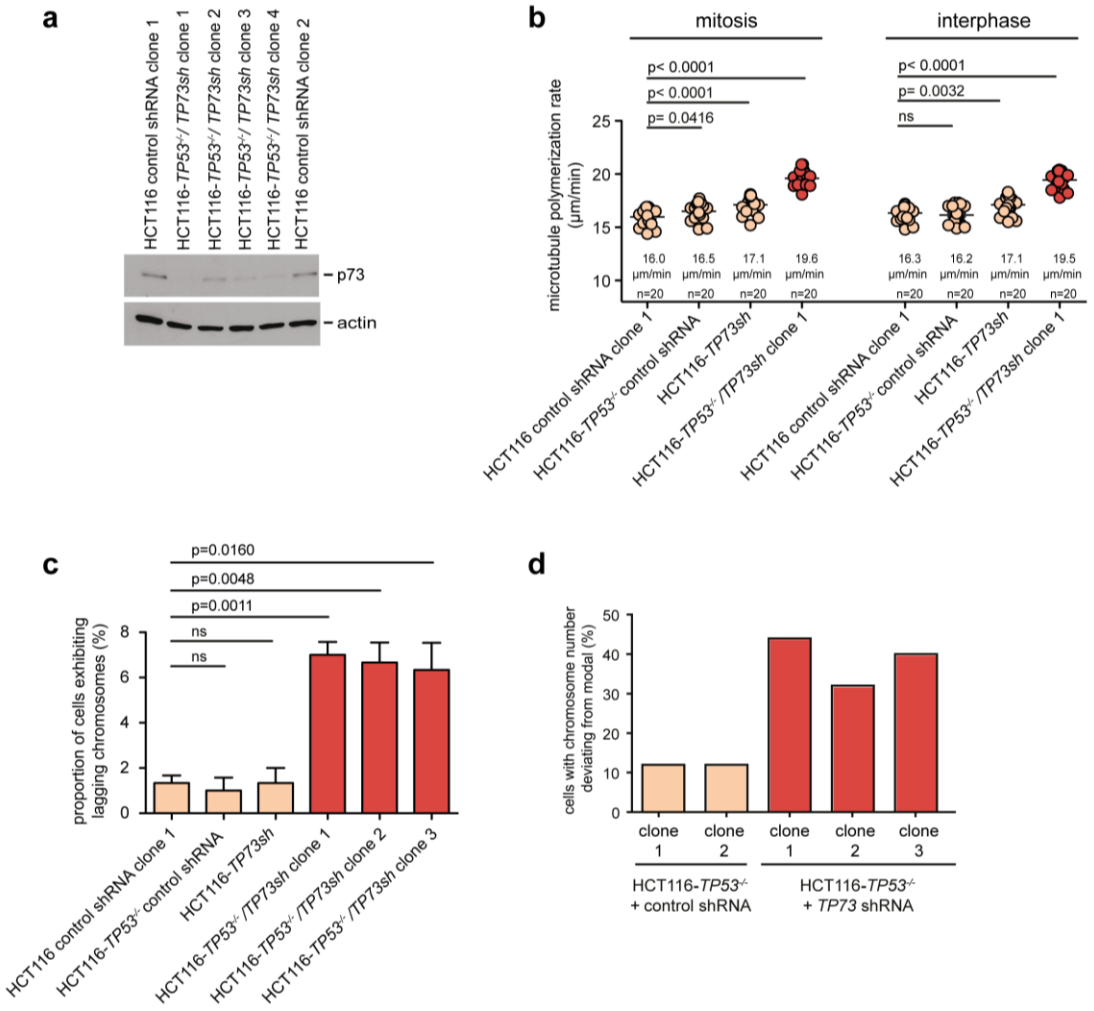

Figure 3.26: The concomitant repression of *TP53* and *TP73* leads to CIN. (a) HCT116-*TP53*$^{-/-}$ cells were stably transfected with a *TP73* shRNA or a control shRNA expression plasmid and single cell clones were isolated. Knock down of *TP73* was verified by western blot, whereby β-actin served as loading control. **(b)** EB3 tracking experiments of cells in mitosis and interphase. The indicated single cell clones were treated with 2 µM DME 1 h prior to EB3 tracking experiments. Scatter dot plots show the average microtubule plus-end assembly rates of 20 microtubules per cell (mean ± sem, *t*-test, n=20 cells from two independent experiments). **(c)** Quantification of cells showing lagging chromosomes during anaphase. The indicated single cell clones were synchronized at G_1/S transition by a double thymidine block and released into the cell cycle. Bar graphs show the proportion of cells exhibiting at least one CREST-positive chromatid (mean ± sem, *t*-test, n=3 with a total of 300 anaphase cells). **(d)** Induction of CIN after repression of *TP53* and *TP73*. Karyotype analyses of single cell clones were performed by chromosome counting in metaphase spreads. The percentage of cells with a chromosome number deviating from modal was calculated (n=100 cells).

These results showed that separate repression of *TP53* or *TP73* is not sufficient to induce chromosomal instability and aneuploidy in HCT116 cells. However, the concomitant repression of *TP53* and *TP73* induces CIN.

To test whether the occurrence of lagging chromosomes and CIN depends on the increased microtubule plus-end assembly rates (Fig. 3.25b), single cell clones repressed of *TP53* and *TP73* were treated with 0.2 nM Taxol over 30 generations followed by drug removal for additional 30 generations. Upon low dose Taxol treatment, cells with low expression of *TP53*

and *TP73* showed decreased microtubule plus-end assembly rates, that were again increased after Taxol removal (Fig. 3.27a). Corresponding to that observation, the proportion of cells displaying lagging chromosomes increased after Taxol removal by about 3-4 fold (Fig. 3.27b). Karyotype analyses by counting individual chromosomes in metaphase spreads revealed between 20% and 25% of cells with a chromosome number deviating from modal upon Taxol treatment. After Taxol removal, the amount of aneuploid cells increased to 40% to 50% in the three different cell clones (Fig. 3.27c).

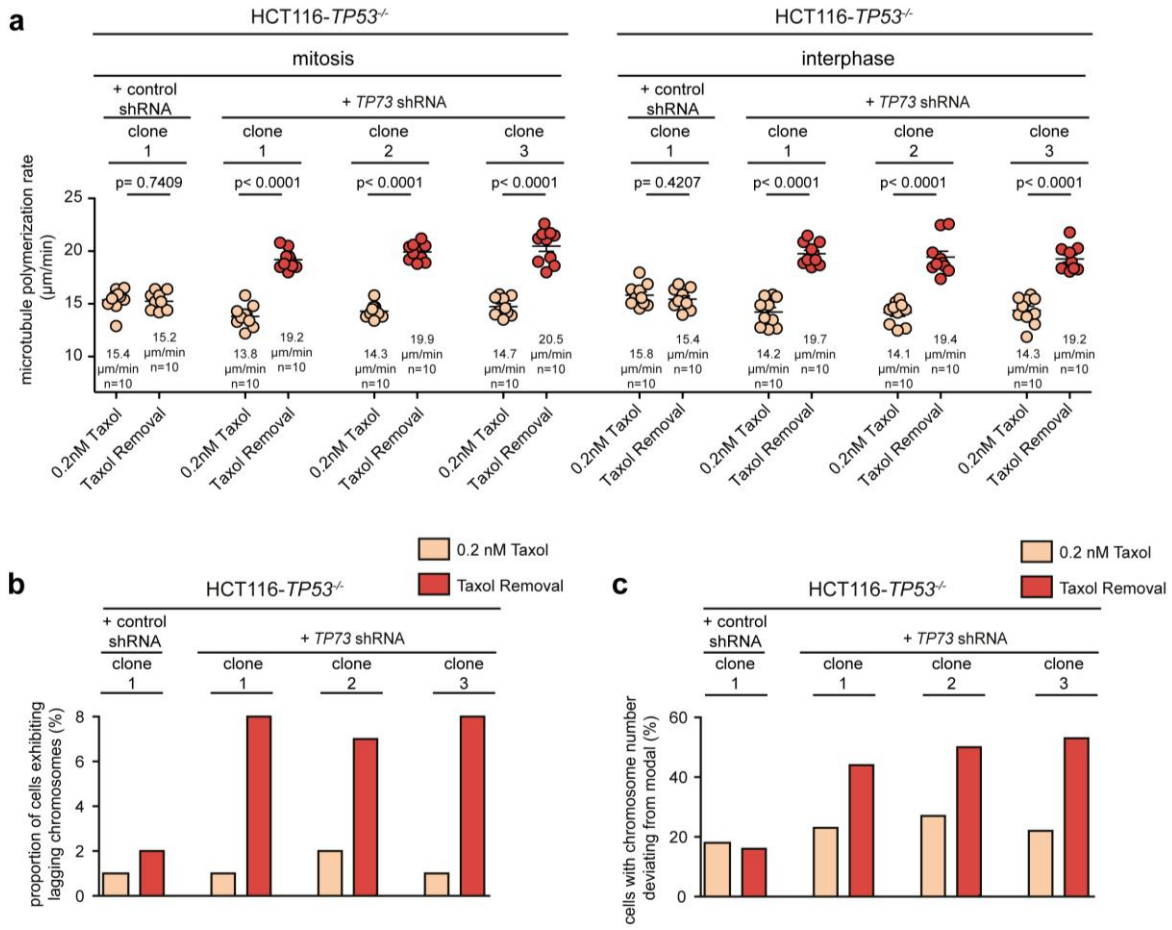

Figure 3.27: The CIN phenotype induced by loss of *TP53* and *TP73* in HCT116 cells can be suppressed by Taxol treatment. (a) Measurements of microtubule plus-end assembly rates in HCT116-*TP53*$^{-/-}$ with a stable repression of *TP73*. Single cell clones were treated with 0.2 nM Taxol for 30 generations, following removal of Taxol and cultivation in DMSO for additional 30 generations. Cells were treated with 2 µM DME 1 h prior to EB3 tracking experiments. Scatter dot plots show the average microtubule plus-end assembly rates of 20 microtubules per cell (mean ± sem, *t*-test, n=10 cells). **(b)** Quantification of the amount of cells exhibiting lagging chromosomes during anaphase. Single cell clones were generated as described in (a). Cells were synchronized at G_1/S transition by double thymidine block, released into the cell cycle for 8.5 h and fixed and stained for immunofluorescence microscopy. Bar graphs show the proportion of cells displaying at least one CREST-positive chromatid (n= 100 anaphase cells counted). **(c)** Karyotype analyses of single cell clones. Single cell clones were generated as described in (a). The proportion of cells with a chromosome number deviating from modal was calculated (n=100 cells).

These results indicate a causal role for increased microtubule plus-end assembly rates induced by loss of p53 and p73 for the development of CIN.

To exclude unspecific effects of the *TP73* shRNA construct, *TAp73* was re-expressed in HCT116-*TP53*$^{-/-}$/*TP73sh* cells. Furthermore, *TAp73* was re-expressed in HCT116 and HCT116-*TP53*$^{-/-}$ cells, which served as control cell lines. Stable cell clones were generated by the use of a doxycycline inducible *TAp73* expression vector. The re-expression of *TAp73* in individual single cell clones was confirmed by western blot analyses (Fig. 3.28a).

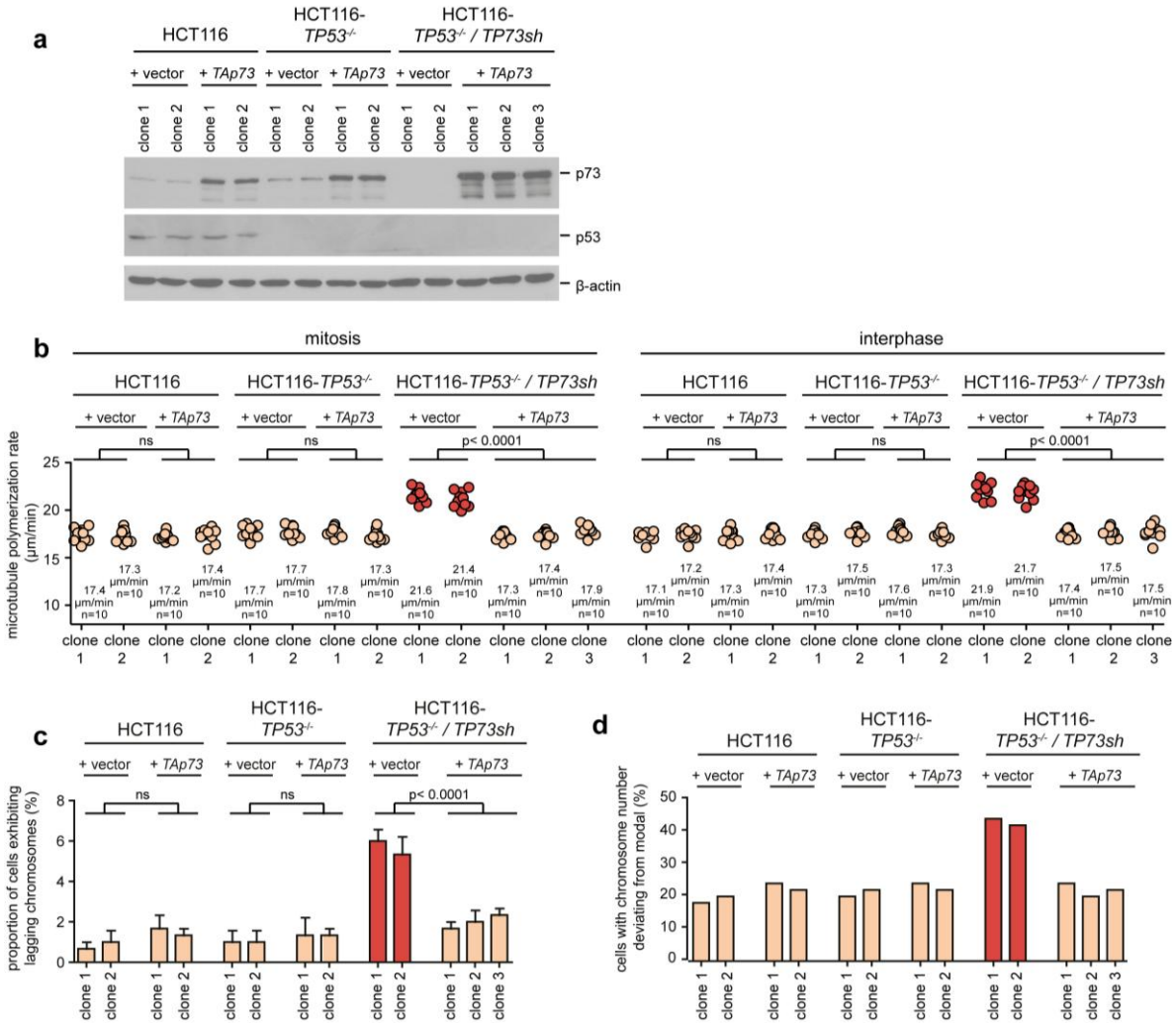

Figure 3.28: The re-expression of *TAp73* suppresses CIN in HCT116-*TP53*$^{-/-}$/*TP73sh* cells. (a) *TAp73* was stably re-expressed in HCT116, HCT116-*TP53*$^{-/-}$ and HCT116-*TP53*$^{-/-}$ /*TP73*sh cells and single cell clones were isolated. The re-expression of *TAp73* was verified by western blot. β-actin served as a loading control **(b)** Measurements of microtubule plus-end assembly rates in single cell clones, that are shown in (a). Cells were treated with 2 µM DME 1 h prior to EB3 tracking experiments. Scatter dot plots show the average microtubule plus-end assembly rates of 20 microtubules per cell (mean ± sem, *t*-test, n=10 cells). **(c)** Quantification of the proportion of cells showing lagging chromosomes in single cell clones, that are shown in (a). Cells were synchronized at G_1/S transition by double thymidine block, released into the cell cycle and fixed and stained for immunofluorescence microscopy after 8.5 h. Bar graphs show the quantification of cells exhibiting at least one CREST-positive chromatid (mean ± sem, *t*-test, n=3 with a total of 300 anaphase cells). **(d)** Karyotype analyses of the indicated single cell clones. The proportion of cells with a chromosome number deviating from modal was determined by chromosome counting in metaphase spreads (n=100 cells).

EB3 tracking experiments were performed to investigate the microtubule plus-end assembly rates. The control cells (HCT116-*TAp73* and HCT116-*TP53*$^{-/-}$-*TAp73*) were not altered in their microtubule plus-end assembly rates, revealing that overexpression of *TAp73* does not affect microtubule dynamics. However, re-expression of *TAp73* in HCT116-*TP53*$^{-/-}$*/TP73sh* cells decreased the microtubule plus-end assembly rates during interphase and mitosis comparable to control transfected HCT116-*TP53*$^{-/-}$*/TP73sh* cells (Fig. 3.28b). Consequently, the amount of cells showing lagging chromosomes was decreased approximately 3-fold upon re-expression of *TAp73* in HCT116-*TP53*$^{-/-}$*/TP73sh* cells, whereas the generation of lagging chromosomes was not affected in HCT116 and HCT116-*TP53*$^{-/-}$ cells (Fig. 3.28c). Karyotype analyses by chromosome counting from metaphase spreads revealed a decreased amount of cells with a chromosome number deviating from modal in HCT116-*TP53*$^{-/-}$*/TP73sh* cells exhibiting a stable re-expression of *TAp73* compared to control transfected HCT116-*TP53*$^{-/-}$*/TP73sh* cells (Fig. 3.28d). These results support the hypothesis that p53 and p73 cooperate in maintaining both, proper microtubule plus-end assembly rates in mitosis and chromosomal stability.

So far, cells with a knock out of *TP53* were used. However, this situation is not a common feature of cancer cells. Instead, human cancer cells rather exhibit a loss of function of p53 due to mutations. Different hot spot mutations were described including a most frequent p53 R175H mutation (Muller & Vousden 2013). HCT116 cells expressing a *TP53* R175H mutant where used to further evaluate the importance of both p53´s and p73´s function for the maintenance of chromosomal stability. HCT116-p53-R175H single cell clones stably transfected with control shRNA or *TP73* shRNA expression plasmids were isolated and the knock down of *TP73* was verified by western blot analyses (Fig. 3.29a). Subsequently, microtubule plus-end assembly rates were determined. While the p53 mutation alone did not affect microtubule plus-end assembly rates, the stable repression of *TP73* in HCT116-p53-R175H cells resulted in an increase in microtubule plus-end assembly rates. Furthermore, the cell clones were treated with 0.2 nM Taxol 2 h prior to EB3 tracking experiments. The low dose Taxol treatment led to a decrease in microtubule plus-end assembly rates to levels similarly observed in the control transfected HCT116-p53-R175H cell clone 1 (Fig. 3.29b). Analyses of HCT116-p53-R175H cells with low *TP73* expression revealed an increased proportion of cells displaying lagging chromosomes in comparison to control transfected HCT116-p53-R175H cells. While the proportion of control cells exhibiting lagging chromosomes was in a range from 1%-2%, on average 5%-5.6% of the single cell clones derived from HCT116-p53-R175H repressed of *TP73* showed lagging chromosomes (Fig. 3.29c). Subsequently, karyotype analyses by chromosome counting from metaphase spreads were conducted. Importantly, HCT116-p53-R175H cell clones with low *TP73* expression also displayed a higher amount of cells with a chromosome number deviating

from modal. This number was increased from 20%-26% in control transfected HCT116-p53-R175H cells to 43%-46% in the three HCT116-p53-R175H cell clones repressed of *TP73* (Fig. 3.29d), indicating that the *TP53* mutation in combination with loss of *TP73* induced CIN.

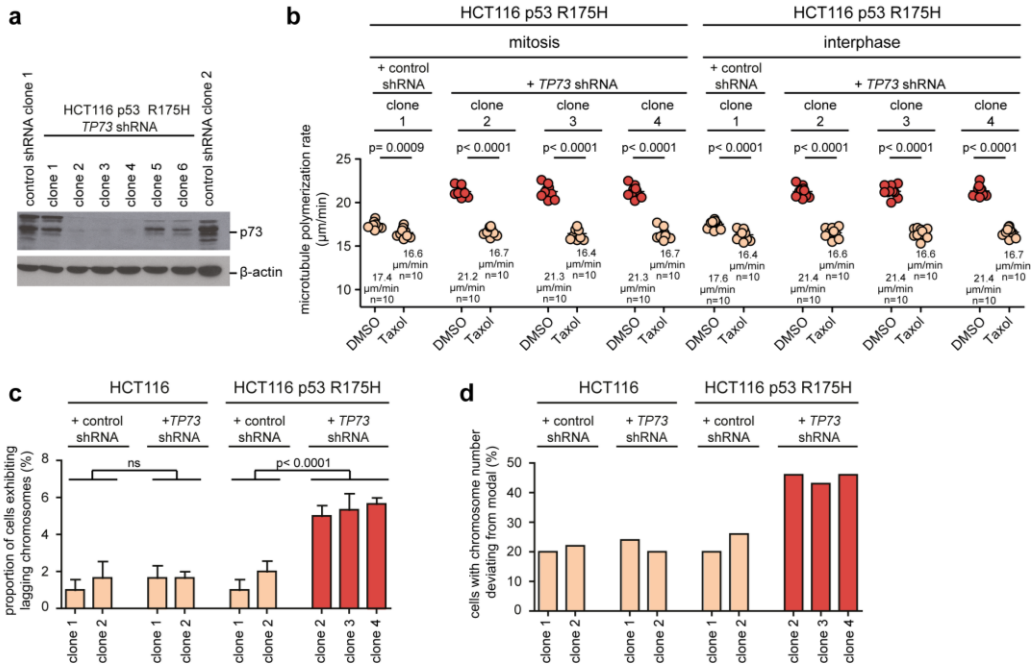

Figure 3.29: Repression of *TP73* in HCT116 cells expressing a mutant form of p53 induces CIN. (a) *TP73* was stably repressed in HCT116 cells expressing mutant *TP53* (p53-R175H) by shRNA and single cell clones were generated. The repression of *TP73* was verified by western blot. β-actin served as loading control. **(b)** Measurements of microtubule plus-end assembly rates in the single cell clones shown in (a). Cells were treated with 2 µM DME 1 h prior to EB3 tracking. Scatter dot plots show the average microtubule plus-end assembly rates of 20 microtubules per cell (mean ± sem, *t*-test, n=10 cells). **(c)** Quantification of proportion of cells with lagging chromosomes in the single cell clones shown in (a). Cells were synchronized by double thymidine block, released into the cell cycle and fixed for immunofluorescence microscopy after 8.5 h. Bar graphs show quantification of cells exhibiting at least one CREST-positive chromatid (mean ± sem, *t*-test, n=3 with a total of 300 anaphase cells). **(d)** Karyotype analyses of the indicated single cell clones by individual chromosome counting from metaphase spreads. The percentage of cells with a chromosome number deviating from modal was determined (n=100 cells).

Another common genetic alteration of cancer cells is the overexpression of a truncated form of p73, which is Δ*Np73*. ΔNp73 is described to inhibit both, p53´s and p73´s function and might act in a dominant negative manner (Zaika *et al.* 2002). To investigate the influence of Δ*Np73* expression on microtubule plus-end assembly rates, Δ*Np73* was overexpressed in HCT116 cells. To verify the inhibition of p53´s function by ΔNp73, cells were treated with 600 nM adriamycin for 16h to induce DNA damage and the activation of p53. Western blot analyses were performed and the protein level of the p53 target p21 was examined. While the overexpression of Δ*Np73* did not alter the protein level of p53 itself, the p53-mediated induction of p21 was greatly decreased suggesting that p53 function is inhibited (Fig. 3.30a).

Furthermore, EB3 tracking experiments were performed. The overexpression of ∆*Np73* in HCT116 cells also increased the microtubule plus-end assembly rates during both, mitosis and interphase in comparison to control transfected cells (Fig. 3.30b). Moreover, in the same cells, the proportion of cells with lagging chromosomes was also increased (Fig. 3.30c).

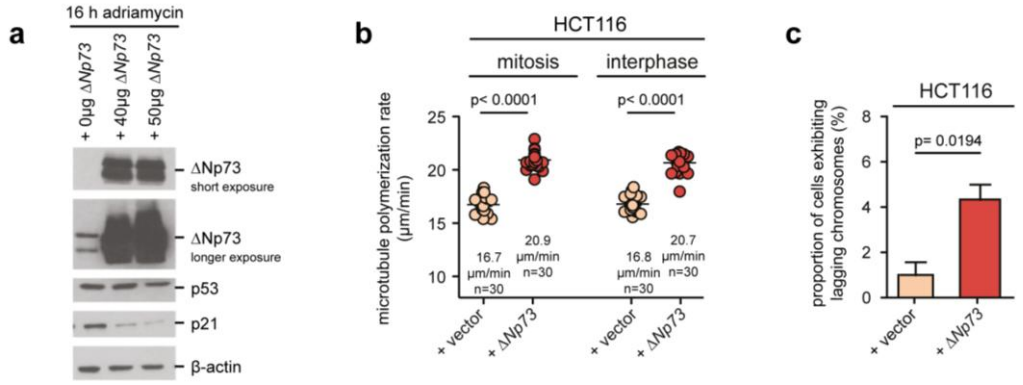

Figure 3.30: The expression of ∆*Np73* increases microtubule plus-end assembly rates and induces the occurrence of lagging chromosomes. (a) *⊿Np73* was transiently overexpressed in HCT116 cells. Cells were treated with 600 nM adriamycin for 16 h and p21 protein levels were detected on western blot. β-actin was used as a loading control. **(b)** Measurements of microtubule plus-end assembly rates after overexpression of *⊿Np73*. Cells were treated with 2 µM DME 1 h prior to EB3 tracking experiments. Scatter dot plots show the average microtubule plus-end assembly rates of 20 microtubules per cell (mean ± sem, *t*-test, n=30 cells from three independent experiments). **(c)** Quantification of cells with lagging chromosomes during anaphase in HCT116 cells after transient overexpression of *⊿Np73*. Cell cycle synchronization at G_1/S transition was achieved by a double thymidine block. Cells were released into the cell cycle for 8.5 h and fixed and stained for immunofluorescence microscopy. Bar graphs show the proportion of cells displaying at least one CREST-positive chromatid (mean ± sem, *t*-test, n=3 with a total of 300 anaphase cells).

These results indicate that expression of ∆*Np73* is sufficient to functionally inactivate both, p53 and p73 and to mediate an increase of microtubule plus-end assembly rates and chromosome segregation defects.

3.2.2 Abnormal Microtubule Dynamics Induced By Loss Of *TP53* And *TP73* Are Mediated By p21

Since p53 and p73 are transcription factors it is likely that upon loss of both various genes might not be transactivated. In collaboration with the Transcriptome and Genome Analysis Laboratory (TAL) of the University Göttingen RNA sequencing of HCT116 cells synchronized in G_2 was performed. For this, HCT116 cells were separately or concomitantly depleted of *TP53* and *TP73*by siRNA. Analyses of the data were performed by Dr. Silvia von der Heyde (former University of Göttingen, Göttingen, Germany). The following table shows an extract of genes, which were deregulated upon separate or concomitant loss of *TP53* and *TP73*.

Table 3.1: Extract of deregulated genes after single or concomitant loss of *TP53* and *TP73*. FC: fold change

***TP53* siRNA vs *LUC* siRNA**		***TP73* siRNA vs *LUC* siRNA**		***TP53/TP73* siRNA vs *LUC* siRNA**	
gene	FC	gene	FC	gene	FC
TP53	0.21	*TP73*	0.46	*TP53*	0.22
CDKN1A	0.39	*CDKN1A*	0.92	*TP73*	0.43
TP53INP1	0.28	*RMRP*	0.27	*CDKN1A*	0.31
MDM2	0.50	*RPPH1*	0.34	*TP53INP1*	0.31
BAX	0.65	*GATA3*	0.46	*MDM2*	0.48
SESN1	0.46	*SNORA21*	0.48	*BAX*	0.60
DNALI1	2.21	*AKAP5*	2.00	*IQGAP2*	2.02
CDH4	2.26	*SH2D3C*	2.03	*TGFBI*	3.96

Among the deregulated genes, the CDK-inhibitor p21 (encoded by the *CDKN1A* gene) was found, which is a key target gene of p53 (El-Deiry *et al.* 1993). To verify the RNA sequencing results, qRT-PCR analyses were performed to investigate the relative *CDKN1A* mRNA levels in cells repressed of either *TP53*, *TP73* or both concomitantly. The analyses verified low expression of *CDKN1A* in HCT116-*TP53*$^{-/-}$ cells compared to parental HCT116 cells. Repression of *TP73* alone also decreased *CDKN1A* mRNA level, but not as strong as observed upon repression of *TP53.* In cells repressed of both *TP53* and *TP73*, the *CDKN1A* mRNA levels were even more decreased compared to HCT116-*TP53*$^{-/-}$ cells (Fig. 3.31a).

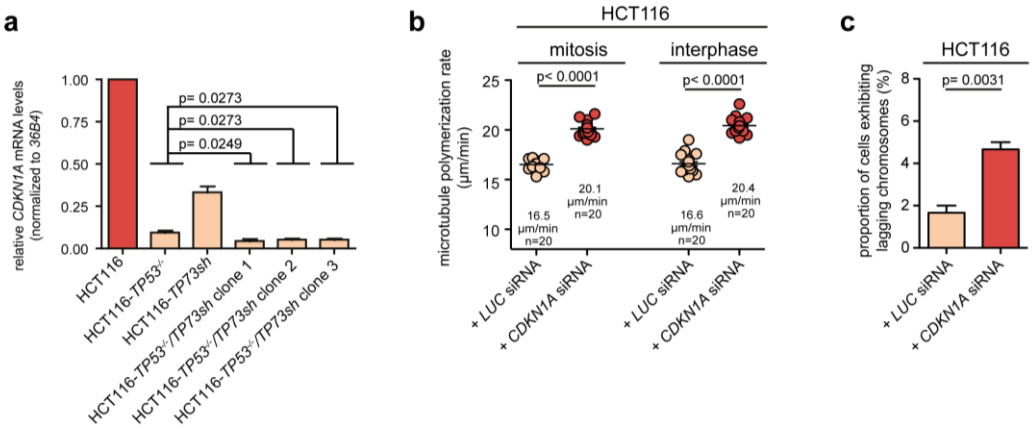

Figure 3.31: Repression of *CDKN1A* induces increased microtubule plus-end assembly rates and lagging chromosomes. (a) qRT-PCR analyses to quantify *CDKN1A* expression in cells repressed of *TP53* and *TP73*. RNA was extracted from asynchronously growing cells and cDNA was synthesized. qRT-PCR was performed with gene specific primers. *CDKN1A* mRNA levels were normalized to the housekeeping gene *36B4*. Bar graphs show relative mRNA expression levels (mean ± sem, *t*-test, n=3) **(b)** Measurements of microtubule plus-end assembly rates in HCT116 cells after transfection with 60 pmol *LUCIFERASE* or *CDKN1A* siRNA. Scatter dot plots show the average microtubule plus-end assembly rates of 20 microtubules per cell (mean ± sem, *t*-test, n=20 cells from two independent experiments). **(c)** Quantification of cells with lagging chromosomes after siRNA-mediated repression of *CDKN1A* in HCT116 cells. Cells were synchronized at G_1/S transition by double thymidine block and released into the cell cycle. After 8.5 h cells were fixed and stained for immunofluorescence microscopy. Bar graphs show proportion of cells exhibiting at least one CREST-positive chromatid (mean ± sem, *t*-test, n=3 with a total of 300 anaphase cells).

Subsequently, *CDKN1A* was repressed in HCT116 cells by siRNA. EB3 tracking experiments showed significantly increased microtubule plus-end assembly rates upon *CDKN1A* repression compared to *LUCIFERASE* siRNA transfected cells (Fig. 3.31b). Furthermore, the occurrence of lagging chromosomes was analyzed. While *LUCIFERASE* siRNA transfected cells exhibited 1.6% lagging chromosomes, this proportion was increased to 4.6% on average in *CDKN1A* siRNA transfected cells (Fig. 3.31c).

To elucidate the relevance of p21 for increased microtubule plus-end assembly rates in HCT116 cells induced by concomitant repression of *TP53* and *TP73*, *CDKN1A* was re-expressed in these cells. The overexpression of *CDKN1A* was verified by western blot analyses (Fig. 3.32a).

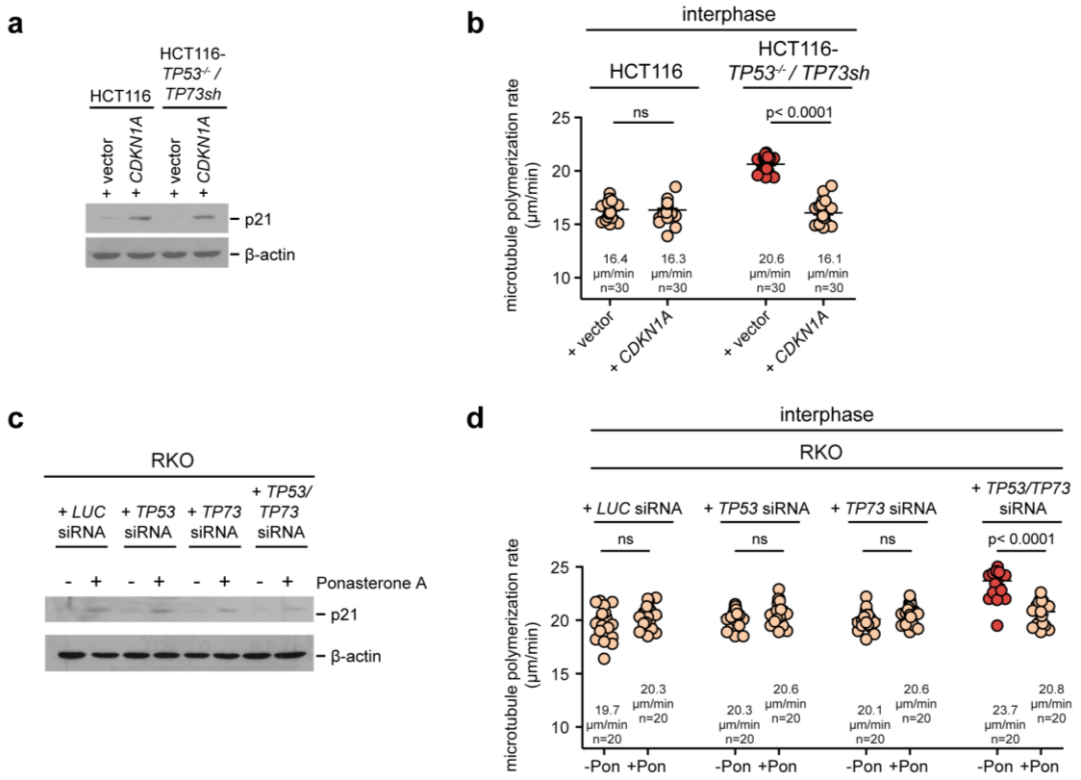

Figure 3.32: The re-expression of *CDKN1A* restores increased microtubule plus-end assembly rates observed upon repression of *TP53* and *TP73* in HCT116 and RKO cells. (a) Representative western blot verifying *CDKN1A* expression in HCT116 cells. β-actin was used as loading control. **(b)** Measurements of microtubule plus-end assembly rates in HCT116 and HCT116-*TP53*$^{-/-}$/*TP73*shRNA upon re-expression of *CDKN1A*. Scatter dot plots show the average microtubule plus-end assembly rates of 20 microtubules per cell (mean ± sem, *t*-test, n=30 cells from three independent experiments). **(c)** Representative western blot showing *CDKN1A* induction upon ponasterone A treatment in RKO cells. β-actin was used as loading control. **(d)** Measurements of interphase microtubule plus-end assembly rates in RKO cells, expressing *CDKN1A* upon ponasterone A (Pon) treatment. Cells were transfected with 60 pmol siRNA and treated with 5 µmol/l ponasterone A for *CDKN1A* induction. Scatter dot plots show the average microtubule plus-end assembly rates of 20 microtubules per cell (mean ± sem, *t*-test, n=20 cells from two independent experiments).

Subsequently, the microtubule plus-end assembly rates were examined. Since the overexpression of *CDKN1A* led to a cell cycle arrest in G_1-phase, the microtubule plus-end assembly rates could solely be measured in interphase cells. The re-expression of *CDKN1A* resulted in a decrease in microtubule plus-end assembly rates in comparison to control vector transfected HCT116-*TP53*$^{-/-}$*/TP73sh* cells (Fig. 3.32b). The microtubule plus-end assembly rates measured upon *CDKN1A* re-expression were comparable to those measured in control HCT116 cells.

To further strengthen these findings, RKO cells harboring a ponasterone A inducible *CDKN1A* expression plasmid were used (Schmidt *et al.* 2000). Also here, the induction of *CDKN1A via* ponasterone A treatment arrested the cells in G_1-phase and microtubule plus-end assembly rates were only measured in interphase. Cells were repressed of either *TP53* or *TP73* or both concomitantly by siRNA transfection and the ponasterone A inducible *CDKN1A* expression plasmid was overexpressed. Treatment with 5 µmol/l ponasterone A led to the induction of *CDKN1A* expression, which was verified by western blot analyses (Fig. 3.32c). EB3 tracking experiments revealed, that also in RKO cells, the loss of both *TP53* and *TP73* resulted in an increase in microtubule plus-end assembly rates during interphase, which was reduced upon re-expression of *CDKN1A* (Fig. 3.32d). Therefore, it is possible that p21 acts as an important effector of both, p53 and p73, for regulating microtubule plus-end assembly rates in these cells.

3.2.3 Loss of *TP53* And *TP73* Causes An Invasive Phenotype In HCT116 Cells

Interestingly, loss of *TP53* and *TP73* induced not only increased microtubule plus-end assembly rates during mitosis but also in interphase. As shown in the first part of this thesis, increased microtubule plus-end assembly rates in interphase are associated with increased cell migration and invasion. Therefore, transwell invasion assays for cells with loss of *TP53* and *TP73* were performed. HCT116, HCT116-*TP53*$^{-/-}$, HCT116-*TP73*shRNA cells and three individual cell clones of HCT116-*TP53*$^{-/-}$ cells with a stable repression of *TP73* were used. Furthermore, one HCT116 *TP53*$^{-/-}$/*TP73*sh cell clone, which was generated in the presence of low dose Taxol (Fig. 3.27), was analyzed to examine the influence of microtubule plus-end assembly rates on invasion (Fig. 3.33a). Transwell invasion assays revealed a significantly increased number of invasive cells after concomitant repression of *TP53* and *TP73* in HCT116 cells (Fig. 3.33a). The repression of either *TP53* or *TP73* alone did not alter the invasion potential in comparison to control HCT116 cells. Importantly, low dose Taxol treatment reduced the amount of invading cells to levels comparable to parental HCT116 cells, suggesting that also in cells with loss of *TP53* and *TP73* the invasive phenotype is mediated by increased microtubule plus-end assembly rates.

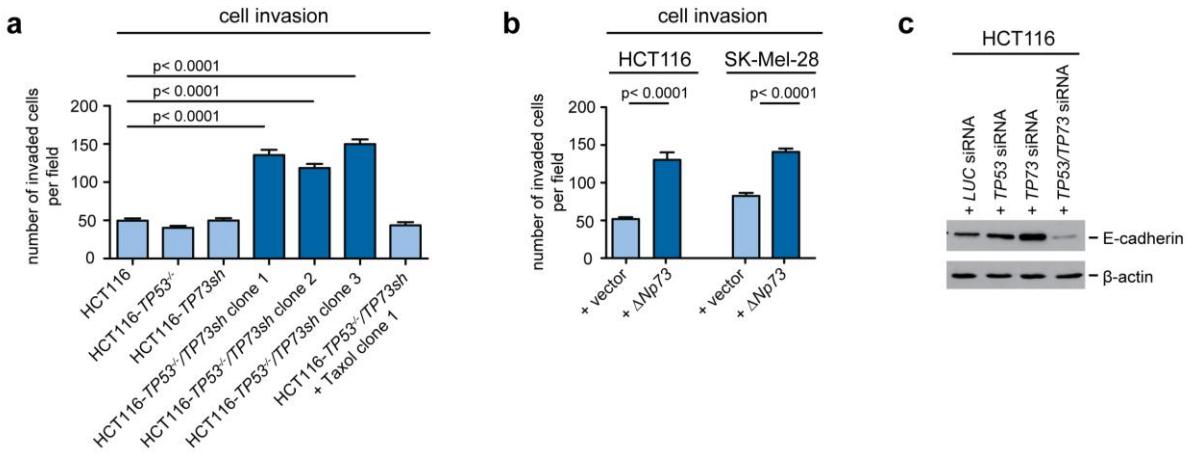

Figure 3.33: Loss of *TP53* and *TP73* induces invasion. (a) Transwell invasion assays using HCT116, HCT116-*TP53*$^{-/-}$, HCT116-*TP73*shRNA cells, three individual cell clones of HCT116-*TP53*$^{-/-}$ cells with a stable repression of *TP73* and one Taxol treated cell clone. Bar graphs show the amount of invaded cells in 30 randomly chosen pictures from three independent experiments (*t*-test, mean ± sem, n=3). **(b)** Transwell invasion assays of HCT116 and SK-Mel-28 cells after overexpression of 50 µg *ΔNp73*. Bar graphs show the amount of invaded cells in 30 randomly chosen pictures from three independent experiments (*t*-test, mean ± sem, n=3). **(c)** Western blot analysis of E-cadherin protein level after transient repression of *TP53*, *TP73* or both concomitantly. Cells were transfected with 60 pmol siRNA and analysis was performed after 48 h. E-cadherin was detected and β-actin was used as a loading control.

This result was also obtained after expression of *ΔNp73* in HCT116 and in non-invasive SK-Mel-28 cells (Fig. 3.33b). As a marker for high motility and invasion, the protein levels of E-cadherin were determined after transient repression of *TP53* and *TP73*. Western blot analysis revealed a strong decrease in E-cadherin protein level after simultaneous repression of *TP53* and *TP73* but not after sole loss of *TP53* or *TP73* (Fig. 3.33c).

3.2.4 *In Vivo* Analyses Of Invasiveness Of HCT116 Cells After Loss Of *TP53* And *TP73*

In order to study the invasive phenotype of the HCT116-*TP53*$^{-/-}$/*TP73*sh cells *in vivo*, chorion allantoic membrane (CAM) assays were performed. CAM assays are an established animal model for cancer research and are widely used to study angiogenesis as well as tumor cell migration and invasion (Deryugina & Quigley 2009). Briefly, fertilized chicken eggs are opened and the CAM becomes accessible. Cells are applied onto the CAM and can be analyzed regarding their growth behavior on and through the membrane.

HCT116 control shRNA, HCT116-*TP53*$^{-/-}$, HCT116-*TP73*sh and HCT116-*TP53*$^{-/-}$/*TP73sh* cells were applied onto the CAM and the grown tumors including the CAM were isolated after seven days. Tumors were fixed and analyzed regarding their overall growth characteristics. Here, the tumors derived from HCT116-*TP53*$^{-/-}$/*TP73*sh macroscopically differed from the tumors derived from the single knock down cells. Whereas the control shRNA transfected

HCT116 cells and the cells repressed of either *TP53* or *TP73* exhibited a polypoid cauliflower-like growth, the cells repressed of both *TP53* and *TP73* exhibited an ulcerative invasive phenotype (Fig. 3.34a), which is often found in invasive carcinoma of the colon.

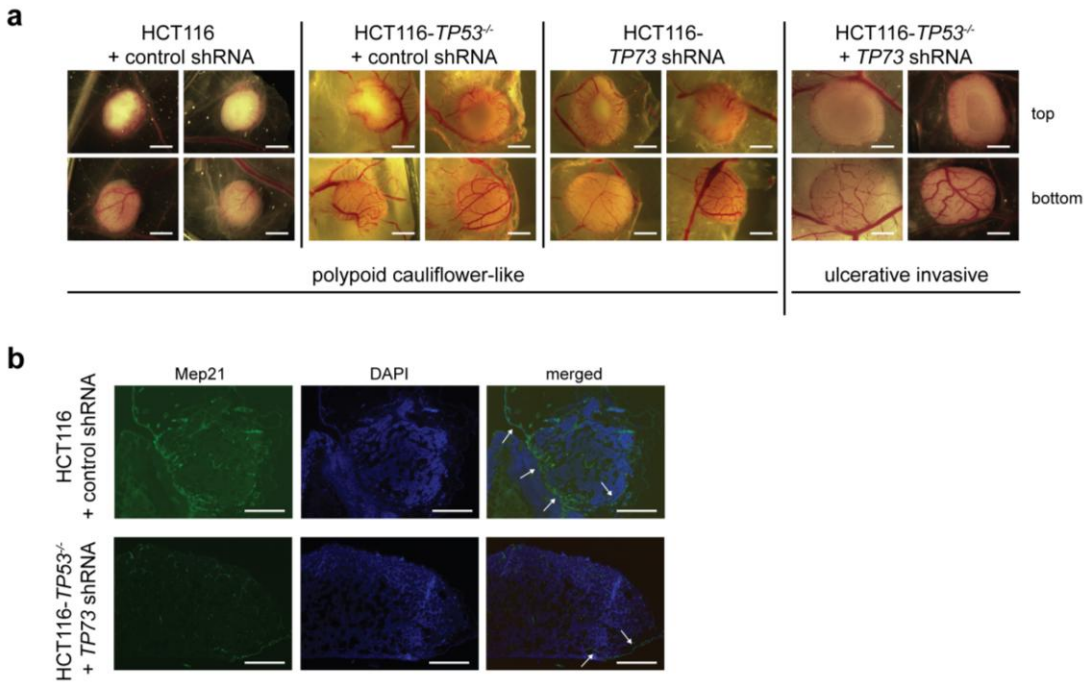

Figure 3.34: Loss of *TP53* and *TP73* causes ulcerative invasive tumor growth *in vivo*. (a) CAM assays of HCT116 control shRNA, HCT116-*TP53*$^{-/-}$ control shRNA, HCT116-*TP73*shRNA and HCT116-*TP53*$^{-/-}$/*TP73*shRNA cells. Two million cells were applied on the CAM on day ten of chicken development. After additional seven days, tumors were isolated and macroscopically analyzed. Two representative tumors derived from each cell line are shown from the top and from the bottom view. Scale bar 200 µm. **(b)** Dissected tumors derived from HCT116 control cells and HCT116-*TP53*$^{-/-}$/*TP73*sh cells were sliced into 12 µM sections and stained for Mep21 and DAPI. Arrows indicate the CAM. Scale bar 100 µm

Immunofluorescence microscopy of cryo-sections of HCT116 control shRNA cells and HCT116-*TP53*$^{-/-}$/*TP73*sh cells gave more insights into the tumor phenotypes. Dissected tumors were sliced into 12 µM sections and stained for Mep21 and DAPI. Staining for Mep21 allowed the discrimination between tumor and blood vessels of the CAM, since Mep21 is a marker for blood endothelial cells of the chicken. Analyses of the tumors derived from HCT116 control cells confirmed the exophytic appearance. The CAM was mainly preserved, but still, the tumor protrudes into the CAM in some sections. Furthermore, the tumor exhibited a very compact and dense structure. In contrast, tumors derived from HCT116-*TP53*$^{-/-}$/*TP73*sh cells showed a mostly destroyed CAM and highly invasive tumor growth. Also, the tumor appeared to be very porous.

These in vivo tumor growth analyses confirmed a highly invasive phenotype induced by the loss of both *TP53* and *TP73*.

4 Discussion

4.1 Increased Activity Of TRIO-Rac1-Arp2/3 Pathway As A Trigger For Migration And CIN

The development of genomic instability is a hallmark of human cancers, which enables the development of certain cancer hallmarks like insensitivity to anti-growth signals, deregulated apoptotic signaling or tissue invasion and metastasis (Hanahan & Weinberg 2000; Hanahan & Weinberg 2011). These newly obtained phenotypes are thought to be acquired by mutations, structural alterations of the genome or chromosomal instability. Thus CIN is associated with tumor progression and an aggressive tumor behavior, which is also characterized by infiltration of nearby tissues and metastases. However, the underlying mechanisms are still largely unknown and a clear link between CIN and cancer cell invasion and metastases is missing so far.

In this thesis, the migration and invasion potential of a panel of MIN/MSI and CIN CRC cell lines and of a panel of melanoma cell lines was examined. Interestingly, not all analyzed CIN cell lines exhibited a migratory and invasive phenotype, but *vice versa* the migratory and invasive cell lines were CIN (Fig. 3.1, Fig. 3.2, Fig. 3.5). Importantly, the migration and invasion potentials of CRC and melanoma cell lines were strongly associated with increased interphase microtubule plus-end assembly rates (Fig. 3.1, Fig. 3.2). Recently, our group established increased microtubule plus-end assembly rates during mitosis as a common cause for CIN (Ertych *et al.* 2014), but the role of increased interphase microtubule plus-end assembly rates has not been investigated yet. This apparent new relationship between microtubule plus-end dynamics in interphase and cell migration was surprising. Therefore, it was of great interest to investigate how enhanced microtubule dynamics contribute to the regulation of cell motility.

In this study, a hyperactive TRIO-Rac1-Arp2/3 pathway was identified as a trigger for the development of a highly migratory and a chromosomally instable phenotype. Furthermore, the studies revealed increased microtubule plus-end assembly rates as an activator of this pathway. During interphase, the hyperactivation of TRIO-Rac1-Arp2/3 due to elevated microtubule plus-end assembly rates presumably results in highly branched actin filaments, which are required for lamellipodia and invadopodia formation during cellular migration and tissue invasion. On the other hand, during mitosis, the microtubule-dependent hyperactivation of TRIO-Rac1-Arp2/3 induces spindle misorientation, the generation of lagging chromosomes and CIN. Therefore, increased microtubule plus-end assembly rates promote the development of a highly aggressive and invasive phenotype.

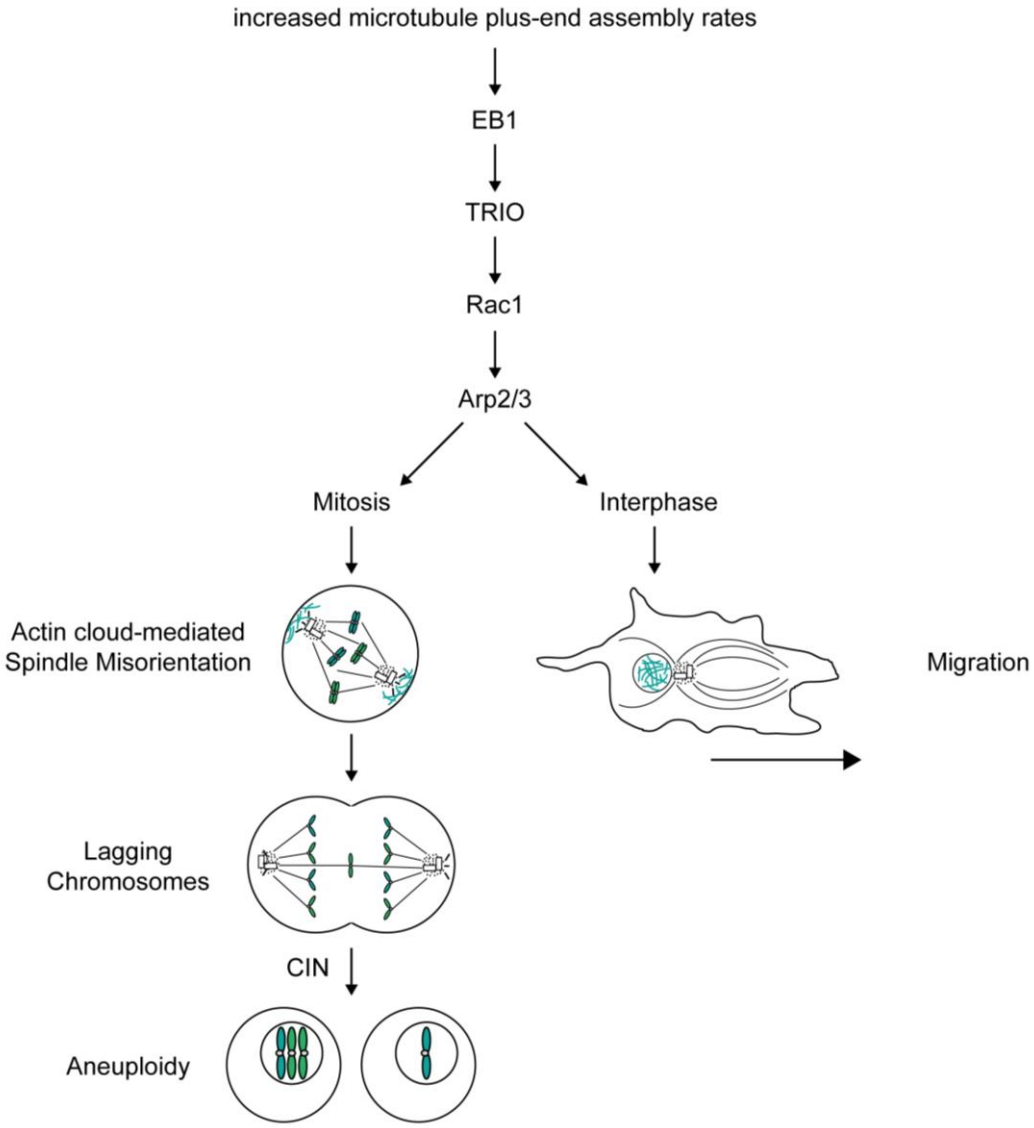

Fig. 4.1: Model showing the microtubule-dependent hyperactivity of the TRIO-Rac1-Arp2/3 pathway that affects both mitosis and interphase. During interphase, in cells exhibiting increased microtubule plus-end assembly rates, TRIO binds to microtubules *via* EB1 and becomes hyperactivated. TRIO activates Rac1, which subsequently leads to Arp2/3-mediated reorganization of the actin cytoskeleton and the formation of lamellipodia thus facilitating migration and invasion. During mitosis, the microtubule dependent increased activity of the Arp2/3 complex leads to spindle misorientation due to enhanced formation of actin clouds. The spindle misorientation causes lagging chromosomes and CIN.

During cell migration, the activation of Rho family GTPases is mediated by GEFs. At least 20 GEFs are known to regulate the activation of Rac1 by catalyzing the exchange of GDP for GTP (Marei & Malliri 2016). Upon them TIAM1, TIAM2, GEF-:H1, ASEF and TRIO are well characterized (Kawasaki *et al.* 2000; Blangy *et al.* 2000; Krendel *et al.* 2002; Rooney *et al.* 2010). TRIO was identified as a microtubule plus-end binding protein in HeLa and neurite cells, whereby binding to microtubules is mediated by the +TIP EB1 (Van Haren *et al.* 2014). EB1 was described to be an important protein in the development of a signaling platform at the microtubule plus-end (Vaughan 2005; Tamura & Draviam 2012), which includes binding

of CLIP-170 (Lantz & Miller 1998), APC, CLASP1 and CLASP2 (Tsvetkov *et al.* 2007). Interestingly, *EB1* is overexpressed in different tumor types and is associated with increased tumor formation (Wang *et al.* 2005). Repression of *EB1* interfered with formation of lamellipodia protrusions in mouse melanoma cells and deregulated Arp2/3 activity during interphase (Schober *et al.* 2009). The binding of TRIO to EB1 enhances its activity. Therefore, the question arises, how binding of TRIO and other GEFs to microtubule plus-ends leads to their activation. In HeLa and neurite cells it was shown, that TRIO binds to microtubules *via* the navigator complex Nav1 and EB1. Thereby, the GEF activity of TRIO and subsequent neurite outgrowth were enhanced. It is hypothesized, that due to binding of TRIO to Nav1 and EB1, the GEF domain of TRIO becomes exposed and the interaction between TRIO and its target GTPase is stabilized (Van Haren *et al.* 2014). Further, the binding of TRIO to microtubules *via* EB1 might lead to a spatial regulated intracellular signaling, which is needed for Rac1-mediated lamellipodia formation at the leading edge of a migrating cell. Microtubule polymerization sequesters and inactivates GEFs whereas microtubule depolymerization releases GEFs (Chang *et al.* 2007). These processes mainly occur at the microtubule plus-ends. During cell motility, the centrosome and the majority of microtubules are oriented towards the leading edge of the cell (Wittmann & Waterman-Storer 2001). Furthermore, microtubule plus-ends, which are oriented towards the leading edge, grow more persistently compared to microtubules oriented towards the rear of a cell (Waterman-Storer & Salmon 1997; Ballestrem *et al.* 2000). However, microtubules usually do not enter the lamellipodium except some so called ´pioneer microtubules´ (Wittmann *et al.* 2003). It seems possible that TRIO might be bound to microtubule plus-ends *via* EB1 and is mainly transported towards the leading edge. Here, microtubule depolymerization would lead to a release of TRIO, which would then in turn be able to activate membrane bound Rac1 in the leading edge, resulting in Arp2/3-activation and actin branching within the lamellipodium.
It remains unclear, whether TRIO directly activates Rac1 or whether also another Rho-family small GTPase, RhoG, which is also a target of TRIO´s GEF activity (Blangy *et al.* 2000), is involved. RhoG is able to activate both Rac1 and Cdc42 in the lamellipodium in a microtubule dependent manner (Gauthier-Rouviere *et al.* 1998), resulting in elevated levels of active Rac1 and active Cdc42. Active Rac1 and Cdc42, in turn, lead to WAVE/WASP-mediated activation of the Arp2/3 complex. The Arp2/3 complex is a well established complex in the formation of branched actin in the lamellipodium, thereby providing a protrusive force (Zheng *et al.* 2008). The hyperactivity of the Arp2/3 complex contributed to growth and invasiveness of gastric carcinoma (Zheng *et al.* 2008), whereas silencing interfered with cell migration in pancreatic cancer (Rauhala *et al.* 2013). Therefore, the hyperactivation of Arp2/3 mediated by the TRIO-Rac1 axis constitutes a greatly important step in tumor cell migration and invasion.

Because only few microtubules reach into the lamellipodium it is questionable whether they are sufficient to transport enough TRIO molecules for the activation of either Rac1 or RhoG to the side of protrusion. Therefore, an amplification of the signaling cascade might be necessary. Rac1 activity can also be stimulated through the Ras GTPase activating like protein IQGAP1, which stabilizes and increases active Rac1 and Cdc42 levels (Briggs & Sacks 2003). IQGAP1 binds to the +TIP CLIP-170, which was detected at microtubules in the leading edge (Fukata *et al.* 2002; Watanabe *et al.* 2004). Furthermore, IQGAP1 is also localized at the cell cortex. A positive feedback loop between IQGAP1 and Rac1 is described: cortical IQGAP1 stimulates Rac1, which in turn promotes microtubule-dependent stabilization of IQGAP1 (Siegrist & Doe 2007). Further, not only TRIO but also other GEFs, like GEF-H1 and ASEF might be delivered to the leading edge. Therefore, different GEF activities and IQGAP1 might contribute to the microtubule-dependent activation of Rac1 in the leading edge and an amplified signaling (Fig. 4.2).

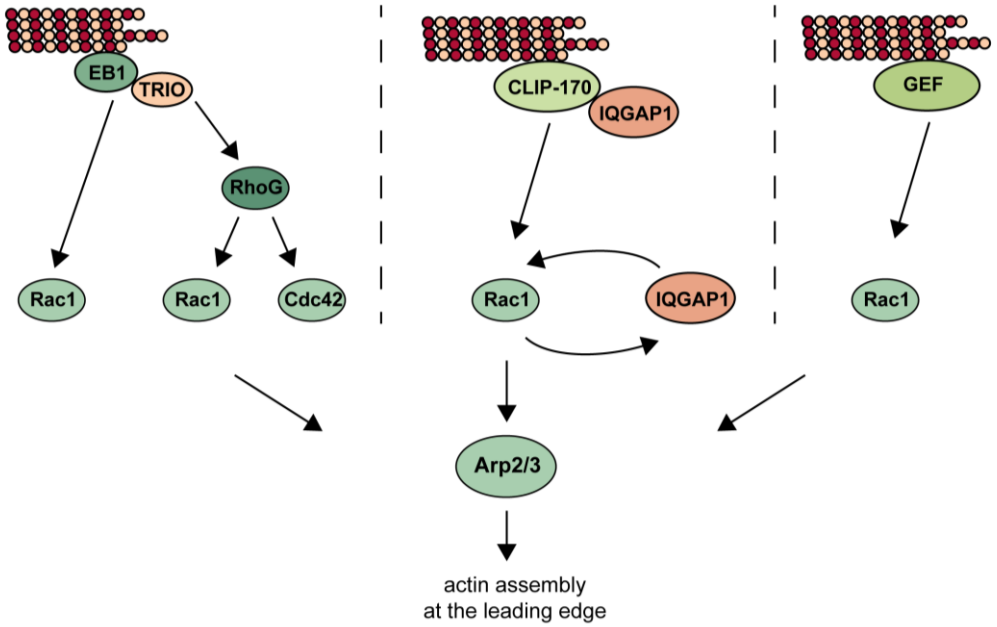

Fig. 4.2: Possible modes of induction of microtubule dependent actin assembly at the leading edge. Microtubule-dependent transport of TRIO to the leading edge might directly activate membrane bound Rac1. But Rac1 activation may also happen due to RhoG activation. Furthermore, IQGAP1 could be transported to Rac1, where a positive feedback loop between Rac1 and IQGAP1 would result in highly active Rac1. Additionally, microtubules could also deliver Rac1-GEFs other than TRIO to the leading edge. These different modes might cooperate to mediate actin assembly through the activation of the Arp2/3 complex.

Recently, also microtubules themselves were described to be capable of actin polymerization (Henty-Ridilla *et al.* 2016). Also here, the +TIP CLIP-170 is involved. It binds to formins, which accelerate actin polymerization by binding to the growing barbed end (Evangelista *et*

al. 2003). Therefore, also TRIO-independent mechanisms could contribute to actin assembly at the leading edge to promote migration.

Interestingly, recent studies linked the amplification of centrosomes with the hyperactivation of Rac1 and an invasive phenotype (Godinho *et al.* 2014). Thereby, an increased number of centrosomes is thought to nucleate increased amounts of microtubules that activate Rac1 by an unknown mechanism. In conformity with my results, an increased microtubule polymer mass might also expose more microtubule plus-ends with, where binding of TRIO can occur. Therefore, more TRIO could be transported towards Rac1 at the invasive front. Whether increased microtubule plus-end assembly rates, which constitute the trigger of increased Rac1-activity in my studies, also lead to increased microtubule polymer mass is not clear and remains to be studied.

In contrast to interphase, the role of TRIO, Rac1 and the Arp2/3 complex in mitotic chromosome segregation is not established, but some reports hint to mitotic roles of different GEFs. The Rac1-GEF TIAM1 was described to play a role during centrosome separation (Woodcock *et al.* 2010). Its depletion resulted in increased centrosome separation and chromosome congression failures (Woodcock *et al.* 2010). Also TRIO was identified as a mitotic Rac1-GEF, acting during cytokinesis at the cleavage furrow (Cannet *et al.* 2014). Unpublished data from our group showed that TRIO is localized to microtubule plus-ends during interphase and mitosis in an EB1-dependent fashion. At the cell cortex, TRIO might be able to activate Rac1 with subsequent actin polymerization triggered by the Arp2/3 complex. During mitosis, a dynamic, revolving cluster of actin filaments was described to be present from prometaphase to anaphase (Mitsushima *et al.* 2010). This cluster, referred to as ´actin clouds´, is located at the cell cortex, extends into the cytoplasm and depends on Arp2/3 activity (Mitsushima *et al.* 2010). Actin clouds might exert pulling forces on centrosomes towards retraction fibers, thus polarizing the cell and orientating the mitotic spindle at the longest cell axis (Fink *et al.* 2011). Unpublished data from our group indeed revealed a decreased formation of actin clouds upon treatment with TRIO-, Rac1- or Arp2/3-inhibitors. Thus, the appearance of a hyperactive TRIO-Rac1-Arp2/3 pathway during mitosis might result in an enhanced branched actin polymerization, leading to the accumulation of dense actin clouds. However, it remains unclear, how actin clouds affect spindle positioning. First hints towards this question were provided recently by the Pellman Group (Kwon *et al.* 2015). Their studies suggest that the actin cloud might exert pulling forces *via* the microtubule binding myosin Myo10, which was shown to link actin and microtubules and move the spindle poles towards actin clouds and retraction fibers (Weber *et al.* 2004; Woolner *et al.* 2008; Kwon *et al.* 2015). Myo10 was described to exhibit overlapping functions with dynein in mammalian cells. Dynein is mainly involved in anchoring the mitotic spindle at the cell cortex *via* a complex of $G_{\alpha i}$-LGN-NuMA and a loss of dynein causes

misorientated mitotic spindles (Kiyomitsu & Cheeseman 2012). But the cortical distribution of dynein is also affected by external stimuli (Morin & Bellaïche 2011). Therefore, it is not clear, whether actin clouds influence the localization of dynein or whether dynein affects the orientation of actin clouds.

Our unpublished data showed that the mitotic localization of TRIO is not restricted to astral microtubules, which grow towards the cell cortex and could possibly interact with membrane bound Rac1. Therefore, TRIO might not only function at the cortex but also at centrosomes, since its localization depends on EB1, which was shown to localize also to centrosomes (Morrison *et al.* 1998; Berrueta *et al.* 1998; Mimori-Kiyosue *et al.* 2000). Furthermore, Rac1 was also described to localize to centrosomal regions in early mitosis (Woodcock *et al.* 2010). Here, it was shown, that the Rac1-GEF TIAM1 facilitates bipolar spindle assembly (Woodcock *et al.* 2010). Therefore, also TRIO might interact with Rac1 at centrosomes thus triggering actin cloud assembly. Besides microtubules, also actin is important for centrosome separation, since depolymerization of actin inhibits splitting of centrosomes (Uzbekov *et al.* 2002). Tyrosine-phosphorylated cortactin (p-cortactin) was identified as a trigger for centrosome separation (Wang *et al.* 2008). Actin filaments can attach to p-cortactin and exert forces to push the centrosomes apart (Wang *et al.* 2008). During interphase, the phosphorylation of cortactin requires Rac1 activity (Head *et al.* 2003). Therefore, also during mitosis, active Rac1 might be important in facilitating cortactin phosphorylation. An abnormal regulated cortactin phosphorylation due to Rac1 hyperactivity might further be associated with deregulated spindle formation and chromosome missegregation.

The overexpression and increased activity of TRIO, Rac1 and Arp2/3 is linked to several tumor types. *TRIO* overexpression, which comes along with hyperactive TRIO, is observed in different cancer types and can be found in the most aggressive forms of malignant glioblastoma, where it is associated with poor patient survival (Schmidt & Debant 2014). Additionally, our unpublished results revealed a correlation of high *TRIO* expression in metastases of colon cancers exhibiting CIN. Thus, TRIO is highly associated with both, invasiveness and aneuploidy in late stage colon tumors. Furthermore, deregulated Rac1-activity is common in cancer. Rac1 overexpression can be found in breast carcinoma, non-small cell lung carcinoma and gastric carcinoma and results in accelerated tumor progression and high mortality rates (Espina *et al.* 2008). Rac1-signaling modulates cell migration and invasion by mediating lamellipodia formation and MMP expression, thereby leading to tumor metastases (Mack *et al.* 2011) but a role of hyperactive Rac1 is not directly associated with CIN so far. Downstream of Rac1, also overexpression of the Arp2/3 complex is associated with highly invasive tumors. In gastric carcinoma, increased activity of the Arp2/3 complex is involved in pathogenesis and progression (Zheng *et al.* 2008). However it remains to be shown whether TRIO, Rac1 or Arp2/3 overexpressing tumors also display

increased actin cloud formation during mitosis and thus, spindle misorientation and CIN. Still, this shared trigger for the development of CIN and cancer cell migration and invasion may constitute an interesting target in cancer therapies. The Rac1 inhibitor NSC23766 was already used in treatment of different breast cancers, where it induced cell cycle arrest and apoptosis (Yoshida *et al.* 2010). However, the efficacy of NSC23766 was not sufficient for its substantial clinical use (Bid *et al.* 2013). But the development of a drug that targets the TRIO-Rac1-Arp2/3 pathway might possibly suppress CIN and cancer cell migration and invasion and thus the two highly relevant phenotypes, which are detected in aggressive cancer.

4.2 p53 And p73 Act As Regulators Of Chromosomal Stability And Cell Invasion

In human cancer, the *TP53* gene encoding for the tumor suppressor p53 is the most frequently mutated gene. Mutations in *TP53* occur late during cancer progression (Baker *et al.* 1990). p53 has two homologs, p63 and p73. Interestingly, the chromosome region coding for p73 is lost in a wide array of tumors, including neuroblastoma (Kaghad *et al.* 1997), melanoma (Dracopoli *et al.* 1989) and hepatocellular carcinoma (Yeh *et al.* 1994). p73 was shown to inhibit aneuploidy in the absence of p53 in mice (Talos *et al.* 2007). Furthermore, a dominant negative form of p73, ΔNp73, which inhibits p53´s and p73´s function, is often overexpressed in tumors and is associated with a highly metastatic phenotype (Steder *et al.* 2013). Thus, we wanted to elucidate how p53 and p73 cooperate in maintaining genomic stability and suppressing invasion.

In this study, p53 and p73 were identified as important regulators of chromosomal stability and cellular migration and invasion. Importantly, the concomitant loss of *TP53* and *TP73* induced aneuploidy (Fig. 3.26d). A complete loss of *TP53* is not common in cancer, but several hot spot mutations of p53 are described (Goldstein *et al.* 2011; Muller & Vousden 2013). These mutants were shown to interact with p73, thereby inhibiting its transcriptional activity (Gaiddon *et al.* 2001). But during my studies, an effect of mutant p53 (p53 R175H) onto chromosomal stability was not detected. However, in combination with *TP73* repression, the development of CIN was observed (Fig. 3.29). A dominant negative form of p73, ΔNp73, was described to negatively regulate both, p53 and p73 function (Grob *et al.* 2001). In my studies, *ΔNp73* overexpression indeed caused increased amounts of cells displaying lagging chromosomes (Fig. 3.30), which constitute a prerequisite for the development of CIN suggesting that concurrent loss of p53 and p73 function is required to induce CIN.

The loss of function of p53 in human colon carcinoma cells is not sufficient to induce aneuploidy (Bunz *et al.* 2002). However, in colorectal cancer CIN is often associated with p53 loss. Since p53 and p73 exhibit functional and structural similarities, such as a highly conserved DNA-binding domain (Levrero *et al.* 2000), they might be able to fulfill redundant

functions and partially transactivate the same genes. Therefore, upon loss of either p53 or p73, the remaining protein might be able to substitute for the other. This is in agreement with findings from Talos *et al.*, who showed that p73 suppresses polyploidy in the absence of functional p53 in mouse embryonic fibroblasts (MEFs) (Talos *et al.* 2007). But while these MEFs developed polyploidy, in my studies the used colorectal cancer cells developed aneuploidy. Thus, on the one hand the maintenance of chromosomal stability seems to be regulated by p53 and p73 but on the other hand different mechanism might account for that in mice and human.

Further, the absence of p53 was shown to correlate with centrosome amplification in mice (Tarapore & Fukasawa 2002). Additionally, in mouse models, a relationship between mutant p53 and p73 was described causing overduplication of centrosomes. In these studies, p53 R172H derived tumors were highly aneuploid due to inhibition of p73 and subsequent centrosome amplification (Murphy *et al.* 2000). Supernumerary centrosomes generate lagging chromosomes, due to transient spindle geometry defects occurring during the assembly of multipolar spindles, that are clustered into a spindle pole. Also human tumors show a strong association between mutant p53 and supernumerary centrosomes, including breast tumors (Carroll *et al.* 1999). However, it was also shown, that loss of p53 alone neither lead to centrosome amplification nor to CIN (Lengauer *et al.* 1997; Bunz *et al.* 2002).

In addition to deregulated mitotic functions, also erroneous replication might result from simultaneous loss of function of p53 and p73. An aberrant activation of CDK-cyclin complexes during S-phase was indeed detected in mice upon loss of p53 and p73 (Talos *et al.* 2007). This resulted in aneuploidy due to a delayed S-phase and re-replication. Indicative for erroneous pre-mitotic defects is the occurrence of acentric chromosomes or chromosome bridges (Burrell *et al.* 2013). Since in my studies, cells concomitantly depleted of *TP53* and *TP73* exhibited high amounts of cells displaying anaphase bridges (Fig 3.25d), it might be possible that replication stress leads also to structural chromosome aberrations (S-CIN) in these cells. Thus, depletion of *TP53* and *TP73* might cause replication stress, which affects the following mitosis (Wilhelm *et al.* 2013; Gelot *et al.* 2015). Recently, an impaired replication fork progression was detected in the absence of p53 (Yeo *et al.* 2016). Thereby, p53 was discovered to prevent conflicts between transcription and replication in S-phase. Upon loss of p53, the timely progression of replication was disturbed by secondary DNA structures, leading to replication fork stalling and collapse (Yeo *et al.* 2016). This in turn results in DNA double strand breaks, which may underlie deletion in mitosis.

My studies showed that the repression of both, *TP53* and *TP73* or the overexpression of *ΔNp73* resulted in an invasive phenotype. Furthermore, the loss of both transcription factors led to a strong reduction in the E-cadherin protein level (Fig. 3.32b), which might be a marker for EMT. Interestingly, *in vivo* studies of HCT116 cells repressed of both *TP53* and *TP73* by

using CAM assays revealed a clinical relevant phenotype: while tumors derived from control shRNA transfected HCT116 cells exhibited a polypoid cauliflower-like phenotype, tumors derived from *TP73* shRNA transfected HCT116-*TP53*$^{-/-}$ cells exhibited an ulcerative invasive tumor growth (Fig. 3.34).

Wild-type p53 was found to inhibit EMT, cancer cell invasion and metastases by Mdm2-mediated degradation of the transcriptional repressor Slug, which leads to enhanced *CDH1* (encoding for E-cadherin) expression (Wang *et al.* 2009). But p53´s function is opposed by another transcription factor, Twist, which is able to hinder DNA binding of p53 (Shiota *et al.* 2008; Smit & Peeper 2008). Therefore, upon loss of *TP53*, both Slug and Twist can drive the repression of *CDH1* and promote EMT. Furthermore, Slug and Twist were described to be increased upon *TP73* repression in MCF-10A cells leading to a highly migratory phenotype of this cell line (Zhang *et al.* 2012). This indicates a regulation of Slug and Twist by both p53 and p73. Thus, the loss of function of p53 and p73 downregulates *CDH1* expression, which is frequently observed in cancer and strongly associated with metastases in mouse models (Derksen *et al.* 2006).

During invasion, the formation of podosomes and invadopodia is an important step. These membrane protrusions are involved in adhesion and invasion and are capable of secretion of matrix-metalloproteinases (MMPs). The formation of podosomes is mediated by Src kinase activity, which is counteracted by p53. Hence, wild-type p53 is involved in suppressing the formation of invadopodia and podosomes. This is mediated by up-regulating PTEN and caldesmon. PTEN antagonizes phosphatidylinositol-3,4,5-trisphosphate (PIP_3) and phosphatidylinositol-4,5-bisphosphate (PIP_2) formation during cell polarization, whereas caldesmon inhibits Arp2/3 induced actin polymerization and also stabilizes actin stress fibers (Yamakita *et al.* 2003; Yoshio *et al.* 2007).

The loss of function of p53 and p73 can also occur due to overexpression of *⊿Np73*. This overexpression results in the gain of highly aggressive traits in cancer (Engelmann *et al.* 2014). ⊿Np73 inhibits p53 and p73 and therefore might work antagonistically to both (Pützer 2013). *⊿Np73* overexpression is found in several cancers including lung cancer (Uramoto *et al.* 2004), neuroblastoma (Douc-Rasy *et al.* 2002) and prostate carcinoma (Guan & Chen 2005). The ⊿Np73 isoform is a regulator of EMT by up-regulating N-cadherin and vimentin as well as Slug, which represses *CHD1*, and was found highly expressed in metastases of skin cancer patients (Engelmann *et al.* 2014). *Vice versa*, the knock down of *⊿Np73* in metastatic cell lines suppressed their invasion potential (Steder *et al.* 2013). Thus ⊿Np73 plays an important role in metastasis induction potentially by inhibiting the repressive functions of p53 and p73. The loss of function of p53 and p73 were accompanied by increased mitotic and interphase microtubule plus-end assembly rates. Based on the findings represented in this thesis, repression of *TP53* and *TP73* might hyperactivate the TRIO-Rac1-

Arp2/3 pathway, which in turn leads to a highly invasive phenotype. Thus, the increased microtubule plus-end assembly rates in mitosis and interphase detected after depletion of *TP53* and *TP73* or overexpression of *⊿Np73* might support the hyperactivation of TRIO and the respective downstream signaling. This might be in line with the observation that the loss of *TP53* alone is not sufficient to induce migration and invasion (Sablina *et al.* 2003; Guo & Zheng 2004) (Fig. 3.32a), since depletion of *TP53* alone did not induce increased microtubule plus-end assembly rates (Fig. 3.25b). In mice, *TP53* deletion was described to result in elevated activities of the PI3K-Rac1-Akt signaling pathway without altering their protein expression (Guo *et al.* 2003). This suggests that cells exhibit enhanced capability of cell migration upon loss of function of p53 but nevertheless also other stimuli are necessary for the development of a migratory and invasive phenotype. These additionally required stimuli could involve various alterations, which affect and enhance microtubule plus-end assembly rates. This may include mutations of *TP53*. Mutations of *TP53* can result in gain of functions, which predispose cells to cancer invasion and metastasis (Oren & Rotter 2010). In mouse models, mutant p53 increases the capability of metastatic carcinomas (Lang *et al.* 2004; Heinlein *et al.* 2008).

RNA-sequencing revealed a pronounced repressed expression of *CDKN1A* upon depletion of *TP53* and *TP73*, which was confirmed by qRT-PCR analyses (Table 3.1, Fig. 3.31a). Furthermore, the re-expression of *CDKN1A* suppressed microtubule plus-end assembly rates in interphase detected upon loss of p53 and p73 (Fig. 3.32b, d). Thus it might be possible, that the observed phenotypes are mediated by p21. p21 acts as a CDK inhibitor, and therefore the loss of function of p21 would lead to an increased CDK activity. Known p21 targets are CDK2 in interphase and CDK1 in mitosis. Whereas CDK2 functions mainly during G_1-S-phase, CDK1 is active during mitosis. A function of CDKs in the regulation of microtubule dynamics is not known, but a few reports have shown a localization of CDKs at centrosomes. For instance, the mitotic CDK1 is transported to the centrosome by the centrosomal protein Cep63 (Löffler *et al.* 2011) and becomes activated there in early mitosis (Jackman *et al.* 2003). Further, CP110 is a target of CDK2, which is involved in centrosome duplication. Loss of CDK-phosphorylation on CP110 led to polyploidy (Chen *et al.* 2002). Also the spindle checkpoint kinase Mps1 is phosphorylated by CDK2 (Fisk & Winey 2001). Moreover, hyperactivation of CDK2 correlates with centrosome amplification (Adon *et al.* 2010). Thus, a relationship between deregulated CDK activity and dysfunction might exist. Therefore, loss of p21 might affect centrosome-mediated microtubule dynamics through increased CDK activity. Whether p21 indeed exerts its microtubule dynamic regulating function *via* its CDK-inhibiting activity needs to be further analyzed in future studies.

References

Abbas, T. & Dutta, A., 2009. P21 in Cancer: Intricate Networks and Multiple Activities. *Nature Reviews Cancer*, 9(6), pp.400–414.

Achard, V. *et al.*, 2010. A “Primer”-Based Mechanism Underlies Branched Actin Filament Network Formation and Motility. *Current Biology*, 20, pp.423–428.

Adachi, A. *et al.*, 1987. Productive, persistent infection of human colorectal cell lines with human immunodeficiency virus. *Journal of Virology*, 61(1), pp.209–213.

Adon, A.M. *et al.*, 2010. Cdk2 and Cdk4 regulate the centrosome cycle and are critical mediators of centrosome amplification in p53-null cells. *Molecular and cellular biology*, 30(3), pp.694–710.

Akhmanova, A. & Steinmetz, M.O., 2015. Control of microtubule organization and dynamics: two ends in the limelight. *Nature Reviews Molecular Cell Biology*, 16(12), pp.711–26.

Akin, O. & Mullins, R.D., 2008. Capping Protein Increases the Rate of Actin-Based Motility by Promoting Filament Nucleation by the Arp2/3 Complex. *Cell*, 133(5), pp.841–851.

Alla, V. *et al.*, 2010. E2F1 in melanoma progression and metastasis. *Journal of the National Cancer Institute*, 102(2), pp.127–133.

Amundson, S.A., Myers, T.G. & Fornace, A.J.J., 1998. Roles for p53 in growth arrest and apoptosis: putting on the brakes after genotoxic stress. *Oncogene*, 17(25), pp.3287–99.

Arellano, M. & Moreno, S., 1997. Regulation of CDK/cyclin Complexes During the Cell. *International Journal of Biochemistry and Cell Biology*, 29(559-573).

Baker, S.J. *et al.*, 1990. P53 Gene Mutations Occur in Combination With 17P Allelic Deletions As Late Events in Colorectal Tumorigenesis. *Cancer Research*, 50(23), pp.7717–7722.

Bakhoum, S.F. *et al.*, 2009. Genome stability is ensured by temporal control of kinetochore-microtubule dynamics. *Nature cell biology*, 11(1), pp.27–35.

Bakhoum, S.F. *et al.*, 2014. The mitotic origin of chromosomal instability. *Current Biology*, 24(4), pp.R148–R149.

Bakhoum, S.F. & Compton, D.A., 2012. Chromosomal instability and cancer : a complex relationship with therapeutic potential. *The Journal of Clinical Investigation*, 122(4), pp.1138–1143.

Ballestrem, C. *et al.*, 2000. Actin-dependent lamellipodia formation and microtubule-dependent tail retraction control-directed cell migration. *Molecular biology of the cell*, 11(9), pp.2999–3012.

Banin, S. *et al.*, 1998. Enhanced Phosphorytation of p53 by ATM in Response to DNA Damage. *Science*, 281(5383), pp.1674–1677.

Barber, T.D. *et al.*, 2008. Chromatid cohesion defects may underlie chromosome instability in human colorectal cancers. *Proceedings of the National Academy of Sciences of the United States of America*, 105(9), pp.3443–3448.

Bartek, J., Lukas, C. & Lukas, J., 2004. Checking on DNA damage in S phase. *Nature reviews. Molecular cell biology*, 5(10), pp.792–804.

Bergstralh, D.T. & St Johnston, D., 2014. Spindle orientation: What if it goes wrong? *Seminars in Cell and Developmental Biology*, 34, pp.140–145.

Berrueta, L. *et al.*, 1998. The adenomatous polyposis coli-binding protein EB1 is associated with cytoplasmic and spindle microtubules. *Proceedings of the National Academy of Sciences of the United States of America*, 95(18), pp.10596–10601.

Bershadsky, A. *et al.*, 1996. Involvement of microtubules in the control of adhesion-dependent signal transduction. *Current biology*, 6(10), pp.1279–1289.

Bershadsky, A.D., Vaisberg, E.A. & Vasiliev, J.M., 1991. Pseudopodial activity at the active edge of migrating fibroblast is decreased after drug-induced microtubule depolymerization. *Cell motility and the cytoskeleton*, 19(3), pp.152–158.

Bertoli, C., Skotheim, J.M. & de Bruin, R.A.M., 2013. Control of cell cycle transcription during G1 and S phases. *Nature reviews. Molecular cell biology*, 14(8), pp.518–28.

Bid, H.K. *et al.*, 2013. RAC1: an emerging therapeutic option for targeting cancer angiogenesis and metastasis. *Molecular cancer therapeutics*, 12(10), pp.1925–1934.

Blanchoin, L. *et al.*, 2014. Actin dynamics, architecture, and mechanics in cell motility. *Physiological reviews*, 94(1), pp.235–63.

Blangy, A. *et al.*, 2000. TrioGEF1 controls Rac- and Cdc42-dependent cell structures through the direct activation of RhoG. *Journal of cell science*, 113, pp.729–39.

Boettner, B. & Van Aelst, L., 2002. The role of Rho GTPases in disease development. *Gene*, 286(2), pp.155–174.

Bos, J.L., Rehmann, H. & Wittinghofer, A., 2007. GEFs and GAPs : Critical Elements in the Control of Small G Proteins. *Cell*, 129, pp.865–877.

Bouquier, N. *et al.*, 2009. A Cell Active Chemical GEF Inhibitor Selectively Targets the Trio/RhoG/Rac1 Signaling Pathway. *Chemistry and Biology*, 16(6), pp.657–666.

Brattain, M.G. *et al.*, 1984. Heterogeneity of human colon carcinoma. *Cancer metastasis reviews*, 3, pp.177–191.

Brattain, M.G. *et al.*, 1981. Heterogeneity of Malignant Cells from a Human Colonic Carcinoma. *Cancer Research*, 41(May), pp.1751–1756.

Bretscher, M.S., 1996. Getting membrane flow and the cytoskeleton to cooperate in moving cells. *Cell*, 87(4), pp.601–606.

Briggs, M.W. & Sacks, D.B., 2003. IQGAP proteins are integral components of cytoskeletal regulation. *EMBO reports*, 4(6), pp.571–4.

Brinkley, B.R., 2001. Managing the centrosome numbers game: From chaos to stability in cancer cell division. *Trends in Cell Biology*, 11(1), pp.18–21.

Brouhard, G.J. *et al.*, 2008. XMAP215 Is a Processive Microtubule Polymerase. *Cell*, 132(1), pp.79–88.

Buccione, R., Orth, J.D. & McNiven, M.A., 2004. Foot and Mouth: Podosomes, Invadopodia and Circular Dorsal Ruffles. *Nature Reviews Molecular Cell Biology* 5(8), pp.647–657.

Bunz, F. *et al.*, 2002. Targeted Inactivation of p53 in Human Cells Does Not Result in Aneuploidy. *Cancer Research*, 62, pp.1129–1133.

Burns, K.M. *et al.*, 2014. Nucleotide exchange in dimeric MCAK induces longitudinal and lateral stress at microtubule ends to support depolymerization. *Structure*, 22(8), pp.1173–1183.

Burrell, R.A. *et al.*, 2013. Replication stress links structural and numerical cancer chromosomal instability. *Nature*, 494(7438), pp.492–496.

Burridge, K. & Wennerberg, K., 2004. Rho and Rac Take Center Stage. *Cell*, 116(2), pp.167–179.

Busson, S. *et al.*, 1998. Dynein and dynactin are localized to astral microtubules and at cortical sites in mitotic epithelial cells. *Current Biology*, 8(9), pp.541–544.

Cain, R.J. & Ridley, A.J., 2009. Phosphoinositide 3-kinases in cell migration. *Biology of the cell*, 101(1), pp.13–29.

Calderwood, D.A., Shattil, S.J. & Ginsberg, M.H., 2000. Integrins and actin filaments: reciprocal regulation of cell adhesion and signaling. *The Journal of biological chemistry*, 275(30), pp.22607–22610.

Cannet, A. *et al.*, 2014. Identification of a mitotic Rac-GEF, Trio, that counteracts MgcRacGAP function during cytokinesis. *Molecular Biology of the Cell*, 25(25), pp.4063–4071.

Carey, T.E. *et al.*, 1976. Cell surface antigens of human malignant melanoma: Mixed hemadsorption assays for humoral immunity to cultured autologous melanoma cells. *Immunology*, 73(9), pp.3278–3282.

Carroll, P.E. *et al.*, 1999. Centrosome hyperamplification in human cancer: chromosome instability induced by p53 mutation and/or Mdm2 overexpression. *Oncogene*, 18(11), pp.1935–1944.

Chambers, A.F. & Matrisian, L.M., 1997. Changing views of the role of matrix metalloproteinases in metastasis. *JNCI Journal of the National Cancer Institute*, 89(17), pp.1260–1270.

Chan, Y.W. *et al.*, 2012. Aurora B controls kinetochore-microtubule attachments by inhibiting Ska complex-KMN network interaction. *Journal of Cell Biology*, 196(5), pp.563–571.

Chang, Y.-C. *et al.*, 2007. GEF-H1 Couples Nocodazole-induced Microtubule Disassembly to Cell Contractility via RhoA. *Molecular biology of the cell*, 19(1), pp.308–317.

Cheeseman, I.M. *et al.*, 2002. Phospho-regulation of kinetochore-microtubule attachments by the Aurora kinase Ipl1p. *Cell*, 111(2), pp.163–172.

Cheeseman, I.M. *et al.*, 2006. The Conserved KMN Network Constitutes the Core Microtubule-Binding Site of the Kinetochore. *Cell*, 127(5), pp.983–997.

Cheeseman, I.M. & Desai, A., 2008. Molecular architecture of the kinetochore-microtubule interface. *Nature reviews. Molecular cell biology*, 9(1), pp.33–46.

Chen, Z. *et al.*, 2002. CP110, a cell cycle-dependent CDK substrate, regulates centrosome duplication in human cells. *Developmental Cell*, 3(3), pp.339–350.

Chew, T.L. *et al.*, 2002. A fluorescent resonant energy transfer-based biosensor reveals transient and regional myosin light chain kinase activation in lamella and cleavage furrows. *Journal of Cell Biology*, 156(3), pp.543–553.

Cimini, D. *et al.*, 2001. Merotelic kinetochore orientation is a major mechanism of aneuploidy in mitotic mammalian tissue cells. *Journal of Cell Biology*, 152(3), pp.517–527.

Cimini, D. *et al.*, 2003. Merotelic kinetochore orientation occurs frequently during early mitosis in mammalian tissue cells and error correction is achieved by two different mechanisms. *Journal of cell science*, 116(Pt 20), pp.4213–4225.

Cimini, D. *et al.*, 2002. Merotelic kinetochore orientation versus chromosome mono-orientation in the origin of lagging chromosomes in human primary cells. *Journal of cell science*, 115(Pt 3), pp.507–515.

Coleman, T.R. & Dunphy, W.G., 1994. Cdc2 regulatory factors. *Current Opinion in Cell Biology*, 6, pp.877–882.

Concin, N. *et al.*, 2005. Clinical relevance of dominant-negative p73 isoforms for responsiveness to chemotherapy and survival in ovarian cancer: Evidence for a crucial p53-p73 cross-talk in vivo. *Clinical Cancer Research*, 11(23), pp.8372–8383.

Concin, N. *et al.*, 2004. Transdominant ΔTAp73 Isoforms Are Frequently Up-regulated in Ovarian Cancer. Evidence for Their Role as Epigenetic p53 Inhibitors in Vivo. *Cancer Research*, 64(7), pp.2449–2460.

Cook, D.R., Rossman, K.L. & Der, C.J., 2013. Rho guanine nucleotide exchange factors: regulators of Rho GTPase activity in development and disease. *Oncogene*, 33(31), pp.4021–4035.

Cortez, D., 1999. Requirement of ATM-Dependent Phosphorylation of Brca1 in the DNA Damage Response to Double-Strand Breaks. *Science*, 286(5442), pp.1162–1166.

Coussens, L.M. & Werb, Z., 1996. Matrix metalloproteinases and the development of cancer. *Chemistry & Biology*, 3(11), pp.895–904.

Crainie, M. *et al.*, 1999. Overexpression of the receptor for hyaluronan-mediated motility (RHAMM) characterizes the malignant clone in multiple myeloma: identification of three distinct RHAMM variants. *Blood*, 93(5), pp.1684–96.

Dalal, B.I., Keown, P. a & Greenberg, a H., 1993. Immunocytochemical localization of secreted transforming growth factor-beta 1 to the advancing edges of primary tumors and to lymph node metastases of human mammary carcinoma. *The American journal of pathology*, 143(2), pp.381–9.

Daub, H. *et al.*, 2001. Rac/Cdc42 and p65PAK regulate the microtubule-destabilizing protein stathmin through phosphorylation at serine 16. *Journal of Biological Chemistry*, 276(3), pp.1677–1680.

DeLuca, J.G. *et al.*, 2006. Kinetochore Microtubule Dynamics and Attachment Stability Are Regulated by Hec1. *Cell*, 127(5), pp.969–982.

Deng, C. *et al.*, 1995. Mice lacking p21CIP1/WAF1 undergo normal development, but are defective in G1 checkpoint control. *Cell*, 82(4), pp.675–684.

Derksen, P.W.B. *et al.*, 2006. Somatic inactivation of E-cadherin and p53 in mice leads to metastatic lobular mammary carcinoma through induction of anoikis resistance and angiogenesis. *Cancer Cell*, 10(5), pp.437–449.

Deryugina, E.I. & Quigley, J.P., 2009. Chick embryo chorioallantoic membrane model systems to study and visualize human tumor cell metastasis. *Cell*, 130(6), pp.1119–1130.

Desai, A. & Mitchison, T.J., 1997. Microtubule Polymerization Dynamics. *Annual review of cell and developmental biology*, 13, pp.83–117.

Douc-Rasy, S. *et al.*, 2002. ΔN-p73α Accumulates in Human Neuroblastic Tumors. *The American Journal of Pathology*, 160(2), pp.631–639.

Dracopoli, N.C. *et al.*, 1989. Loss of alleles from the distal short arm of chromosome 1 occurs late in melanoma tumor progression. *Proc.Natl.Acad.Sci.USA*, 86(12), pp.4614–4618.

Drewinko, B. *et al.*, 1976. Establishment of a human carcinoembryonic antigen-producing colon adenocarcinoma cell line. *Cancer research*, 36(2 Pt 1), pp.467–75.

Dujardin, D.L. *et al.*, 2003. A role for cytoplasmic dynein and LIS1 in directed cell movement. *Journal of Cell Biology*, 163(6), pp.1205–1211.

Efimov, A. *et al.*, 2008. Paxillin-dependent stimulation of microtubule catastrophes at focal adhesion sites. *Journal of cell science*, 121, pp.196–204.

Elbashir, S.M. *et al.*, 2001. Duplexes of 21-nucleotide RNAs meditae RNA interference in cultured mammalian cells. *Nature*, 411(May), pp.1–5.

El-Deiry, W.S. *et al.*, 1993. WAF1, a potential mediator of p53 tumor suppression. *Cell*, 75(4), pp.817–825.

El-sibai, M. *et al.*, 2009. RhoA/ROCK-mediated switching between Cdc42- and Rac1-dependent protrusion in MTLn3 carcinoma cells. *Experimental Cell Research*, 314(7), pp.1540–1552.

Engelmann, D. *et al.*, 2014. A balancing act: orchestrating amino-truncated and full-length p73 variants as decisive factors in cancer progression. *Oncogene*, (August), pp.1–13.

Ertych, N. *et al.*, 2014. Increased microtubule assembly rates influence chromosomal instability in colorectal cancer cells. *Nature cell biology*, 16(8), pp.779–91.

Espina, C. *et al.*, 2008. A critical role for Rac1 in tumor progression of human colorectal adenocarcinoma cells. *The American journal of pathology*, 172(1), pp.156–66.

Etienne-Manneville, S., 2013. Microtubules in cell migration. *Annual review of cell and developmental biology*, 29, pp.471–99.

Etienne-Manneville, S. & Hall, A., 2003. Cdc42 regulates GSK-3 b and adenomatous polyposis coli to control cell polarity. *Nature*, 421(February), pp.753–756.

Evangelista, M., Zigmond, S. & Boone, C., 2003. Formins: signaling effectors for assembly and polarization of actin filaments. *Journal of cell science*, 116(Pt 13), pp.2603–2611.

Fife, C.M., Mccarroll, J.A.. & Kavallaris, M., 2014. Movers and shakers: Cell cytoskeleton in cancer metastasis. *British Journal of Pharmacology*, pp.5507–5523.

Fink, J. *et al.*, 2011. External forces control mitotic spindle positioning. *Nature cell biology*, 13(7), pp.771–8.

Fisk, H.A. & Winey, M., 2001. The mouse Mps1p-like kinase regulates centrosome duplication. *Cell*, 106(1), pp.95–104.

Friedl, P. & Wolf, K., 2003. Tumour-cell invasion and migration: diversity and escape mechanisms. *Nature reviews. Cancer*, 3(5), pp.362–374.

Fukata, M. *et al.*, 2002. Rac1 and Cdc42 capture microtubules through IQGAP1 and CLIP-170. *Cell*, 109(7), pp.873–885.

Gadde, S. & Heald, R., 2004. Mechanisms and molecules of the mitotic spindle. *Current Biology*, 14(18), pp.797–805.

Gaiddon, C. *et al.*, 2001. A subset of tumor-derived mutant forms of p53 down-regulate p63 and p73 through a direct interaction with the p53 core domain. *Mol Cell Biol*, 21(5), pp.1874–1887.

Ganem, N.J., Godinho, S.A. & Pellman, D., 2009. A mechanism linking extra centrosomes to chromosomal instability. *Nature*, 460(7252), pp.278–82.

Gard, D.L. & Kirschner, M.W., 1987. A microtubule-associated protein from Xenopus eggs that specifically promotes assembly at the plus-end. *Journal of Cell Biology*, 105(5), pp.2203–2215.

Gauthier-Rouviere, C. *et al.*, 1998. RhoG GTPase controls a pathway that independently activates Rac1 and Cdc42Hs. *Mol.Biol.Cell*, 9(6), pp.1379–1394.

Gelot, C., Magdalou, I. & Lopez, B.S., 2015. Replication stress in mammalian cells and its consequences for mitosis. *Genes*, 6(2), pp.267–298.

Godinho, S.A. *et al.*, 2014. Oncogene-like induction of cellular invasion from centrosome amplification. *Nature*, 510(7503), pp.167–171.

Goldstein, I. *et al.*, 2011. Understanding wild-type and mutant p53 activities in human cancer: new landmarks on the way to targeted therapies. *Cancer Gene Ther*, 18(1), pp.2–11.

Goode, B.L., Drubin, D.G. & Barnes, G., 2000. Functional cooperation between the microtubule and actin cytoskeletons. *Current Opinion in Cell Biology*, 12(1), pp.63–71.

Gorbsky, G.J., 2004. Mitosis: MCAK under the Aura of Aurora B. *Current Biology*, 14(9), pp.346–348.

Grego, S., Cantillana, V. & Salmon, E.D., 2001. Microtubule treadmilling in vitro investigated by fluorescence speckle and confocal microscopy. *Biophysical journal*, 81(1), pp.66–78.

Grill, S.W. *et al.*, 2003. The distribution of active force generators controls mitotic spindle position. *Science*, 301(5632), pp.518–521.

Grob, T.J. *et al.*, 2001. Human delta Np73 regulates a dominant negative feedback loop for TAp73 and p53. *Cell death and differentiation*, 8(12), pp.1213–1223.

Gruis, N.A. *et al.*, 1995. Genetic evidence in melanoma and bladder cancers that p16 and p53 function in separate pathways of tumor suppression. *American Journal of Pathology*, 146(5), pp.1199–1206.

Guan, M. & Chen, Y., 2005. Aberrant expression of DeltaNp73 in benign and malignant tumours of the prostate: correlation with Gleason score. *Journal of clinical pathology*, 58(11), pp.1175–1179.

Gundersen, G.G. & Bulinski, J.C., 1988. Selective stabilization of microtubules oriented toward the direction of cell migration. *Proceedings of the National Academy of Sciences of the United States of America*, 85(16), pp.5946–50.

Guo, C.P. *et al.*, 2011. Potent anti-tumor effect generated by a novel human papillomavirus (HPV) antagonist peptide reactivating the pRb/E2F pathway. *PLoS ONE*, 6(3).

Guo, F. *et al.*, 2003. P19Arf-p53 tumor suppressor pathway regulates cell motility by suppression of phosphoinositide 3-kinase and Rac1 GTPase activities. *Journal of Biological Chemistry*, 278(16), pp.14414–14419.

Guo, F. & Zheng, Y., 2004. Rho family GTPases cooperate with p53 deletion to promote primary mouse embryonic fibroblast cell invasion. *Oncogene*, 23(33), pp.5577–85.

Hall, A., 2012. Rho family GTPases. *Biochemical Society transactions*, 40(6), pp.1378–82.

Hanahan, D. & Weinberg, R. a., 2011. Hallmarks of cancer: The next generation. *Cell*, 144(5), pp.646–674.

Hanahan, D. & Weinberg, R.A., 2000. The hallmarks of cancer. *Cell*, 100, pp.57–70.

Van Haren, J. *et al.*, 2014. Dynamic microtubules catalyze formation of navigator-TRIO complexes to regulate neurite extension. *Current Biology*, 24(15), pp.1778–1785.

Harper, J.W. *et al.*, 1995. Inhibition of cyclin-dependent kinases by p21. *Molecular biology of the cell*, 6(4), pp.387–400.

Harper, J.W. *et al.*, 1993. The p21 Cdk-Interacting Protein Cipl Is a Potent Inhibitor of G l Cyclin-Dependent Kinases. *Cell*, 75, pp.805–816.

Head, J.A. *et al.*, 2003. Cortactin tyrosine phosphorylation requires Rac1 activity and association with the cortical actin cytoskeleton. *Molecular biology of the cell*, 14(May), pp.3216–3229.

Heinen, D. *et al.*, 1995. Microsatellite Instability in Colorectal Adenocarcinoma Cell Lines That Have Full-Length Adenomatous Polyposis Coli Protein. *Cancer*, pp.4797–4799.

Heinlein, C. *et al.*, 2008. Mutant p53R270H gain of function phenotype in a mouse model for oncogene-induced mammary carcinogenesis. *International Journal of Cancer*, 122(8), pp.1701–1709.

Henty-Ridilla, J.L. *et al.*, 2016. Accelerated actin filament polymerization from microtubule plus ends. *Science*, 352(6288).

Hofmann, U.B. *et al.*, 2000. Matrix metalloproteinases in human melanoma. *The Journal of investigative dermatology*, 115(3), pp.337–344.

Holland, A.J. & Cleveland, D.W., 2012. Losing balance: the origin and impact of aneuploidy in cancer. *EMBO reports*, 13(6), pp.501–14.

Holland, G.J. *et al.*, 2009. Sensing Chromosome Bi-Orientation Kinase from Kinetochore Substrates. *Science*, 323(March), pp.1350–1353.

Hunter, A.W. *et al.*, 2003. The kinesin-related protein MCAK is a microtubule depolymerase that forms an ATP-hydrolyzing complex at microtubule ends. *Molecular Cell*, 11(2), pp.445–457.

Jackman, M. *et al.*, 2003. Active cyclin B1-Cdk1 first appears on centrosomes in prophase. *Nature cell biology*, 5(2), pp.143–148.

Jordan, M.A. & Wilson, L., 2004. Microtubules as a target for anticancer drugs. *Nature Reviews. Cancer*, 4, pp. 253-265

Kaghad, M. *et al.*, 1997. Monoallelically expressed gene related to p53 at 1p36, a region frequently deleted in neuroblastoma and other human cancers. *Cell*, 90(4), pp.809–819.

Kardon, J.R. & Vale, R.D., 2009. Regulators of the cytoplasmic dynein motor. *Nature reviews Molecular cell biology*, 10(12), pp.854–865.

Kaverina, I., Rottner, K. & Small, J.V., 1998. Targeting, capture, and stabilization of microtubules at early focal adhesions. *Journal of Cell Biology*, 142(1), pp.181–190.

Kaverina, I. & Straube, A., 2011. Regulation of cell migration by dynamic microtubules. *Seminars in Cell and Developmental Biology*, 22(9), pp.968–974.

Kawasaki, Y. *et al.*, 2000. Asef, a link between the tumor suppressor APC and G-protein signaling. *Science*, 289(5482), pp.1194–1197.

Kessenbrock, K., Plaks, V. & Werb, Z., 2010. Matrix Metalloproteinases: Regulators of the Tumor Microenvironment. *Cell*, 141(1), pp.52–67.

Kim, E. & Deppert, W., 2004. Transcriptional activities of mutant p53: When mutations are more than a loss. *Journal of Cellular Biochemistry*, 93(5), pp.878–886.

Kimura, K. *et al.*, 1996. Regulation of myosin phosphatase by Rho and Rho-associated kinase (Rho-kinase). *Science*, 273(5272), pp.245–248.

Kirschner, M.W. & Mitchison, T.J., 1986. Beyond self assembly: from microtubules to morphogenesis. *Cell*, 45, pp.329–342.

Kita, K. *et al.*, 2006. Adenomatous Polyposis Coli on Microtubule Plus Ends in Cell Extensions Can Promote Microtubule Net Growth with or without EB1. *Molecular biology of the cell*, 17, pp.2331–2345.

Kiyomitsu, T. & Cheeseman, I.M., 2012. Chromosome- and spindle-pole-derived signals generate an intrinsic code for spindle position and orientation. *Nature cell biology*, 14(3), pp.311–7.

Knowlton, A.L., Lan, W. & Stukenberg, P.T., 2006. Aurora B Is Enriched at Merotelic Attachment Sites, Where It Regulates MCAK. *Current Biology*, 16(17), pp.1705–1710.

Kohn, K.W. *et al.*, 2012. Gene expression profiles of the NCI-60 human tumor cell lines define molecular interaction networks governing cell migration processes. *PLoS ONE*, 7(5).

Komarova, Y. *et al.*, 2009. Mammalian end binding proteins control persistent microtubule growth. *Journal of Cell Biology*, 184(5), pp.691–706.

Kops, G.J.P.L., Foltz, D.R. & Cleveland, D.W., 2004. Lethality to human cancer cells through massive chromosome loss by inhibition of the mitotic checkpoint. *Proceedings of the National Academy of Sciences of the United States of America*, 101(23), pp.8699–704.

Krendel, M., Zenke, F.T. & Bokoch, G.M., 2002. Nucleotide exchange factor GEF-H1 mediates cross-talk between microtubules and the actin cytoskeleton. *Nature cell biology*, 4(4), pp.294–301.

Krylyshkina, O. *et al.*, 2002. Modulation of substrate adhesion dynamics via microtubule targeting requires kinesin-1. *Journal of Cell Biology*, 156(2), pp.349–359.

Krylyshkina, O. *et al.*, 2003. Nanometer targeting of microtubules to focal adhesions. *Journal of Cell Biology*, 161(5), pp.853–859.

Kuroda, S. *et al.*, 1999. Cdc42, Rac1, and their effector IQGAP1 as molecular switches for cadherin-mediated cell-cell adhesion. *Biochemical and biophysical research communications*, 262(1), pp.1–6.

Kurokawa, K. & Matsuda, M., 2005. Localized RhoA Activation as a Requirement for the Induction of Membrane Ruffling. *Molecular biology of the cell*, 16(8), pp.4294–4303.

Kwon, M. *et al.*, 2015. Direct Microtubule-Binding by Myosin-10 Orients Centrosomes toward Retraction Fibers and Subcortical Actin Clouds. *Developmental Cell*, 34, pp.1–15.

Labrecque, M.P. *et al.*, 2016. The retinoblastoma protein regulates hypoxia-inducible genetic programs, tumor cell invasiveness and neuroendocrine differentiation in prostate cancer cells. *Oncotarget*, 5(17).

Lang, G.A. *et al.*, 2004. Gain of function of a p53 hot spot mutation in a mouse model of Li-Fraumeni syndrome. *Cell*, 119(6), pp.861–872.

Langermann, S., 1998. Requirement for p53 and p21 to Sustain G 2 Arrest After DNA Damage. *Science*, 282(November), pp.1497–1502.

Lansbergen, G. *et al.*, 2004. Conformational changes in CLIP-170 regulate its binding to microtubules and dynactin localization. *Journal of Cell Biology*, 166(7), pp.1003–1014.

Lantz, V.A. & Miller, K.G., 1998. A class VI unconventional myosin is associated with a homologue of a microtubule-binding protein, cytoplasmic linker protein-170, in neurons and at the posterior pole of Drosophila embryos. *Journal of Cell Biology*, 140(4), pp.897–910.

Lara-Gonzalez, P., Westhorpe, F.G. & Taylor, S.S., 2012. The spindle assembly checkpoint. *Current Biology*, 22(22), pp.R966–R980.

Larsson, N. *et al.*, 1997. Control of microtubule dynamics by oncoprotein 18: dissection of the regulatory role of multisite phosphorylation during mitosis. *Molecular and cellular biology*, 17(9), pp.5530–5539.

Lauffenburger, D.A. & Horwitz, A.F., 1996. Cell migration: A physically integrated molecular process. *Cell*, 84(3), pp.359–369.

Lawson, C.D. & Burridge, K., 2014. The on-off relationship of Rho and Rac during integrin-mediated adhesion and cell migration. *Small GTPases*, 5(1), pp.37–41.

Lee, S.H. & Dominguez, R., 2010. Regulation of actin cytoskeleton dynamics in cells. *Molecules and cells*, 29(4), pp.311–325.

Leibovitz, A. *et al.*, 1976. Classification of human colorectal adenocarcinoma cell lines. *Cancer Research*, 36(12), pp.4562–4569.

Lengauer, C., Kinzler, K.W. & Vogelstein, B., 1997. Genetic instability in colorectal cancers. *Nature*, 386, pp.623-627.

Leung, T. *et al.*, 1995. A novel serine/threonine kinase binding the ras-related RhoA GTPase which translocates the kinase to peripheral membranes. *Journal of Biological Chemistry*, 270(49), pp.29051–29054.

Leve, F. & Morgado-Díaz, J.A., 2012. Rho GTPase signaling in the development of colorectal cancer. *Journal of Cellular Biochemistry*, 113(8), pp.2549–2559.

Levrero, M. *et al.*, 2000. The p53/p63/p73 family of transcription factors: overlapping and distinct functions. *Journal of cell science*, 113, pp.1661–1670.

Liao, G., Nagasaki, T. & Gundersen, G.G., 1995. Low concentrations of nocodazole interfere with fibroblast locomotion without significantly affecting microtubule level: implications for the role of dynamic microtubules in cell locomotion. *Journal of cell science*, 108, pp.3473–3483.

Ligon, L.A. *et al.*, 2003. The Microtubule Plus-End Proteins EB1 and Dynactin Have Differential Effects on Microtubule Polymerization. *Molecular biology of the cell*, 14(May), pp.1405–1471.

Liu, Q. *et al.*, 2000. Chk1 is an essential kinase that is regulated by Atr and required for the G2/M DNA damage checkpoint. *Genes and Development*, 14(12), pp.1448–1459.

Lochter, A. *et al.*, 1997. Matrix metalloproteinase stromelysin-1 triggers a cascade of molecular alterations that leads to stable epithelial-to-mesenchymal conversion and a premalignant phenotype in mammary epithelial cells. *Journal of Cell Biology*, 139(7), pp.1861–1872.

Löffler, H. *et al.*, 2011. Cep63 recruits Cdk1 to the centrosome: Implications for regulation of mitotic entry, centrosome amplification, and genome maintenance. *Cancer Research*, 71(6), pp.2129–2139.

Lolli, G. & Johnson, L.N., 2005. CAK-Cyclin-Dependent Activating Kinase: A key kinase in cell cycle control and a target for Drugs? *Cell Cycle*, 4(4), pp.572–577.

Losada, A., Hirano, M. & Hirano, T., 1998. Identification of Xenopus SMC protein complexes required for sister chromatid cohesion. *Genes and Development*, 12, pp.1966–1997.

De Luca, M. *et al.*, 2008. Aurora-A and ch-TOG act in a common pathway in control of spindle pole integrity. *Oncogene*, 27(51), pp.6539–6549.

Machacek, M. *et al.*, 2009. Coordination of Rho GTPase activities during cell protrusion. *Nature*, 461(7260), pp.99–103.

Mack, N.A. *et al.*, 2011. The diverse roles of Rac signaling in tumorigenesis. *Cell Cycle*, 10(10), pp.1571–1581.

Malumbres, M. & Barbacid, M., 2009. Cell cycle, CDKs and cancer: a changing paradigm. *Nature reviews. Cancer*, 9(3), pp.153–166.

Malumbres, M. & Barbacid, M., 2005. Mammalian cyclin-dependent kinases. *Trends in Biochemical Sciences*, 30(11), pp.630–641.

Maney, T. *et al.*, 1998. Mitotic Centromere–associated Kinesin Is Important for Anaphase Chromosome Segregation. *J Cell Biol*, 142(3), pp.787–801.

Marei, H. & Malliri, A., 2016. GEFs: Dual regulation of Rac1 signaling. *Small GTPases*, 0(0), pp.1–10.

Margolis, R.L. & Wilson, L., 1998. Microtubule treadmilling: What goes around comes around. *BioEssays*, 20(10), pp.830–836.

Matsuoka, S., Huang, M. & Elledge, S.J., 1998. Linkage of ATM to cell cycle regulation by the Chk2 protein kinase. *Science*, 282(5395), pp.1893–1897.

Maxwell, C.A., McCarthy, J. & Turley, E., 2008. Cell-surface and mitotic-spindle RHAMM: moonlighting or dual oncogenic functions? *Journal of cell science*, 121, pp.925–932.

Meulmeester, E. & Ten Dijke, P., 2010. The dynamic roles of TGF-beta in cancer. *The Journal of pathology*, (October 2010), pp.205–218.

Michaelis, C., Ciosk, R. & Nasmyth, K., 1997. Cohesins: Chromosomal proteins that prevent premature separation of sister chromatids. *Cell*, 91(1), pp.35–45.

Mimori-Kiyosue, Y. *et al.*, 2005. CLASP1 and CLASP2 bind to EB1 and regulate microtubule plus-end dynamics at the cell cortex. *Journal of Cell Biology*, 168(1), pp.141–153.

Mimori-Kiyosue, Y., Shiina, N. & Tsukita, S., 2000. The dynamic behavior of the APC-binding protein EB1 on the distal ends of microtubules. *Current Biology*, 10(14), pp.865–868.

Mitsushima, M. *et al.*, 2010. Revolving movement of a dynamic cluster of actin filaments during mitosis. *Journal of Cell Biology*, 191(3), pp.453–462.

Montenegro-Venegas, C. *et al.*, 2010. MAP1B Regulates Axonal Development by Modulating Rho-GTPase Rac1 Activity. *Molecular biology of the cell*, 21(22), pp.4042–4056.

Morin, X. & Bellaïche, Y., 2011. Mitotic Spindle Orientation in Asymmetric and Symmetric Cell Divisions during Animal Development. *Developmental Cell*, 21(1), pp.102–119.

Morrison, E.E. *et al.*, 1998. EB1, a protein which interacts with the APC tumour suppressor, is associated with the microtubule cytoskeleton throughout the cell cycle. *Oncogene*, 17(26), pp.3471–3477.

Muller, P.A.J. & Vousden, K.H., 2013. P53 Mutations in Cancer. *Nature cell biology*, 15(1), pp.2–8.

Mullins, R.D. & Hansen, S.D., 2013. In vitro studies of actin filament and network dynamics. *Current Opinion in Cell Biology*, 25(1), pp.1–8.

Murphy, K.L., Dennis, A.P. & Rosen, J.M., 2000. A gain of function p53 mutant promotes both genomic instability and cell survival in a novel p53-null mammary epithelial cell model. *Faseb J*, 14(14), pp.2291–2302.

Musacchio, A. & Salmon, E.D., 2007. The spindle-assembly checkpoint in space and time. *Nature reviews. Molecular cell biology*, 8(5), pp.379–93.

Nabi, I.R., 1999. The polarization of the motile cell. *Journal of cell science*, 112, pp.1803–1811.

Nakajima, M. *et al.*, 2007. The complete removal of cohesin from chromosome arms depends on separase. *Journal of cell science*, 120, pp.4188–4196.

Nalbant, P. *et al.*, 2010. Guanine Nucleotide Exchange Factor-H1 Regulates Cell Migration via Localized Activation of RhoA at the Leading Edge. *Molecular biology of the cell*, 21(22), pp.4042–4056.

Narumiya, S., Tanji, M. & Ishizaki, T., 2009. Rho signaling, ROCK and mDia1, in transformation, metastasis and invasion. *Cancer and Metastasis Reviews*, 28(1-2), pp.65–76.

Nezi, L. & Musacchio, A., 2009. Sister chromatid tension and the spindle assembly checkpoint. *Current Opinion in Cell Biology*, 21(6), pp.785–795.

Nigg, E.A., 2001. Mitotic kinases as regulators of cell division and its checkpoints. *Nature reviews. Molecular cell biology*, 2(1), pp.21–32.

Nigg, E.A. & Stearns, T., 2011. The centrosome cycle: Centriole biogenesis, duplication and inherent asymmetries. *Nature Cell Biology*, 13(10), pp.1154–1160.

Nobes, C.D. & Hall, A., 1995. Rho, Rac, and Cdc42 GTPases regulate the assembly of multimolecular focal complexes associated with actin stress fibers, lamellipodia, and filopodia. *Cell*, 81(1), pp.53–62.

Noë, V. *et al.*, 2001. Release of an invasion promoter E-cadherin fragment by matrilysin and stromelysin-1. *Journal of cell science*, 114(114), pp.111–118.

O'Connor, K. & Chen, M., 2013. Dynamic functions of RhoA in tumor cell migration and invasion. *Small GTPases*, 4(3), pp.141–147.

O'Connor, K.L., Chen, M. & Towers, L.N., 2012. Integrin α6β4 cooperates with LPA signaling to stimulate Rac through AKAP-Lbc-mediated RhoA activation. *American journal of physiology. Cell physiology*, 302(3), pp.C605–14.

O'Connor, K.L., Nguyen, B.K. & Mercurio, A.M., 2000. RhoA function in lamellae formation and migration is regulated by the α6β4 integrin and cAMP metabolism. *Journal of Cell Biology*, 148(2), pp.253–258.

Ogino, S. *et al.*, 2010. Down-regulation of p21 (CDKN1A/CIP1) is inversely associated with microsatellite instability and CpG island methylator phenotype (CIMP) in colorectal cancer. *The Journal of pathology*, 220(September), pp.114–125.

Ohuchi, E. *et al.*, 1997. Membrane-Type metalloproteinase digests extracellular matrix macromolecules including interstitial collagens. *Matrix Biology*, 16(2), pp.76–77.

Oren, M. & Rotter, V., 2010. Mutant p53 gain-of-function in cancer. *Cold Spring Harbor perspectives in biology*, 2(2), p.a001107.

Orr, B. & Compton, D.A., 2013. A double-edged sword: how oncogenes and tumor suppressor genes can contribute to chromosomal instability. *Front Oncol*, 3(June), p.164.

Osmani, N. *et al.*, 2010. Cdc42 localization and cell polarity depend on membrane traffic. *Journal of Cell Biology*, 191(7), pp.1261–1269.

Palamidessi, A. *et al.*, 2008. Endocytic Trafficking of Rac Is Required for the Spatial Restriction of Signaling in Cell Migration. *Cell*, 134(1), pp.135–147.

Parri, M. & Chiarugi, P., 2010. Rac and Rho GTPases in cancer cell motility control. *Cell communication and signaling : CCS*, 8, p.23.

Pellinen, T. & Ivaska, J., 2006. Integrin traffic. *Journal of cell science*, 119(Pt 18), pp.3723–3731.

Peters, J.-M., 2006. The anaphase promoting complex/cyclosome: a machine designed to destroy. *Nature reviews. Molecular cell biology*, 7(9), pp.644–56.

Petitjean, A. *et al.*, 2006. TP53 Impact of Mutant p53 Functional Properties on Mutation Patterns and Tumor Phenotype: Lessons from Recent Developments in the IARC TP53 Database. *Human Mutation*, 27(July), pp.796–802.

Pinsky, B.A. & Biggins, S., 2005. The spindle checkpoint: Tension versus attachment. *Trends in Cell Biology*, 15(9), pp.486–493.

Pollard, T.D. & Earnshaw, W.C., 2007. Cell Biology. Springer Verlag Berlin Heidelberg

Potter, D.A. *et al.*, 1997. Calpain Regulates Actin Remodeling during Cell Spreading. *The Journal of Cel Biology*. 139(4), pp.895–905.

Pützer, B.M., 2013. DNp73 : oncotarget in invasion and metastasis. *Oncotarget*, 5(1), pp.1–2.

Radisky, D.C. *et al.*, 2005. Rac1b and reactive oxygen species mediate MMP-3-induced EMT and genomic instability. *Nature*, 436(7047), pp.123–7.

Radisky, E.S. & Radisky, D.C., 2010. Matrix metalloproteinase-induced epithelial-mesenchymal transition in breast cancer. *Journal of Mammary Gland Biology and Neoplasia*, 15(2), pp.201–212.

Rauhala, H.E. *et al.*, 2013. Silencing of the Arp2/3 complex disturbs pancreatic cancer cell migration. *Anticancer Research*, 33(1), pp.45–52.

Ren, X.D., Kiosses, W.B. & Schwartz, M.A., 1999. Regulation of the small GTP-binding protein Rho by cell adhesion and the cytoskeleton. *EMBO Journal*, 18(3), pp.578–585.

Ricke, R.M., van Ree, J.H. & van Deursen, J.M., 2008. Whole chromosome instability and cancer: a complex relationship. *Trends in Genetics*, 24(9), pp.457–466.

Ridley, A.J. *et al.*, 2003. Cell migration: integrating signals from front to back. *Science*, 302(5651), pp.1704–1709.

Ridley, A.J., 2006. Rho GTPases and actin dynamics in membrane protrusions and vesicle trafficking. *Trends in Cell Biology*, 16(10), pp.522–529.

Ridley, A.J. *et al.*, 1992. The small GTP-binding protein rac regulates growth factor-induced membrane ruffling. *Cell*, 70(3), pp.401–410.

Rieder, C.L. *et al.*, 1995. The checkpoint delaying anaphase in response to chromosome monoorientation is mediated by an inhibitory signal produced by unattached kinetochores. *Journal of Cell Biology*, 130(4), pp.941–948.

Rieder, C.L. & Salmon, E.D., 1994. Motile kinetochores and polar ejection forces dictate chromosome position on the vertebrate mitotic spindle. *Journal of Cell Biology*, 124(3), pp.223–233.

Rieder, C.L. & Salmon, E.D., 1998. The vertebrate cell kinetochore and its roles during mitosis. *Trends in Cell Biology*, 8(8), pp.310–318.

Rohatgi, R. *et al.*, 1999. The interaction between N-WASP and the Arp2/3 complex links Cdc42-dependent signals to actin assembly. *Cell*, 97(2), pp.221–231.

Rooney, C. *et al.*, 2010. The Rac activator STEF (Tiam2) regulates cell migration by microtubule-mediated focal adhesion disassembly. *EMBO reports*, 11(4), pp.292–298.

Rossman, K.L., Der, C.J. & Sondek, J., 2005. GEF means Go: turning on Rho GTPases with guanine nucleotide-exchange factors. *Nature Reviews Molecular Cell Biology*, 6(2), pp.167–180.

Rudolph-Owen, L.A. *et al.*, 1998. The Matrix Metalloproteinase Matrilysin Influences Early-Stage Mammary Tumorigenesis. *Cancer Research*, 55(19), pp.5500–5506.

Rufini, A. *et al.*, 2011. p73 in Cancer. *Genes and Cancer*, 2(4), pp.491–502. A

Sablina, A.A., Chumakov, P.M. & Kopnin, B.P., 2003. Tumor suppressor p53 and its homologue p73alpha affect cell migration. *Journal of Biological Chemistry*, 278(30), pp.27362–27371.

Sadok, A. & Marshall, C.J., 2014. Rho GTPases: Masters of Cell Migration. *Small GTPases*, 5(4).

Sahai, E., 2005. Mechanisms of cancer cell invasion. *Current opinion in genetics & development*, 15(1), pp.87–96.

Salaycik, K.J. *et al.*, 2005. Quantification of microtubule nucleation, growth and dynamics in wound-edge cells. *Journal of cell science*, 118(Pt 18), pp.4113–4122.

Sanchez, Y., 1997. Conservation of the Chk1 Checkpoint Pathway in Mammals: Linkage of DNA Damage to Cdk Regulation Through Cdc25. *Science*, 277(5331), pp.1497–1501.

Sanhaji, M. *et al.*, 2011. Mitotic centromere-associated kinesin (MCAK): a potential cancer drug target. *Oncotarget*, 2(12), pp.935–47.

Schmidt, J.C. *et al.*, 2012. The Kinetochore-Bound Ska1 Complex Tracks Depolymerizing Microtubules and Binds to Curved Protofilaments. *Developmental Cell*, 23(5), pp.968–980.

Schmidt, M. *et al.*, 2000. Differential modulation of paclitaxel-mediated apoptosis by p21 Waf1 and p27 Kip1. *Oncogene*, 19, pp.2423–2429.

Schmidt, S. & Debant, A., 2014. Function and regulation of the Rho guanine nucleotide exchange factor Trio. *Small GTPases*, 5(June), p.e29769.

Schober, J.M. *et al.*, 2009. Migration and actin protrusion in melanoma cells are regulated by EB1 protein. *Cancer Letters*, 284(1), pp.30–36.

Schuyler, S.C. & Pellman, D., 2001. Microtubule “plus-end-tracking proteins”: The end is just the beginning. *Cell*, 105(4), pp.421–424.

Semple, T.U. *et al.*, 1978. Tumor and Lymphoid Cell Lines from a Patient with Carcinoma of the Colon for a Cytotoxicity Model. *Cancer Research*, 38(MAY), pp.1345–1355.

Sheltzer, J.M., 2013. A transcriptional and metabolic signature of primary aneuploidy is present in chromosomally-unstable cancer cell and informs clinical prognosis. *Cancer research*, 73(21), pp.6401–6412.

Sheltzer, J.M. & Amon, A., 2011. The aneuploidy paradox: Costs and benefits of an incorrect karyotype. *Trends in Genetics*, 27(11), pp.446–453.

Shiota, M. *et al.*, 2008. Twist and p53 reciprocally regulate target genes via direct interaction. *Oncogene*, 27(42), pp.5543–5553.

Siegrist, S.E. & Doe, C.Q., 2007. Microtubule-induced cortical cell polarity. *Genes & Development*, 21(5), pp.483–496.

Smit, M.A. & Peeper, D.S., 2008. Deregulating EMT and Senescence: Double Impact by a Single Twist. *Cancer Cell*, 14(1), pp.5–7.

Spaderna, S. *et al.*, 2006. A Transient, EMT-Linked Loss of Basement Membranes Indicates Metastasis and Poor Survival in Colorectal Cancer. *Gastroenterology*, 131(3), pp.830–840.

Steder, M. *et al.*, 2013. DNp73 Exerts Function in Metastasis Initiation by Disconnecting the Inhibitory Role of EPLIN on IGF1R-AKT/STAT3 Signaling. *Cancer Cell*, 24(4), pp.512–527.

Stepanova, T. *et al.*, 2003. Visualization of microtubule growth in cultured neurons via the use of EB3-GFP (end-binding protein 3-green fluorescent protein). *The Journal of neuroscience : the official journal of the Society for Neuroscience*, 23(7), pp.2655–2664.

Straube, A. & Merdes, A., 2007. EB3 Regulates Microtubule Dynamics at the Cell Cortex and Is Required for Myoblast Elongation and Fusion. *Current Biology*, 17(15), pp.1318–1325.

Suardet, L. *et al.*, 1992. Responsiveness of three newly established human colorectal cancer cell lines to transforming growth factors beta 1 and beta 2. *Cancer research*, 52(13), pp.3705–3712.

Sumara, I. *et al.*, 2000. Characterization of vertebrate cohesin complexes and their regulation in prophase. *Journal of Cell Biology*, 151(4), pp.749–761.

Talos, F. *et al.*, 2007. p73 Suppresses Polyploidy and Aneuploidy in the Absence of Functional p53. *Molecular Cell*, 27(4), pp.647–659.

Tamura, N. & Draviam, V.M., 2012. Microtubule plus-ends within a mitotic cell are “moving platforms” with anchoring, signalling and force-coupling roles. *Open biology*, 2(11), p.120132.

Tanenbaum, M.E. *et al.*, 2008. Dynein, Lis1 and CLIP-170 counteract Eg5-dependent centrosome separation during bipolar spindle assembly. *The EMBO journal*, 27(24), pp.3235–45.

Tanenbaum, M.E. & Medema, R.H., 2010. Mechanisms of Centrosome Separation and Bipolar Spindle Assembly. *Developmental Cell*, 19(6), pp.797–806.

Tarapore, P. & Fukasawa, K., 2002. Loss of p53 and centrosome hyperamplification. *Oncogene*, 21(40), pp.6234–40.

Théry, M. *et al.*, 2005. The extracellular matrix guides the orientation of the cell division axis. *Nature cell biology*, 7(10), pp.947–953.

Thiery, J.P. & Sleeman, J.P., 2006. Complex networks orchestrate epithelial-mesenchymal transitions. *Nature reviews. Molecular cell biology*, 7(2), pp.131–42.

Thompson, S.L., Bakhoum, S.F. & Compton, D.A., 2010. Mechanisms of Chromosomal Instability. *Current Biology*, 20(6), pp.R285–R295.

Thompson, S.L. & Compton, D.A., 2008. Examining the link between chromosomal instability and aneuploidy in human cells. *Journal of Cell Biology*, 180(4), pp.665–672.

Thukral, S.K. *et al.*, 1995. Discrimination of DNA binding sites by mutant p53 proteins. *Molecular and cellular biology*, 15(9), pp.5196–202.

Tighe, A. *et al.*, 2001. Aneuploid colon cancer cells have a robust spindle checkpoint. *EMBO Reports*, 2(7), pp.609–614.

Torres, E.M. *et al.*, 2007. Effects of aneuploidy on cellular physiology and cell division in haploid yeast. *Science*, 317(5840), pp.916–24.

Toyoshima, F. & Nishida, E., 2007. Integrin-mediated adhesion orients the spindle parallel to the substratum in an EB1- and myosin X-dependent manner. *The EMBO journal*, 26(6), pp.1487–1498.

Tran, A.D.A. *et al.*, 2007. HDAC6 deacetylation of tubulin modulates dynamics of cellular adhesions. *Journal of cell science*, 120, pp.1469–1479.

Tsvetkov, A.S. *et al.*, 2007. Microtubule-binding proteins CLASP1 and CLASP2 interact with actin filaments. *Cell Motility and the Cytoskeleton*, 64(7), pp.519–530.

Tuve, S. *et al.*, 2004. Alterations of dTA-p73 splice transcripts during melanoma development and progression. *International Journal of Cancer*, 108(1), pp.162–166.

Uramoto, H. *et al.*, 2004. Expression of ∆ Np73 Predicts Poor Prognosis in Lung Cancer Expression. *Clinical Cancer Research*, 10, pp.6905–6911.

Uzbekov, R., Kireyev, I. & Prigent, C., 2002. Centrosome separation: Respective role of microtubules and actin filaments. *Biology of the Cell*, 94(4-5), pp.275–288.

Vasiliev, J.M. *et al.*, 1970. Effect of colcemid on the locomotory behaviour of fibroblasts. *Journal of embryology and experimental morphology*, 24(3), pp.625–640.

Vaughan, K.T., 2005. TIP maker and TIP marker; EB1 as a master controller of microtubule plus ends. *Journal of Cell Biology*, 171(2), pp.197–200.

Vega, F.M. *et al.*, 2011. RhoA and RhoC have distinct roles in migration and invasion by acting through different targets. *Journal of Cell Biology*, 193(4), pp.655–665.

Wang, S.-P. *et al.*, 2009. p53 controls cancer cell invasion by inducing the MDM2-mediated degradation of Slug. *Nature cell biology*, 11(6), pp.694–704.

Wang, W. *et al.*, 2008. Centrosome separation driven by actin-microfilaments during mitosis is mediated by centrosome-associated tyrosine-phosphorylated cortactin. *Journal of cell science*, 121(Pt 8), pp.1334–43.

Wang, W. *et al.*, 2004. Identification and testing of a gene expression signature of invasive carcinoma cells within primary mammary tumors. *Cancer Research*, 64(23), pp.8585–8594.

Wang, Y. *et al.*, 2005. Overexpression of EB1 in human esophageal squamous cell carcinoma (ESCC) may promote cellular growth by activating beta-catenin/TCF pathway. *Oncogene*, 24(44), pp.6637–45.

Watanabe, T. *et al.*, 2004. Interaction with IQGAP1 links APC to Rac1, Cdc42, and actin filaments during cell polarization and migration. *Developmental Cell*, 7(6), pp.871–883.

Waterman-Storer, C.M. *et al.*, 1999. Microtubule growth activates Rac1 to promote lamellipodial protrusion in fibroblasts. *Nature cell biology*, 1(1), pp.45–50.

Waterman-Storer, C.M. & Salmon, E., 1999. Positive feedback interactions between microtubule and actin dynamics during cell motility. *Current opinion in cell biology*, 11(1), pp.61–67.

Waterman-Storer, C.M. & Salmon, E.D., 1997. Actomyosin-based retrograde flow of microtubules in the lamella of migrating epithelial cells influences microtubule dynamic instability and turnover and is associated with microtubule breakage and treadmilling. *Journal of Cell Biology*, 139(2), pp.417–434.

Watson, P. & Stephens, D.J., 2006. Microtubule plus-end loading of p150(Glued) is mediated by EB1 and CLIP-170 but is not required for intracellular membrane traffic in mammalian cells. *Journal of cell science*, 119, pp.2758–2767.

Weber, K.L. *et al.*, 2004. A microtubule-binding myosin required for nuclear anchoring and spindle assembly. *Nature*, 431(7006), pp.325–329.

Wen, Y. *et al.*, 2004. EB1 and APC bind to mDia to stabilize microtubules downstream of Rho and promote cell migration. *Nature cell biology*, 6(9), pp.820–830.

Whalley, H.J. *et al.*, 2015. Cdk1 phosphorylates the Rac activator Tiam1 to activate centrosomal Pak and promote mitotic spindle formation. *Nature Communications*, 6(May), p.7437.

Whitehead, C.M. & Rattner, J.B., 1998. Expanding the role of HsEg5 within the mitotic and post-mitotic phases of the cell cycle. *Journal of cell science*, 111 (Pt 1, pp.2551–2561.

Wilhelm, T. *et al.*, 2013. Spontaneous slow replication fork progression elicits mitosis alterations in homologous recombination-deficient mammalian cells. *Proceedings of the National Academy of Sciences of the United States of America*, 111(2), p.201311520.

Wittmann, T., Bokoch, G.M. & Waterman-Storer, C.M., 2003. Regulation of leading edge microtubule and actin dynamics downstream of Rac1. *Journal of Cell Biology*, 161(5), pp.845–851.

Wittmann, T., Hyman, A. & Desai, A., 2001. The spindle: a dynamic assembly of microtubules and motors. *Nature cell biology*, 3(1), pp.E28–E34.

Wittmann, T. & Waterman-Storer, C.M., 2001. Cell motility: can Rho GTPases and microtubules point the way? *Journal of cell science*, 114, pp.3795–3803.

Woodcock, S.A. *et al.*, 2010. Tiam1-Rac Signaling Counteracts Eg5 during Bipolar Spindle Assembly to Facilitate Chromosome Congression. *Current Biology*, 20(7), pp.669–675.

Woolner, S. *et al.*, 2008. Myosin-10 and actin filaments are essential for mitotic spindle function. *Journal of Cell Biology*, 182(1), pp.77–88.

Yamada, K.M. & Araki, M., 2001. Tumor suppressor PTEN: modulator of cell signaling, growth, migration and apoptosis. *Journal of cell science*, 114(Pt 13), pp.2375–2382.

Yamaguchi, H., Lorenz, M., *et al.*, 2005. Molecular mechanisms of invadopodium formation: The role of the N-WASP-Arp2/3 complex pathway and cofilin. *Journal of Cell Biology*, 168(3), pp.441–452.

Yamaguchi, H. & Condeelis, J., 2007. Regulation of the actin cytoskeleton in cancer cell migration and invasion. *Biochimica et Biophysica Acta - Molecular Cell Research*, 1773(5), pp.642–652.

Yamaguchi, H., Wyckoff, J. & Condeelis, J., 2005. Cell migration in tumors. *Current Opinion in Cell Biology*, 17, pp.559–564.

Yamakita, Y. *et al.*, 2003. Caldesmon inhibits Arp2/3-mediated actin nucleation. *Journal of Biological Chemistry*, 278(20), pp.17937–17944.

Yang, A. *et al.*, 1998. P63, a P53 Homolog At 3Q27–29, Encodes Multiple Products With Transactivating, Death-Inducing, and Dominant-Negative Activities. *Molecular Cell*, 2(3), pp.305–16.

Yang, A. & McKeon, F., 2000. P63 and P73: P53 mimics, menaces and more. *Nature reviews. Molecular cell biology*, 1(3), pp.199–207.

Yeh, S. *et al.*, 1994. Frequent Genetic Alterations at the Distal Region of Chromosome ip in Human Hepatocellular Carcinomas. *Cancer Research*, 54, pp.4188–4192.

Yeo, C.Q.X. *et al.*, 2016. P53 Maintains Genomic Stability by Preventing Interference between Transcription and Replication. *Cell Reports*, 15(1), pp.132–146.

Yoshida, T. *et al.*, 2010. Blockade of Rac1 activity induces G1 cell cycle arrest or apoptosis in breast cancer cells through downregulation of cyclin D1, survivin, and X-linked inhibitor of apoptosis protein. *Molecular cancer therapeutics*, 9(6), pp.1657–1668.

Yoshio, T. *et al.*, 2007. Caldesmon suppresses cancer cell invasion by regulating podosome/invadopodium formation. *FEBS Letters*, 581(20), pp.3777–3782.

Zaika, A.I. *et al.*, 2002. DeltaNp73, a dominant-negative inhibitor of wild-type p53 and TAp73, is up-regulated in human tumors. *The Journal of experimental medicine*, 196(6), pp.765–780.

Zhang, J. *et al.*, 2005. Silencing p21(Waf1/Cip1/Sdi1) expression increases gene transduction efficiency in primitive human hematopoietic cells. *Gene therapy*, 12(19), pp.1444–1452.

Zhang, Y. *et al.*, 2012. Mammary epithelial cell polarity is regulated differentially by p73 isoforms via epithelial-to-mesenchymal transition. *Journal of Biological Chemistry*, 287(21), pp.17746–17753.

Zheng, H.C. *et al.*, 2008. Arp2/3 overexpression contributed to pathogenesis, growth and invasion of gastric carcinoma. *Anticancer Research*, 28(4 B), pp.2225–2232.

Zheng, Y., 2001. Dbl family guanine nucleotide exchange factors. *Trends in Biochemical Sciences*, 26(12), pp.724–732.

Van Zijl, F., Krupitza, G. & Mikulits, W., 2011. Initial steps of metastasis: Cell invasion and endothelial transmigration. *Mutation Research - Reviews in Mutation Research*, 728(1-2), pp.23–34.

Acknowledgement

At this point, I would like to thank everyone who contributed to this thesis and who supported me during the last four years.

First of all, I want to thank my doctorate supervisor Prof. Dr. Holger Bastians for giving me the opportunity to work on this exciting topic in his lab. Thanks for the constant guidance as well as valuable ideas and discussions on the project.

Besides, I would like to thank my thesis committee members Prof. Dr. Michael Thumm and Prof. Dr. Dieter Kube for their comments and suggestions throughout my project.

Furthermore, I thank Prof. Dr. Heike Krebber for providing working materials. I also want to thank Prof. Dr. Jörg Wilting and his lab members, especially Berti Manshausen and Sonja Schwoch, for introducing and supervising the CAM assays, providing the main working materials and supporting the processing and analyses of the samples. Thanks to Silvia von der Heyde for bioinformatical analyses of the RNA sequencing results and to Prof. Dr. Maik Kschischo for discussion on statistical tests.

I am extremely grateful to all current and former members of the Bastians lab for the fantastic working atmosphere, constant support, motivation and all the fun we had during and after working in the lab. I want to thank Dr. Norman Ertych and Dr. Ailine Stolz for sharing their knowledge and teaching me the essential techniques. Thanks to Nadine Schermuly, Elina Glaubke and Magdalena Kistner for vivid discussions on failed and successive experiments and also all the non-scientific related topics as well as constructive coffee breaks and cocktail hours. Further, I would particularly like to thank Dr. Sina Lüddecke for reading and commenting on the manuscript, cheery words whenever necessary and being a friend also outside the lab.

Last but not least, I want to express my special and greatest appreciation to my family for practically and morally supporting me throughout my thesis and my life in general. I want to thank them for their continuous love and motivation. I could not have done it without them.

Curriculum Vitae

Personal Data

Katharina Berger

Born on 11th of January 1988
in Brandenburg an der Havel

School Education

08/94-06/00	Konrad-Sprengel-Grundschule in Brandenburg an der Havel
08/00-06/07	Bertolt-Brecht-Gymnasium in Brandenburg an der Havel

Scientific Education

10/07-09/10	Bachelor of Science in Life Sciences University of Potsdam Bachelor Thesis Institute for Molecular Biology "Analysis of H_2O_2 responsive gene expression in *Arabidopsis thaliana*"
10/10-08/12	Master of Science in Biochemistry and Molecular Biology University of Potsdam Master Thesis Institute for Cell Biology "Functional Characterization of CP55 in *Dictyostelium*"
since 10/12	PhD student in the group of Prof. Dr. Holger Bastians, Institute for Molecular Oncology Section of Cellular Oncology University Medical School Member of the GGNB program "Molecular Biology of Cells"